ČESKÁ ZEMĚDĚLSKÁ UNIVERZITA V PRAZE
Fakulta životního prostředí
Katedra biotechnických úprav krajiny

Příspěvek k hodnocení různých přístupů v modelování ztráty půdy vodní erozí v prostředí GIS

Disertační práce

Autor práce: Ing. Michaela Hrabalíková

Školitel práce: prof. Ing. Miloslav Janeček, CSc.

Praha 2015

Prohlašuji, že jsem disertační práci vypracovala samostatně s použitím výsledků vlastní práce nebo společné práce s kolegy a s pomocí dalších zdrojů, které jsou řádně citovány.

V Praze dne 27. 11. 2015

PODĚKOVÁNÍ

Děkuji svému školiteli prof. Ing. Miloslavu Janečkovi, DrSc. za cenné rady, připomínky a konzultace během zpracovávání disertační práce a pomoc během celého doktorského studia.

Abstrakt

Disertační práce: *Příspěvek k hodnocení různých přístupů v modelování ztráty půdy vodní erozí v prostředí GIS* je souborem pěti studií publikovaných nebo přijatých k publikaci ve vědeckých časopisech. Tematicky se práce zaobírá otázkou propojení erozního modelování s geografickými informačními systémy. Práce je rozdělena do pěti kapitol. V první kapitole je uvedena problematika erozního a srážko-odtokového modelování se zaměřením zejména na koncept a základní rovnice, na nichž je modelování eroze postaveno. Druhá kapitola obsahuje 2 studie, které se zabývají modelováním srážko-odtokových poměrů v experimentální lokalitě modelem KINFIL. Kapitola se také zaobírá výběrem vhodného modelu a zdrojovými daty, které tvoří základ pro vyhodnocení fyziografických parametrů povodí. Třetí kapitola se tematicky věnuje výpočtu faktoru erozní účinnosti srážek z dlouhodobých záznamů 32 meteorologických stanic v České republice. Částečné se prolíná s předchozí kapitolou a tím, že jedním z výstupů studie je databáze REDES obsahující hodnoty *R*-faktoru. Kapitola se ovšem více zaměřuje na časové měřítko v modelování a to zejména na vliv časového kroku v modelování na výsledné hodnoty. Čtvrtá kapitola se tematicky věnuje modelování eroze v prostředí GIS na základě analýzy digitálního modelu terénu. Obsahuje jednu studii, která řeší vliv různých algoritmů a rovnic na výpočet topografického faktoru a celkové ovlivnění predikce ztráty půdy.

Abstract

Dissertation thesis: *Contribution to the evaluation of different approaches to the modelling of soil loss by water erosion in GIS*, is a set of five studies published or accepted for publication in scientific journals. Thematically the work deals with the question of linking the erosion modelling together with geographic information systems. The work is divided into five chapters. In the first chapter, the issue of erosion and rainfall-runoff modelling is described. A particular focus is placed on the concept and the basic equations underlying erosion modelling. The second chapter contains 2 studies that deal with modelling rainfall-runoff conditions in the area of experimental area using KINFIL model. The chapter also discusses the selection of a suitable model and source datasets that forms the basis for the evaluation of physiographic parameters of a catchment. The third chapter is thematically focused in calculating the rainfall factor based on long-term precipitation records from 32 meteorological stations in the Czech Republic. It partially overlaps with the previous chapter because one of the outcomes of the study is the REDES database containing values of *R*-factor. However, the chapter focuses more on the time scale, and especially the influence of the time step in the simulation on resulting outcomes of the model. The fourth chapter is dealing by erosion modelling in GIS based on analysis of digital terrain models. It contains a study that addresses the influence of various algorithms and/or equations to calculate topographical factor and its effect on the overall prediction of soil loss.

Obsah

1 Úvod

Modelování eroze půdy je důležité nejen pro pochopení erozního procesu jako takového, ale především pro predikci chování hydrologických a erozních procesů v určitém systému, za stanovených podmínek, a umožňuje tak identifikaci nebo výběr vhodných protierozní opatření.

Modelování erozních jevů, a s tím souvisejících srážko-odtokových poměrů, v systému (pole, povodí) umožňuje:

- Pochopení hlavních řídících faktorů,
- Hodnocení dopadů na produkční a mimoprodukční funkce půdy a znečištění vodních zdrojů,
- Identifikace strategií v protierozní a protipovodňové ochraně,
- Hodnocení efektivity půdo-ochranných opatření.

Půdní eroze je výsledkem složité interakce systému půda-rostlina-atmosférické jevy. Tudíž, modelování půdní eroze vyžaduje multidisciplinární přístup mezi pedology, agronomy, hydrology a dalšími skupinami odborníků. Řádný model musí být schopen integrovat procesy, faktory a příčiny v různých prostorových a časových měřítcích. Správně kalibrovaný model poskytuje tak dobré odhady rizik spojených s erozí půdy.

Během posledních 60 let byly vyvinuty různé modely lišící se ve schopnosti predikce, prostorovém a časovém měřítku. Ovšem, s datovou otevřeností (viz projekt Copernicus, CENIA atd.) a rozvojem moderních technologických nástrojů, jako jsou geografické informační systémy (GIS) a dálkový průzkum země, vznikají další modifikace stávajících modelů (Nearing a Hairsine, 2010, Karydas et al., 2014, Tetzlaff et al., 2013, Thalacker, 2014)anebo nové algoritmy (Tarboton, 1997) či modely (Moore and Burch, 1986) za účelem zpřesňování predikce degradace půdy erozí. GIS pracuje na základě shromažďování, transformaci a zobrazování prostorových dat (Longley et al., 2004). V důsledku toho, se očekává, že implementace erozních modelů do prostředí GIS a zvyšování podrobnosti dat bude poskytovat podstatně realističtější odhady. Nicméně, v oblasti erozního modelování stále existují jisté problémy (Boardman, 2006), mis-koncepce a mis-aplikace modelů (Govers, 2010). Proto je zde potřeba dále zkoumat roli GIS v hydrologicko-erozním modelování a vyhodnotit tak potenciál ke zlepšení predikcí na základě volby vhodného modelu popř. algoritmu, datových zdrojů, časového a prostorového měřítka.

Tato disertační práce prezentuje soubor studií zaměřených na propojení GIS s modelováním erozních a srážko-odtokových procesů. První dvě studie jsou obsaženy v kapitole 2., která se

zaměřuje na vyhodnocení dostupných datových zdrojů pro modelování vodní eroze a srážko-odtokových procesů v prostředí GIS a výběr vhodného modelu. Další dvě studie jsou součástí kapitoly 3, která se zejména zaměřuje na vyhodnocení vlivu časového a prostorového měřítka v modelování na příkladu výpočtu faktoru erozní účinnosti deště. Poslední studie je zařazena do kapitoly 4. Tato kapitola shrnuje různé přístupy v predikci ztráty půdy v prostředí GIS, kdy základním vstupním parametrem je digitální model reliéfu (DMR).

Disertační práce celkem obsahuje 5 studií publikovaných nebo přijatých k publikaci ve vědeckých impaktovaných časopisech. Formát citací a jednotky v jednotlivých studií jsou vždy na základě instrukcí pro autory daného časopisu.

1.1 Koncepce erozního modelování a současný vývoj modelování

Modelování půdní eroze má poměrně dlouhou historii, kdy první modely již začaly vznikat ve 40. letech 20. století (Garen et al., 1999). Od té doby se modelování vodní eroze stále vyvíjí, i když ne zrovna nepřetržitě (Morgan a Nearing, 2011). Erozní modely byly v počátku založeny pouze na definování hlavních řídících faktorů erozních procesů (viz obr. 1) a určení jejich vlivu na erozní procesy na základě výsledků pozorování, měření, experimentů a statistických metod (Wischmeier and Smith, 1965). Byly zaměřeny převážně na zjišťování nebo prognózu ztráty půdy.

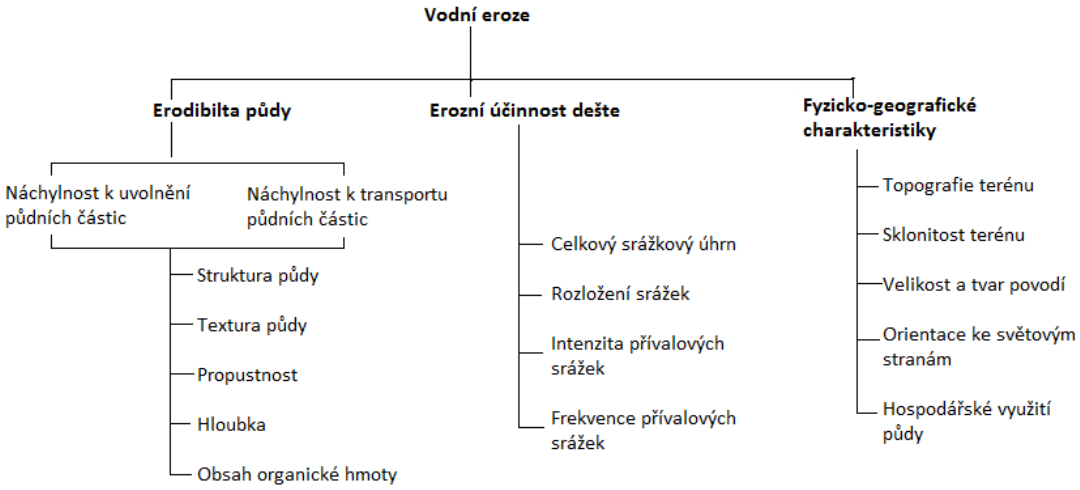

Obr. 1: Hlavní faktory podmiňující erozi půdy (Zhang et al., 1996)

Průkopnická práce Meyera a Wischmeiera (1969) představuje základní koncepční rámec pro modelování vodní eroze (viz obr. 2), který položil základ mnoha dalším modelům, jako je např.

v praxi stále nejčastěji užívaný model USLE (Wischmeier a Smith, 1965, 1978) nebo jeho revidovaná forma RUSLE (Renard, 1997).

Meyer a Wishmeier (1969) navázali na výzkum Ellisona (1947) a koncipovali erozní proces jako dvoufázový proces zahrnující rozrušení půdního krytu, čili uvolnění půdní částice, a následně její transport povrchovým odtokem (viz obr. 2). Erozní proces popsali jakožto výsledek:

- Oddělení půdních částic následkem dopadu dešťové kapky;
- Oddělení půdních částic následkem povrchového odtoku;
- Transport půdních částic srážkami;
- Transport půdních části povrchovým odtokem.

Tento popis byl z velké části odvozen na základě laboratorních experimentů. Krajina, jako taková, byla v rámci těchto experimentů podle Morgana (2010) reprezentována jako profil jednoho svahu (od hřbetnice do údolnice), který byl následně rozdělen do několika segmentů. Erozní proces byl simulován na základě výpočtu, kdy se pro každý segment vypočítalo množství uvolněných půdních částic a kapacity transportovat půdní částice z daného segmentu po spádnici do dalšího.

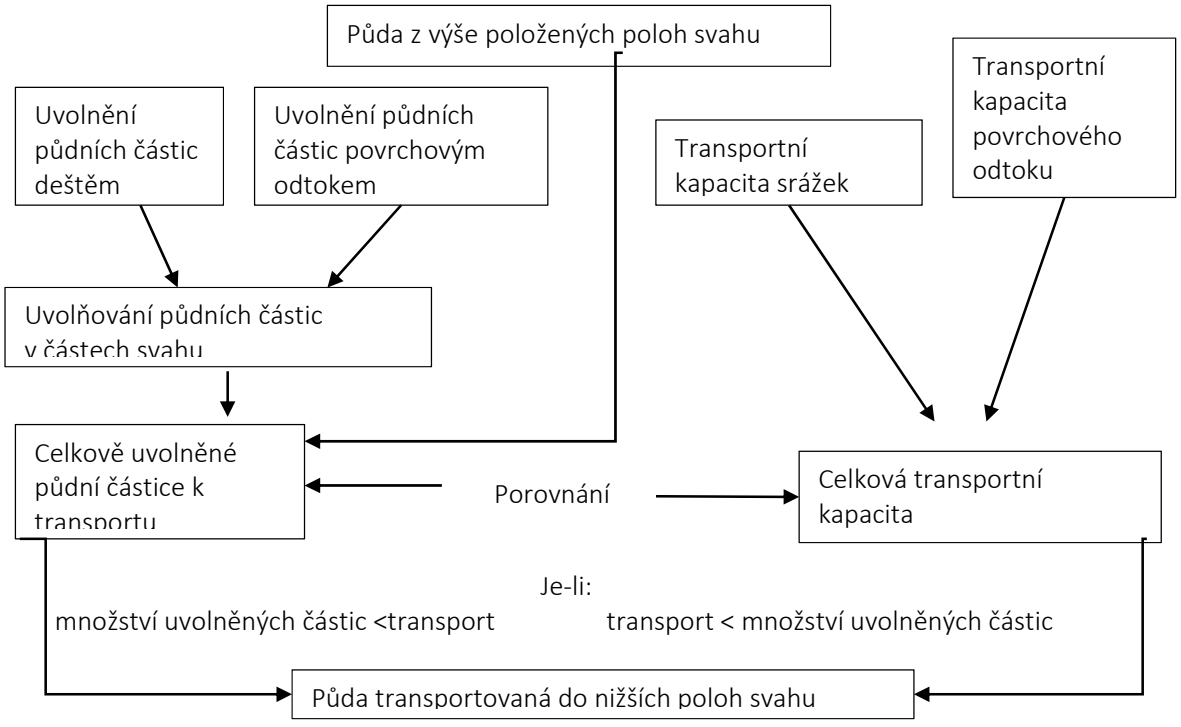

Obr. 2: Koncept modelování vodní eroze (převzato z Meyer a Wishcmeier, 1969)

Jedny z prvních koncepčních erozních modelů, které adaptovaly přístup Meyera a Wischmeiera (1969) generují povrchový odtok a transport sedimentů na základě koncepce stavby

hydrologických modelů. Jedná se např. o AGNPS (Young et al., 1989, Young and Onstad, 1990) a ANSWERS (Beasley et al., 1980). Tyto modely uživateli nabízí volbu simulace v denním časovém kroku na základě čísel odtokové křivky (Boughton, 1989) a simulace jedné události na základě výpočtu odtokového součinitele a infiltrace vody do půdy. Tato generace modelů má však koncepčně zpracovanou pouze hydrologickou část, v popisu erozního procesu se opírá o faktory USLE – erodovatelnost půdy (*K*), délka svahu, vliv vegetačního pokryvu (*C*) a protierozních opatření (*P*).

Další zásadní přístup v popisu erozního procesu uvádí Morgan (2005), kdy erozi už popisuje jako tří fázový systém:

- fáze uvolnění půdních částic,
- fáze transportu půdních částic, a
- fáze sedimentace půdních částic.

V podstatě se jedná o tři na sebe navazující vzájemně podmiňující procesy (Beven, 2011, Morgan, 2005):

- Hydrologická část, kdy vzniká povrchový odtok a půdní částice se uvolní k transportu.
- Eroze, způsobená dopadem dešťových kapek anebo vlastním povrchovým odtokem.
- Sedimentace a odhad transportní kapacity povrchového odtoku.

Další generace modelů, jako např. WEPP (Nearing a Nicks, 1998) již nahrazuje faktory týkající se erodibility půdy, vegetačního pokryvu a sklonu parametry, které vychází fyzikálních zákonů a přímých měření. Tudíž modely popisují, např. náchylnost půdy k erozi parametry, jako jsou koheze, drsnost povrchu a tangenciální napětí (Moussa, 2003). Pokrok a nové směry v modelování shrnuje ve své práci Brazier (2004).

V průběhu let, tak vznikla řada modelů, které sice nebyly prostorově orientované (Boughton, 1989, Moore and Burch, 1986, Grayson et al., 1992), Další vývoj v modelování se již výhradně orientuje na vývoj prostorově distribuovaných modelů (Beven a Alcock, 2012, Quinn et al., 1991, Quinn et al., 1995, Grayson et al., 1992, Moore et al., 1991, Zhang et al., 2013). Řada modelů (viz obr. 3), tak disponuje svým vlastním GIS prostředím, např. LISEM, WATEM/SEDEM, tvoří jeho nadstavbu, např. WEPP (Nearing a Nicks, 1998), SWAT, anebo jsou přímo implantovány do GIS prostředí, např. USPED, RUSLE 3D, TOPMODEL (Beven, 2011), MMF. Tyto všechny simulace v prostředí GIS vychází z analýzy digitálního modelu terénu (DMT), kde základ tvoří výpočet primárních (např. sklonitost, orientace ke světovým stranám, směr a akumulace povrchového odtoku) a sekundárních atributů (např. specifická přispívající plocha, zakřivení svahů atd.) (Zhang

et al., 1996, Oliveira et al., 2013, Moore et al., 1991). Problematikou modelování vodní eroze v prostředí GIS se podrobněji zabývá kapitola 4. (viz studie: *Comparison of different approaches of LS factor calculations based on measured soil loss under simulated rainfall*)

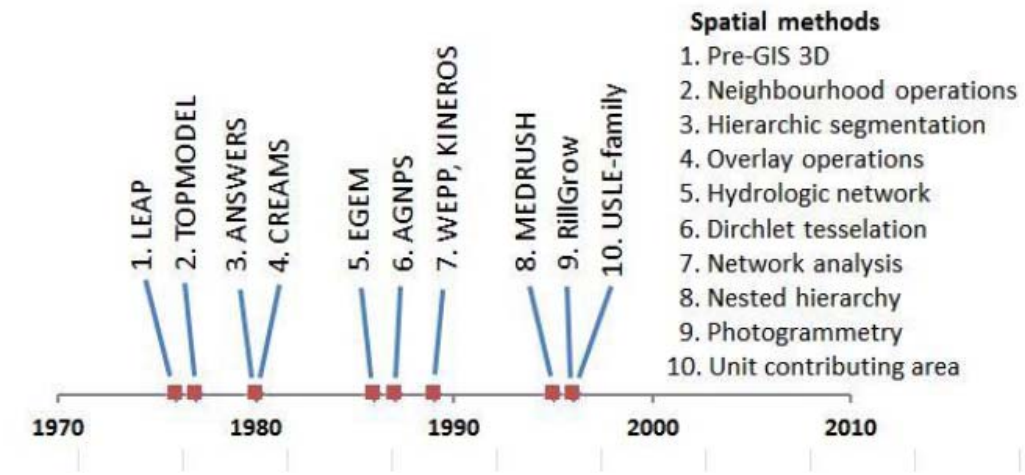

Obr. 3: Mezníky ve vývoji a modifikaci vybraných erozních modelů (Karydas et al., 2014)

1.2 Rozdělení modelů a jejich základní operační rovnice

Govers (2010) poukazuje na zásadní zlom, který nastal v 80 letech minulého století, ve vývoji erozních modelů a to v přechodu z tzv. empiricky založených modelů k tzv. fyzikálně založeným. V současnosti je k dispozici více než 80 erozních modelů (Karydas et al., 2014), které mohou být založené na empirickém základu, mohou být koncepční nebo mohou být fyzikálně založené. Současně dostupné modely se také liší v komplexnosti a nárocích na vstupní data.

Pro obyčejného uživatele tak mohou nastat otázky:

- Jaká vstupní data jsou potřeba a v jakém formátu?
- V jakém detailu mají data být (tzn. Prostorové měřítko)?
- Je třeba mít dlouhodobou řadu dat, v jakém horizontu, v jakém časovém záznamu (tzn. Časové měřítko – viz kapitola 3, studie 4)
- Jaký algoritmus zvolit? (viz kapitola 4, studie 5)
- Jak přesné jsou predikce modelu?

Samotným výběrem modelu (viz více studie 1) a datových zdrojů se podrobněji zabývá kapitola 2 (viz studie 1, studie 2 a také studie 3).

Následující podsekce uvádí přehled základních operačních rovnic, na jejichž základě pracuje většina erozních modelů a algoritmů v prostředí GIS.

1.2.1 Základní operační rovnice empirických modelů

Nejznámějším a i světově nejvyužívanějším empirickým erozním modelem je USLE (Wischmeier a Smith, 1978) a její revidovaná forma RUSLE (Renard, 1997). Tyto modely, a erozní modely z nich vycházející, jsou založeny na jedné základní rovnici o šesti členech:

$$A = R \times K \times L \times S \times C \times P \quad (1)$$

Kde: *A* je průměrná roční ztráta půdy, *R* je faktor erozní účinnosti deště, *K* je faktor erodibility půdy, *S* je faktor sklonitosti, *L* je faktor délky svahu, *C* je faktor ochranného vlivu vegetačního pokryvu a *P* je faktor účinnosti protierozních opatření. Doplňující rovnice jsou vyžadovány pro stanovení topografického faktoru LS a také mohou být použity další rovnice pro stanovení R faktoru a K faktoru (Wishmeier et al., 1978).

(R)USLE je pro uživatele velmi jednoduchý model k pochopení. Ovšem, studie provedená Fosterem (1982) ukázala na příkladu aplikace USLE v malém povodí, že tento model má jisté limity a při nerespektování těchto limitů vede k chybným závěrům. Vzhledem ke kritice modelu, Wischmeier a Smith (1978) popsali limity modelu:

- Model je platný pouze pro plošnou, mezirýžkovou a rýžkovou vodní erozi. Ostatní typy vodní eroze nejsou v modelu brány v úvahu.
- Model neřeší depozici sedimentů, tudíž model nesmí být použit pro části svahu (oblasti), kde dochází k depozici sedimentu.
- Faktor délky svahu a sklonu musí být určeny pouze v oblasti, kde se tvoří povrchový odtok.

Nearing et al. (1998) jako největší nevýhodu u tohoto typu modelu uvádí, že je naprosto neefektivní, pokud je aplikován mimo podmínky, pro které byl vyvinut.

V současnosti problematickými faktory v rovnici jsou faktory L, S a R (viz Studie 3). Následující tabulka 1 uvádí přehled možných rovnic a algoritmů pro výpočet topografického faktoru (viz více Studie 5).

Tab. 1: Různé přístupy k výpočtu topografického faktoru *LS* (β – sklon v radiánech; s – sklon v %; λ – délka s vahu v metrech, As – "specific catchment area"*)

Autor & Reference	LS Faktor		Model	Poznámka
	S	L		
Smith a Wishmeier (1965)	$S = \frac{0.043s^2 + 0.3s + 0.43}{6.613}$ Rovnice může být také zapsána jako: $S = 0.0065s^2 + 0.0453s + 0.065$	$(\lambda/22.13)^m$ kde m = 0.5pokud β > 0.05 m = 0.4 pokud 0.03 < β > 0.05 m = 0.3 pokud 0.01 < β > 0.03 m = 0.2 pokud β < 0.01	-	Rovnice odvozena na základě experimentu za přirozených srážek na plochách o sklonu 3-18%
Wishmeier a Smith (1978)	$65.4sin^2\beta + 4.56sin\beta + 0.0654$		USLE, USLE2D, GIS, WATEM/SEDEM,	
Böhner a Selige (2006)	$LS = (A_s^{0.5}/22.13)^{0.5}(65.4sin^2\beta_{A_s} + 4.56sin\beta_{A_s} + 0.0654)$ pro β_{As} >0.0505 $LS = (A_s^{0.5}/22.13)^{3\beta_{As}^{0.6}}(65.4sin^2\beta_{As} + 4.56sin\beta_{As} + 0.0654)$		SAGA	
Foster a Wishmeier (1974)	$LS = \sum_{j=1}^{N} \frac{S_j\lambda_j^{m+1} - S_j\lambda_{j-1}^{m+1}}{(\lambda_j - \lambda_{j-1})(22.13)^m}$ tato rovnice může být rozšířena a aplikována na 3-D reliéf: $LS = \sum_{i,j}^{N} \frac{S_{i,j}(\lambda_{i,j}^{m+1})_{outlet} - S_{i,j}(\lambda_{i,j}^{m+1})_{inlet}}{(\lambda_{i,j-outlet} - \lambda_{i,j-inlet})(22.13)^m}$		USLE, USLE2D, SAGA GIS, WATEM/SEDEM,	
Desmet, Govers (1996), Govers (1991)	$S = 1.45\left(\frac{tan\beta}{0.09}\right)$	$L_{(i,j)} = \frac{\left(A_{(i,j),in} + D^2\right)^{(m+1)} - A_{(i,j),in}^{(m+1)}}{x_{(i,j)}^m \cdot D^{(m+2)} \cdot 22.13^m}$ Popis rovnice viz studie 5 - metodika	SAGA GIS, USLE2D, WATEM/SEDEM,	Rovnice pro L faktor vychází z rovnice Fostera a Wischmeiera (1974)
McCool et al. (1987)	$10.8sin\beta + 0.03$ když $\beta < 0.09$ $16.8sin\beta - 0.5$; když $\beta \geq 0.09$ $3sin^{0.8}\beta + 0.56$; když $\lambda < 4.5\ m$	$(\lambda/22.13)^m$ kde $m = F/(1+F)$ kde $F = (sin\beta/0.0896)/(sin^{0.8}\beta + 0.56)$ nebo F=0 pokud nastane depozice λ≤4.5 m	RUSLE, SAGA GIS, WATEM/SEDEM, USLE2D, RUSLE -IDRISI	Simulované srážky na sklonu 0.1-3% plochy pod přirozenými srážkami os klonu 8-18%. Předpokládá se střední poměr mezi rýžkovou a mezirýžkovou erozí
McCool et al. (1993)	$10.8sin\beta + 0.03$ když $\tan\beta < 0.09$ $(sin\beta/0.0869)^{0.6}$ když $\tan\beta \geq 0.09$		-	Na základě měření rýžkové eroze v terénu (na více než 2100 segmentů svahu) o sklonech 1.5-56%
Moore a Burch (1986)	$LS = (A_s/22.13)^m(sin\beta/0.0896)^n$ Kde *m*=0.4; *n*=1.3; a A_s= specific catchment area		Tzv. STI (Sediment Transport Index)	Odvozeno na základě tzv. „ unit stream power theory" z koncepčních rovnic modelu WEPP, vývoje povodí
Griffin (1988), Mitášová (1996)	-	$L = (m+1)(A_s/22.13)^m$ kde *m*=0.2-0.6 (0.4)	GRASS, USPED	Tzv. bodová metoda
Liu et al. (1994)	$S = 21.91sin\theta - 0.96$	-		
Nearing (1997)	$S = -1.5 + \frac{17}{(1 + e^{(2.3 - 6.1sin\beta)})}$	-		

**Specific catchment area = volně přeloženo jako specifická přispívající plocha*

1.2.2 Základní operační rovnice v koncepčních modelech

Koncepční erozní modely vychází ze tří forem nebo fází vodní eroze. Morgan (2005) uvádí, že tyto fáze na sebe navazují a to jak v čase, tak i v určitém bodě a v určitém rozsahu vždy po spádnici. Podle Zhanga (1996) se jedná v první fázi o plošnou erozi, která je následována vznikem drobných rýžek (mezirýžková eroze a rýžková eroze), kde se koncentruje povrchový odtok. Tyto rýžky se různě tvoří na základě agregátové stability půdy a mikroreliéfu prostředí (tj. změnám v nadmořské výšky a sklonitosti). Povrchový odtok z rýžek se poté koncentruje a vytváří rýhy, brázdy až strže.

Foster et al. (1977) odvodili rovnici, která vychází z podstaty výše popsaného procesu. Rovnice je založena vývoji uvolnění půdní částice a jejím transportem srážkou nebo povrchovým odtokem. Rovnice, tak matematicky popisuje proces eroze a sedimentace.

$$\frac{dq_s}{dx} = D_r + D_i \quad (2)$$

Kde: *q* je množství sedimentu na jednotku šířky rýžky, *x* je délka ve směru toku vody v rýžce, *Dr* je čisté množství uvolnění nebo ukládání materiálu v rýžkách a Di množství uvolněného nebo uloženého materiálu v mezirýžkách.

Mezi hlavní faktory, které ovlivňují proces tvorby mezirýžek a rýžek, jsou zde podle Fostra (1982) uvažovány:

- Hydrologie,
- Topografie,
- Erodovatelnost půdy,
- Transport půdních částic,
- Vegetace,
- Drsnost povrchu a způsob obhospodařování pozemků.

Do kategorie koncepčních modelů se také řadí podle Zhanga (1996) kinematický model vytvoření Rose et al. (1983a, 1983b), který pracuje na principu matematického popisu procesu:

1. Uvolnění půdní částice energií dešťové kapky.
2. Depozice sedimentu jakožto výsledek gravitačních sil.
3. Vstup již usazeného sedimentu do transportu.

Dalším modelem, který je založený na kinematickém řešení model KINFIL (Kovář and Vaššová, 2010), který je podrobně popsán ve studii 1 v kapitole 2. Tento model neřeší přímo ztrátu půdy erozí, ale je založený na kombinaci teorie infiltrace a transformace přímého odtoku kinematickou vlnou. Jako jeden ze vstupních dat se zde používají fyziografické, hydraulické a

klimatické parametry povodí (viz studie 1 a studie 2) a tudíž při rozšíření o popis erozních procesů by se jednalo velmi robustní nástroj k vyhodnocování různých variantních nejen situací v povodí, což již Kovář et al. (2012) prokázali ve své studii v lokalitě Třebsín.

Holý et al. (1988) vyvinul simulační model povrchového odtoku a erozního procesu SMODERP (Kavka and Zajicek, 2013) řeší srážko-odtokové vztahy a erozní procesy na jednotlivém svahu (pozemku). Jedná se o koncept, který řeší erozní proces na základě pohybu vody po svahu s prostorovým členěním na dílčí plochy. Je odvozen pro výpočet svahového odtoku z přívalových dešťů (pouze ve vegetační sezóně), s obecně proměnnou intenzitou v čase

1.2.3 Základní operační rovnice ve fyzikálně založených modelech

Fyzikálně založené erozní modely vychází z mechanizmů, které kontrolují erozní proces a také zahrnují fyzikální charakteristiky vývoje rostlin a klimatu.

Rovnice kontinuity pro objem sedimentu procházející daným bodem po povrchu v daném čase je podle Morgana a Nearinga (2011):

$$\frac{\partial(AC)}{\partial t} + \frac{\partial(QC)}{\partial x} - e(x,t) = q_s(x,t) \quad (3)$$

Kde: *A* je plocha průřezu toku, *C* je koncentrace sedimentu v toku, *t* je čas, *x* je horizontální vzdálenost po svahu, *e* je transport sedimentu v dané části svahu a q_s je množství vstupu sedimentu z vnějších zdrojů do dané části svahu na jednotku délky toku, např. při konvergentním proudění ze strany svahu. Na lineárních svazích q_s = 0, a rovnice kontinuity může být zapsána ve tvaru:

$$\frac{\partial(AC)}{\partial t} + \frac{\partial(QC)}{\partial x} = e_i + e_r \quad (4)$$

Kde e_i je míra eroze v mezirýžkách a e_r míra eroze v rýžkách.

Tato forma rovnice je použita ve většině fyzikálně založených erozních modelech jako je WEPP (Nearing and Nicks, 1998), EUROSEM (Morgan et al., 1998), LISEM (De Roo and Jetten, 1999). V GUEST (Yu and Rose, 1999) má ovšem rovnice trochu jiný tvar. V tomto modelu je půda pospána zrnitostí s 50 třídami, které jsou určeny podle usazovací rychlosti půdních částic. Také se zde rozlišuje, zda se jedná o materiál erodovaný nově nebo materiál, který již jednou byl erodovaný, tzn. erodovaný sediment. Depozice materiálu je modelována explicitně. Rovnice má tvar:

$$\frac{\partial(AC_j)}{\partial t} + \frac{\partial(QC_j)}{\partial x} = e_{ij} + e_{idj} + e_{rj} + e_{rdj} - d_i \quad (5)$$

Kde: C_j je koncentrace sedimentu v toku o velikosti částice *j*, e_{ij} rychlost eroze částice sedimentu o velikosti *j* v originálním materiálu v mezirýžkách, e_{idj} rychlost eroze částice sedimentu o velikosti *j* z již dříve uvolněného materiálu v mezirýžkách, e_{rj} rychlost eroze částice sedimentu o velikosti *j* v originálním materiálu v rýžkách, e_{rdj} rychlost eroze částice sedimentu o velikosti *j* z již dříve uvolněného materiálu v rýžkách a d_j je míra depozice částic o velikosti *j*.

I když fyzikálně založené modely vychází ze stejné rovnice kontinuity, tak se liší v parametrech popisujících erozi a depozici erodovaného materiálu (Nearing a Nicks, 1998, Morgan et al., 1998, De Roo a Jetten, 1999)

1.3 Cíle práce

Disertační práce předkládá aktuální otázky a přístupy spojené s modelováním potenciální ztráty půdy vodní erozí a povrchového odtoku. Zejména se jedná o propojení klasických přístupů v modelování, především univerzální rovnice ztráty půdy (USLE), s geografickými informačními systémy (GIS).

Specifické oblasti práce jsou následující:

1) Výběr vhodného modelu a možné datové zdroje v prostředí GIS:
    - Porovnání různých modelů a identifikace jejich silných a slabých stránek,
    - Vyhodnocení protierozní funkce historických mezí na základě vstupních dat odvozených v prostředí GIS,

2) Vliv různého časového kroku v modelování:
    - Do nově vzniklé databáze REDES přispět za Českou republiku výpočtem faktoru erozní účinnosti deště (*R*-faktor) pro 32 stanic v České republice za období 1960 – 2000,
    - Výpočet kalibrační funkce pro harmonizaci datové sady erozní účinnosti deště v evropském měřítku

3) Vliv topografie na ztrátu půdy erozí v prostředí GIS:
    - Porovnání různých přístupů ve výpočtu topografického (*LS*) faktoru
    - Vyhodnocení vlivu použitého algoritmu na výpočet *LS*-faktoru na celkový výstup výpočtu ztráty půdy v (R)USLE.

2 Výběr vhodného modelu a zpracování charakteristik povodí v GIS

Volba nejen erozního, ale i srážko-odtokového modelu, je závislá na povaze mnoha parametrů, ale především na tom, co daný uživatel od modelu chce. Boardman (2006) a Morgan (2010) shrnují podmínky a faktory, které je třeba vzít v úvahu při výběru modelu (viz tab. 2), z nich tři jsou nejzásadnější:

- Datové zdroje,
- Efektivita modelu,
- Časové a prostorové měřítko modelu.

Tab. 2: Hlavní parametry modelu a relevantní volby v erozním modelování

Parametr	Volba
Rozsah	Svah/ malé povodí/střední povodí/ velké povodí
Trvání	Epizoda/dlouhodobý průměr
Faktory	Klima/ topografie/ půdy/ vegetace
Proces	Uvolnění půdní částice deštěm/ srážko-odtokový proces/ uvolnění částice povrchovým odtokem
Prvky	Ztráta půdy/ Sedimentace/ transport splavenin
Forma	Kapková/ rýžková/ brázdová až stržová/ břehová eroze
Operační základ	Empirický/koncepční
Vyhodnocení	Kvalitativní/ kvantitativní

V literatuře je možné nalézt velké množství porovnání modelů a jejich parametrů, jako je tomu např. ve studii 1: *Choosing an Appropriate Hydrological Model for Rainfall-Runoff Extremes in Small Catchments*. Např. Amore et al. (2004) porovnával efektivitu modelu WEPP a USLE na třech povodích v Sicílii. Zhang et al. (1996) hodnotil simulace modelu WEPP pro roční ztrátu půdy před optimalizací parametrů (R^2 = 0.50 – 0.65) a po optimalizaci parametrů (R^2 = 0.54 – 0.68). K podobným výsledkům také došel Tiwari (2000).

Využitím prostorových a GIS konceptu v modelování se také zabývalo mnoho autorů, jako např. Zhang et al. (1996), Vrieling (2006), de Vente et al.(2009, 2014) a další.

STUDIE 1: Choosing an Appropriate Hydrological Model for Rainfall-Runoff Extremes in Small Catchments

Pavel Kovář, Michaela Hrabalíková, Martin Neruda, Roman Neruda, Jan Šrejber, Andrea Jelínková and Hana Bačinová

Soil & Water Res., 10, 2015 (3): 137–146

Abstract: Real and scenario prognosis in engineering hydrology often involves using simulation techniques of mathematical modelling the rainfall-runoff processes in small catchments. These catchments are often up to 50 km^2 in area, their character is torrential, and the type of water flow is super-critical. Many of them are ungauged. The damage in the catchments is enormous, and the length of the torrents is about 23% of the total length of small rivers in the Czech Republic. The Smědá experimental mountainous catchment (with the Bílý potok downstream gauge) in the Jizerské hory Mts. was chosen as a model area for simulating extreme rainfall-runoff processes using two different models. For the purposes of evaluating and simulating significant rainfall-runoff episodes, we chose the KINFIL physically-based 2D hydrological model, and ANN, an artificial neural network mathematical "learning" model. A neural network is a model of the non-linear functional dependence between inputs and outputs with free parameters (weights), which are created by iterative gradient learning algorithms utilizing calibration data. The two models are entirely different. They are based on different principles, but both require the same time series (rainfall-runoff) data. However, the parameters of the models are fully different, without any physical comparison. The strength of KINFIL is that there are physically clear parameters corresponding to adequate hydrological process equations, while the strength of ANN lies in the "learning procedure". Their common property is the rule that the greater the number of measured rainfall-runoff events (pairs), the better fitted the simulation results can be expected.

Keywords: flood prediction; infiltration; Jizerské hory Mts.; kinematic wave; neural network

INTRODUCTION

Rapidly developing catastrophic situations caused by extreme rainfall-runoff episodes can often be encountered in small mountainous catchments, where changes in the runoff and sediment regime can be enormous. This is the situation for the creeks in the Jizerské Hory Mts., where the Smědá catchment was chosen as the case study for this paper. Convective

high-intensity precipitation on a relatively small catchment area, its high inclination and the slope of the longitudinal profile of the river, channel destruction and its surroundings impacted by erosion often cause a great damage (Kovář & Křovák 2002).

An improvement in runoff prediction methods and in determining the volumes of flooding waves are of economic as well as environmental importance (Čamrová & Jílková 2006). *N*-year flood discharges are the basic hydrological sources for proposing measures against floods and erosion. Over the past few decades, growing importance has been given to the use of mathematical models of the rainfall runoff process, based physically on infiltration, and to monitoring surface runoff and its movement on slopes and on hydrographic networks. This case study shows the ways of identifying the design runoff in small basins using the KINFIL model (Kovář 1992). This model combines the *CN* curves method and the solution of infiltration equations (Morel-Seytoux & Verdin 1981). The simulation of surface runoff is resolved by the kinematic wave model (Singh 1976, 1996), taking into account the detailed topography of the basin. The topographic terrain values are calculated by ArcGIS software. The accuracy of these mathematical modelling methods and their connection to GIS systems is adequate for the accuracy of the mathematical description of physical processes and to the range and reliability of the data set used herein.

The second model used in this paper is an artificial neural network consisting of units called neurons that transfer and process information in the form of excitations. The training of the neural network can be imagined as modifications to the network parameters in such a way that the output neurons are excited by certain combinations of input signals (Rumelhart & McClelland 1986). The number of neurons and their connections are determined by the topology of the network. According to the function, we distinguish input, output, and intermediate neurons. The input neurons correspond with receptors, the output neurons are connected to effectors, and the intermediate neurons constitute the mediators of the information transfer between inputs and outputs (Lippmann 1987). These ways of excitation transfer are referred to as paths. The information is processed on paths by means of changes in the states of neurons along the corresponding paths. The states of all neurons and connections (synaptic weights) represent the configuration of a network. Training the neural network involves setting the configuration on the basis of data representing pairs of inputs with desired outputs. This approach is called supervised learning, and it most often utilizes gradient-based nonlinear algorithms, called error back propagation (Neruda *et al.* 2005).

The goal of our study is to compare the KINFIL and ANN approaches, to identify their strengths and weaknesses.

MATERIAL AND METHODS

Description of the Smědá catchment. The river Smědá rises in the peat lands of the Jizerské hory Mts. It is the border flow between the Czech Republic and Poland (Figure 1a). Since 1957, a water level recorder has been installed in the Bílý potok station and a number of precipitation gauges have been set up in Hejnice, Nové Město pod Smrkem, Višňová, and Bílý Potok. This catchment with its measured rainfall-runoff episodes is often a source of flood disasters, which will be analyzed in this study. Table 1 shows the major physical-geometric catchment characteristics of the Bílý Potok downstream water level recorder.

Table 1. Physical-geometric characteristics of the Smědá catchment, Bílý Potok downstream gauge

Characteristics	Value
Basin area (km2)	26.58
Thalweg length (km)	13.3
Thalweg slope (–)	0.069
Altitude (m a.s.l.)	497–1123
Basin average width (km)	1.96
Basin slope (Herbst) (%)	22.2

The Smědá brook is classified as having class I and class II basic water quality – the water is classified as unpolluted or slightly polluted. Table 2 shows the basic hydrological data in the Smědá catchment, e.g. the average yearly precipitation and the *N*-years runoff values.

Table 2. Hydrological data of the Smědá basin at Bílý Potok, the outlet station (Czech Hydrometeorological Institute)

Smědá basin	Precipitation annual (mm)		N-year runoffs ($m^3 \cdot s^{-1}$)						
	precipitation	outflow	Q_1	Q_2	Q_5	Q_{10}	Q_{20}	Q_{50}	Q_{100}
Bílý potok	1426	1116	21	33	54	74	97	132	162

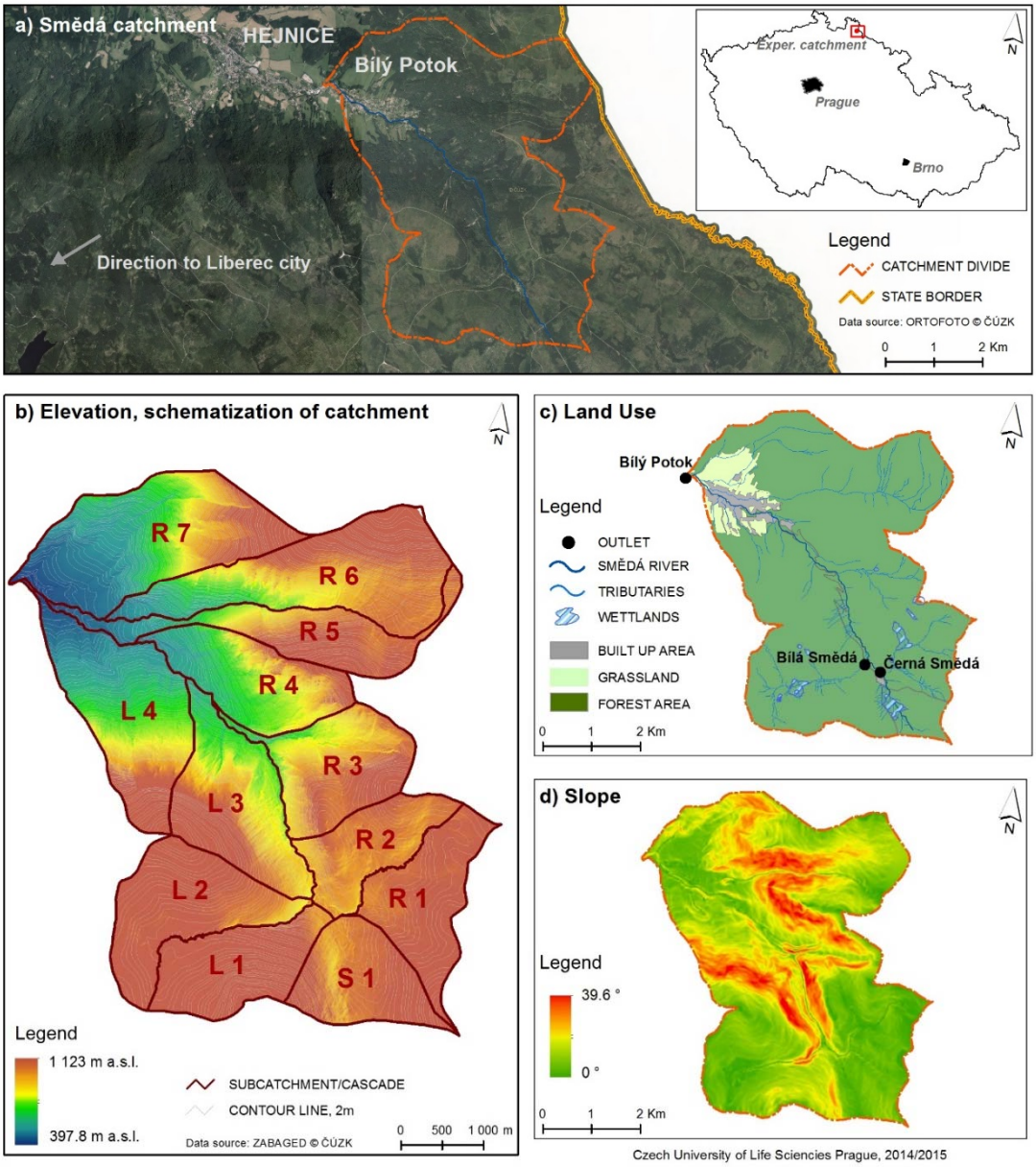

Figure 1. Main characteristics of the Smědá catchment

In the following description, the basic geological, soil, geomorphological, and land use characteristics of this part of the Jizerské hory Mts. are presented as a consequence of the effects of major rainfall-runoff episodes. For understanding the destruction in the area caused by high surface outflow and erosion processes, the following considerations should be taken into account:

- The geological basement of the Jizerské hory massif is composed of biotic coarse granular or porphyritic granite, easily eroded and crumbled into fine fractions.
- Most of the soils are shallow, light, coarse granular loamy-sandy soils of peat mountain Podzosol type, peaty soils, and rocky rubble on steep slopes.

- The unsuitable structure and texture of the soils and the softness of the soil profile with a lack of humus means that the soils are easily eroded.
- The Jizerské hory Mts. have one of the highest precipitation frequencies and amplitudes of all Central Europe.
- Steep terrain slopes (30–50%) and quite long slope lengths (400–1000 m) provide conditions for gully erosion of whole areas.

The vegetation in the Smědá basin consists mainly of spruce (80–90%), beech and maple trees (up to 15%). Dwarf pines occur in the peatlands, and birches and rowans are scattered in coppices. However, there is an intensive new planting programme, and the herbaceous small reed vegetation that has grown up in the clearings after deforestation is gradually being replaced. The species composition now being planted is different from the old species composition, and includes species that are more resilient to natural disasters, and that help preventing forest erosion and infiltration.

GIS mapping of the Smědá catchment. In the present study, GIS tools were used to create a digital model of the terrain (DMT), hydrological soil groups, economic land use, and the distribution into the sub-catchments. We used ArcGIS 10.2 software tools, with the Spatial Analyst extension. The starting-point materials were vector base datasets derived from the Orthophoto map and the Basic Map of the Czech Republic 1:10 000 (ZABAGED II), digital map BPEJ, and datasets downloaded from the HEIS database. The resulting products are the maps shown in Figure 1: Major characteristics of the Smědá catchment, comprising: (a) orthophotos, (b) height ratios and schematization of sub-catchments, (c) slope, and (d) land use. The synthetic product is a geographical map containing the hydrological information required for the KINFIL model. This data is compiled in Table 3 and shown in Figure 2, which provides a geometrical schematization of the sub-catchments, including land use. Table 3 provides a numbering system for the geometrized areas of the catchment (see Figure 2) away from the catchment boundary to the downstream gauge profile, distinguishing the upper segment (S) and the plates of the left (L) and right (R) side of the flow direction of the Smědá river.

The KINFIL model. The KINFIL model is based on a combination of infiltration theory, put forward by Green and Ampt and modified by Morel-Seytoux (Morel-Seytoux & Verdin 1981), and direct runoff transformation, resolved using a kinematic wave (Lax & Wendroff 1960; Kibler & Woolhiser 1970; Beven 1979; Singh 1996).

The task of the infiltration part of the model is to determine the parameters of saturated hydraulic conductivity *Ks* and the retention coefficient of the suction pressure *Sf* (for the state of field capacity *FC*).

Table 3: Schematization of the Smědá catchment

Cascade/ subcatchment	Area (km^2)	Length of basin (km)	Plate	Area (km^2)	Aver. Width (km)	Length (km)	Slope (-)	Grassland (%)	Forest (%)	Other area (%)	Built up area (%)
S1	1.64	1.86	S 11	1.12	0.88	1.26	0.178	-	99.30	-	0.70
			S 12	0.53		0.60	0.114	-	94.60	-	5.40
R1	1.84	1.35	R 1	1.84	1.36	1.35	0.070	-	99.60	-	0.40
R2	1.44	0.75	R 21	0.96	1.93	0.50	0.097	-	99.60	-	0.40
			R 22	0.48		0.25	0.204	-	99.90	-	0.10
R3	1.99	1.80	R 31	1.08	1.10	0.98	0.213	-	100.00	-	-
			R 32	0.91		0.83	0.394	-	99.90	-	0.10
R4	1.91	1.75	R 41	0.97	1.09	0.89	0.243	-	91.50	-	7.80
			R 42	0.95		0.87	0.424	-	100.00	-	-
R5	1.79	0.78	R 51	0.10	2.29	0.05	0.119	-	100.00	-	-
			R 52	0.41		0.18	0.216	-	100.00	-	-
			R 53	1.27		0.56	0.269	1.10	81.10	1.70	16.10
R6	3.3	1.49	R 61	0.50	2.22	0.23	0.156	-	100.00	-	-
			R 62	1.33		0.60	0.218	-	100.00	-	-
			R 63	1.47		0.66	0.380	0.65	93.75	3.06	2.54
R7	3.46	3.50	R 71	0.40	0.99	0.41	0.180	-	100.00	-	-
			R 72	1.68		1.70	0.317	2.90	95.40	1.70	-
			R 73	1.38		1.40	0.147	34.70	42.50	15.00	7.80
L1	1.79	1.18	L 11	0.62	1.51	0.41	0.193	-	100.00	-	-
			L 12	1.17		0.77	0.147	-	99.70	-	0.30
L2	2.25	1.23	L 21	1.34	1.83	0.73	0.086	-	100.00	-	-
			L 22	0.91		0.50	0.154	-	99.93	-	0.07
L3	2.33	1.48	L 31	0.36	1.58	0.23	0.157	-	100.00	-	-
			L 32	1.61		1.02	0.415	-	98.40	-	1.60
			L 33	0.36		0.23	0.273	-	94.60	-	5.40
L4	2.75	2.67	L 41	0.23	1.03	0.23	0.171	-	100.00	-	-
			L 42	1.03		1.00	0.403	-	100.00	-	-
			L 43	1.49		1.45	0.164	24.70	52.00	2.00	21.30

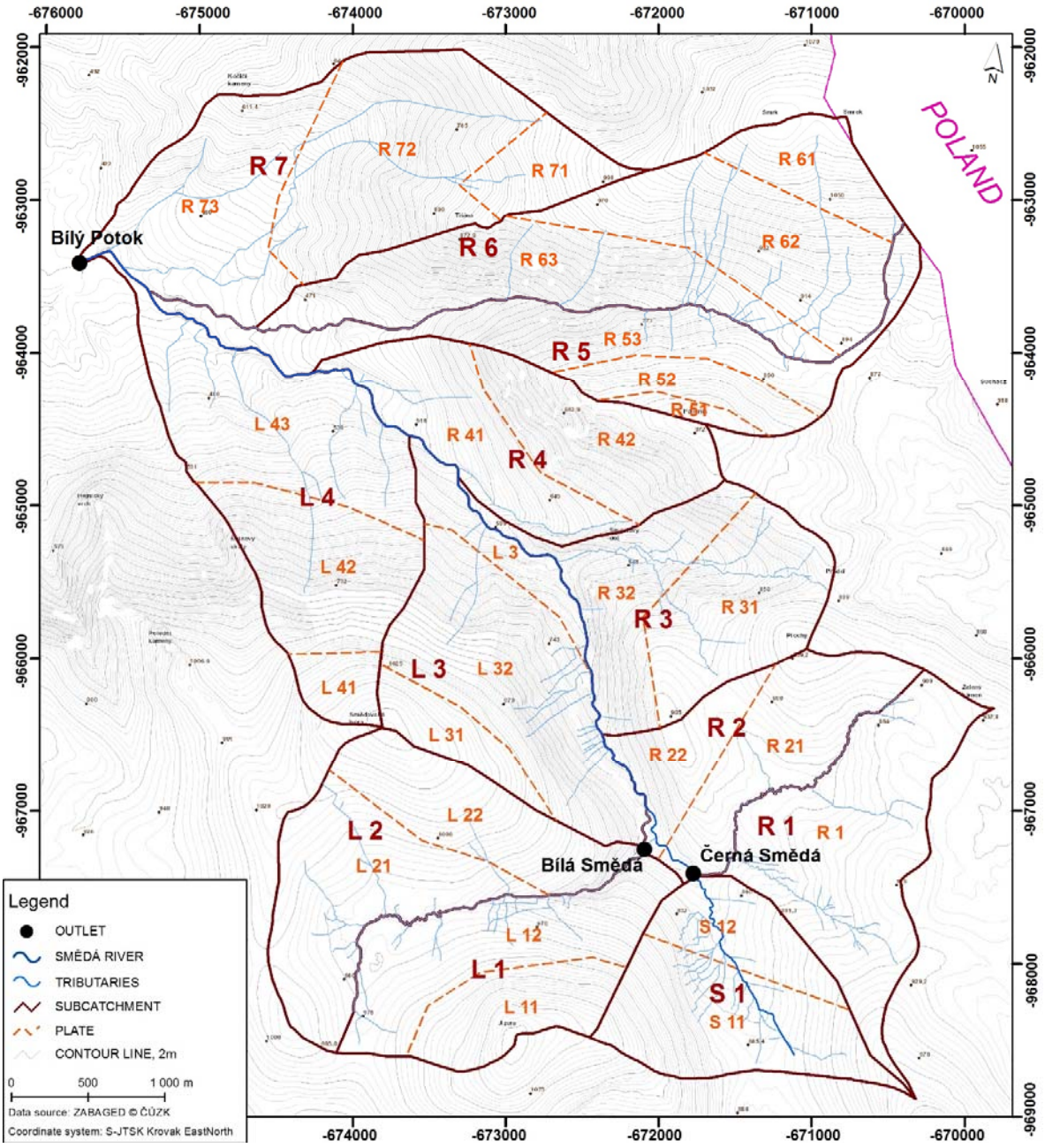

Figure 2. The Smědá catchment (BP) – distribution into sub-catchments

The solution makes use of previously derived relationships between these parameters and the values of the runoff curve numbers *CN* (US SCS 1986). The *CN* index values correspond with the conceptual values for soil parameters *Ks* and *Sf* (*FC*): *CN* = *f* (*Ks*, *Sf*) (Kovář 1992; Kovář *et al.* 2014). The second component of the KINFIL model is the direct runoff transformation. The equation describes an unsteady flow, which is approximated by a kinematic wave. The kinematic equation has been converted into the finite difference form and resolved by the Lax-Wendroff explicit

numerical scheme (Lax & Wendroff 1960). For practical solutions, the basin has been geometrized by being divided into two components: the cascade of planes and the convergent segments, so that the simulation of the runoff process corresponds with the topographical catchment areas.

For the rain files of rainfall-runoff episodes, the KINFIL model simulation is important for correct determining the value for the runoff curve numbers *CN* (US SCS 1992) for antecedent moisture conditions (average: *AMC* II), and also the default values for other parameters (actual: CN_A, volumetric: CN_{vol}), and consequently the hydraulic conductivity *Ks* and sorptivity *S* (at the field capacity *FC*). The *CN* values, and therefore the value for the potential retention of the active upper soil zone, are influenced by the uses to which the mostly forested land is put. The forest hydrological conditions affect especially the interception, infiltration, and retention of water in depressions with no runoff and a ground cover layer of forest soil (humus leaf litter, *HLL*). The class of forest hydrological conditions (*CFHC*) is determined on the basis of the depth of the litter (*HLL* from 0 to 15 cm) and its compactness (*C*) classification. For these *CFHC* values, the average numbers of runoff *CN* curves have been derived by hydrologic soil groups (Kovář & Vaššová 2012).

The average value representation of the first grain category I^{st} is 25–30%. To this class reaches saturated hydraulic conductivity *Ks* values as high as 10 mm/h. On the basis of the humus compactness grade *CG* = 1 (depth to 5 cm), the forested surface of the basin may be classified into two hydraulic conditions (*CFHC* = 2) and for soil group C, subsequent CN_{II} = 79 and for soil group B CN_{II} = 69.

Table 4 provides a clear record of the numbers of runoff curve values. To calibrate the parameters of the model, it is necessary to choose characteristic couples of rainfall-runoff episodes in such a way that the rains were short and heavy, that the basin has already been saturated by previous rain, and that the peak flow was attained as soon as possible. This means that the episode should preferably be in category *AMC* III of the *CN* curve validity (i.e. low values for hydraulic conductivity and sorptivity at *FC*). Episodes with the characteristics reported in Table 5 were selected for calibration.

Table 4. Land division in the Smědá catchment, Bílý Potok downstream gauge

Representation	% of area	HSG[1]	weighted CN[2]
Forests	88	70 % C	$0.70 \cdot 79 = 55.3$
		18 % B	$0.18 \cdot 69 = 12.4$
Pastures (clearings)	7	7 % C	$0.07 \cdot 79 = 5.5$
Arable land	3	3 % B	$0.03 \cdot 79 = 2.4$

Representation	% of area	HSG[1]	weighted CN[2]
Built-up (urbanized)	2	2 % –	0.02 · 98 = 1.9
TOTAL	**100**	100 %	**CN_{II} = 77.0 (rounded)** **CN_{III} = 89.0**

[1]Hydrological soil groups
[2]The weighted average of CN values

Variable i_{max} in Table 5 is the highest rainfall intensity, H_s is rain depth, H_{s5} is the sum of previous rains for five days before the start of the episode, and Q_{max} is peak flow. For the selected calibration episodes, we were aware that the period of 35–45 years that elapsed between the calibration and the validation period in the KINFIL model has changed the status of land use in the Smědá basin to some extent. The simulation rating for the parameters used for calibrating the KINFIL model is shown in Table 6.

Table 5. Selected runoff episodes (KINFIL) in the Smědá catchment (calibration)

Episode number	Date (start) of episode	i_{max} ($mm \cdot h^{-1}$)[1]	H_s (mm)[2]	H_{s5} (mm)[3]	Q_{max} ($m^3 \cdot s^{-1}$)[4]
03	01/07/1971	10.1	77.3	50.5	33.75
04	20/06/1977	12.4	37.7	37.0	37.89

[1]The highest rainfall intensity
[2]The rain depth
[3]The sum of the previous rains for five days before the start of the episode
[4]The peak flow

Table 6: Simulation rating of episodes selected for parameters calibration in the Smědá catchment

Episode number	Date (start) of episode	Measured Q_{max}($m^3 \cdot s^{-1}$)	Calculated QC_{max}($m^3 \cdot s^{-1}$)	Difference peak (%)	Nash-Sutcliff coefficient (–)
03	01/07/1971	33.75	40.22	19.17	0.62
04	20/06/1977	37.89	35.45	3.14	0.99

From the calibration criteria, only episode number 04 is fully acceptable (WMO 1984). When selecting the validation episodes, we focused on recent episodes (after 2008) (Table 7), indicating the volume of effective rainfall (i.e. runoff volumes) for each rain gauge station. Table 7 also shows the previous rainfall totals, the API_{30} index, and the saturation class (II–III) for each episode. Table 8 provides the episodic volume values for *CN* and the volume of the retention zone.

Table 7: Status of catchment saturation 30 days before the start of episode

Episode No.	Start of episode	Total rainfall 30 days before the start of the episode (mm)			API_{30} (mm)[1]	Saturation class
		Hejnice	Nové Město	Weighted average		
Weight		0.830	0.170	1		
1	29. 10. 2008	84.2	94.5	86.0	79.9	II
2	24. 06. 2009	195.4	226.1	200.6	186.6	III
3	02. 06. 2010	144.8	150.8	145.8	135.6	III
4	23. 07. 2010	88.9	97.3	90.3	84.0	II
5	06. 08. 2010	164.0	175.2	165.9	154.3	III

[1]The index of the previous saturation

Table 8: Runoff episodes heights and CN_{vol} volume

Episode No.	Start of episode	Rainfall	Runoff Q (mm)	A (mm)[1]	Volume value CN_{vol} (–)[2]
1	29. 10. 2008	54.6	26.3	37.3	87.2
2	24. 6. 2009	21.1	15.7	5.4	97.9
3	02. 06. 2010	44.8	38.6	5.7	97.8
4	23. 07. 2010	79.1	29.1	76.3	76.9
5	06. 08. 2010	199.7	136.8	63.5	80.0

[1] Retention zone volume
[2] Volume value of Curve Number CN_{vol}

The volume values for the CN_{vol} curves and the values for the retention zone volumes were calculated from the rainfall and runoff volumes according to a well-known methodology (Ponce & Hawkins 1996).

The ANN model. The inputs for the ANN model are short-history values of hourly precipitation and runoffs; the output of the network, representing the runoff value one hour ahead, is predicted on the basis of the history of hourly values of precipitation and runoff. The experiments demonstrated that a period of two or three hours was sufficient for good predictions. A further objective of the experiments was to minimize the free parameters, i.e. the size of the network. A two-hour runoff and precipitation history was therefore used during the experiments. The number of layers in the network has also been kept as limited as possible. It is known that, in theory, one hidden layer should be sufficient to obtain an arbitrarily relevant approximation of the functional dependence represented in the data. However, in our experiments there was a

confirmation that the use of two (and sometimes more than two) hidden layers results in a smaller network. In all our experiments we have therefore used networks with four input neurons, one output neuron, and two layers of eight and five neurons, respectively. This rather small size has proved to be specific enough for the quantity of available data; larger networks have a tendency to over-fit the training data and achieve poor generalization.

RESULTS

Results of the KINFIL model calibration and validation. The results of parameter calibration for the KINFIL model are shown in Figure 3. The peak flows of the tested hydrographs were in accordance with the criteria assessment that was used (WMO 1984) only in the case of episode 04. The data for calibrating the KINFIL model parameters is presented in Table 6, and the results of the hydrograph simulations used by the model are shown in Figure 4.

According to the criteria of the World Meteorological Organization (WMO 1984), simulations with resulting coefficients in the range of 0.75–1.0 are applicable, using the same coefficient for model assessment (Table 9). The quality of the results is described by means of the Nash-Sutcliffe coefficient (Nash & Sutcliffe 1970) in Table 9.

Table 9: Validation results (KINFIL)

Episode		Nash – Sutcliffe coefficient	
1.	29. – 30. 10. 2008	0.61	NO
2.	24. – 25. 06. 2009	**0.77**	**YES**
3.	23. – 25. 06. 2010	**0.89**	**YES**
4.	06. – 08. 08. 2010	**0.81**	**YES**

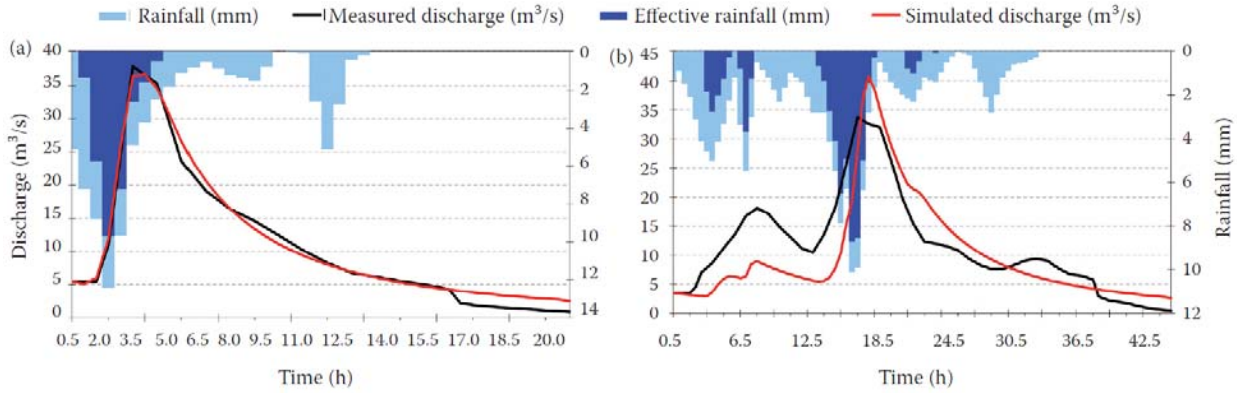

Figure 3. KINFIL calibration: Smědá 04, 20–21/6 1977 (a) and Smědá 03, 1–2/7 1971 (b)

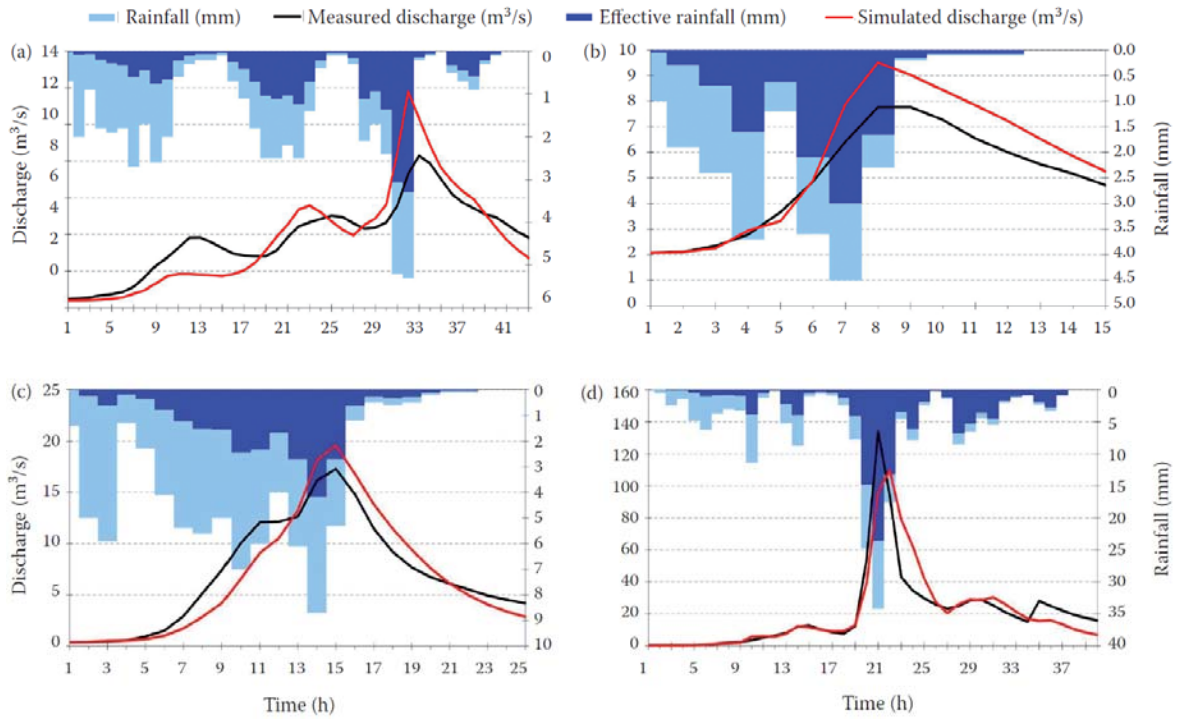

Figure 4. KINFIL validation Smědá: 29–30/10 2008 – episode 1 (a), 24–25/6 2009 – episode 2 (b), 23–25/7 2010 – episode 3 (c) and 6–8/8 2010 – episode 4 (d)

Results of the ANN Model calibration and validation. During the experiments, we employed the leave-one out methodology – the model was always calibrated using four episodes out of five, and the remaining fifth episode was used for validation. Figure 5 shows the calibration and validation results. In this case, a history of two hour worth runoff and precipitation values is used as an input of one training example with the output of runoff value one hour ahead. The main problem when calibrating the network was not the quality of approximation, but rather the generalization of the model for previously unseen data. The validation data error was therefore used during calibration as a stop criterion to prevent over-fitting. In particular, the relevant increase in the validation error was used as an indicator to stop the iterative training algorithm. The models were calibrated by the error back propagation method with a momentum term. The quality of the results is described by means of the Nash-Sutcliffe coefficient (Nash & Sutcliffe 1970) in Table 10.

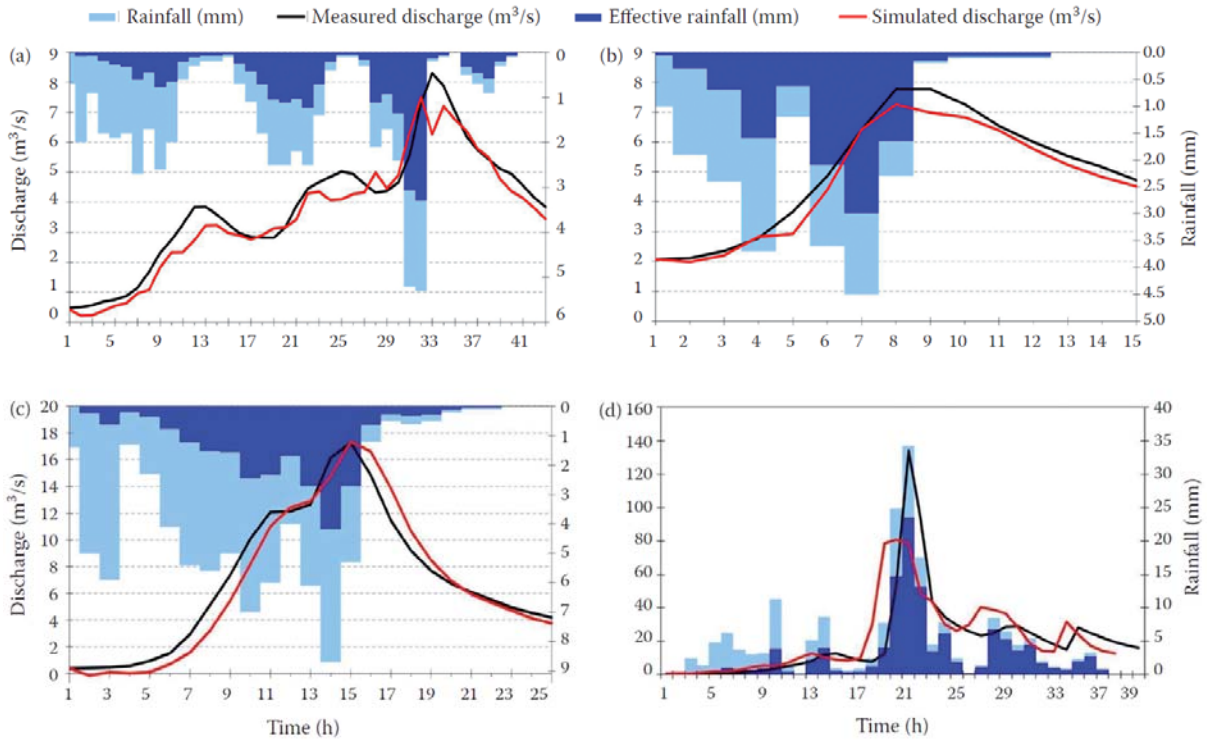

Figure 5. ANN Smědá: 29–30/10 2008 – episode 1 (a), 24–25/6 2009 – episode 2 (b), 23–25/7 2010 – episode 3 (c) and 6–8/8 2010 – episode 4 (d)

Table 10 Validation results for MLP

Episode		Nash – Sutcliffe coefficient	
1.	29. – 30. 10. 2008	**0.92**	**YES**
2.	24. – 25. 06. 2009	**0.96**	**YES**
3.	02. – 04. 06. 2010	**0.94**	**YES**
4.	23. – 25. 07. 2010	**0.95**	**YES**

DISCUSSION

Concerning the KINFIL model, the essential question for hydrologists is which simplifications are right. Physically-based rainfall-runoff models attempt to link catchment behaviour with measurable properties (Beven 2001). However, scaling is a problem of magnitude. It is currently unclear whether this upscaling premise is correct. Catchment behaviour at larger scales can hardly be described by the same governing equations with effective parameters that somehow subsume the heterogeneity of the catchment (Kirchner 2009). Not only the subsurface conditions for unsaturated flow, but also the spatial distribution of the rainfall over a catchment area serve as good examples of heterogeneity. However, we tested the KINFIL model with four parameters

only in order to avoid over-parametrization while keeping an adequate model structure (Perrin *et al*. 2001; Andréassian 2004).

The Smědá catchment in the Jizerské hory Mts. has a very non-linear rainfall-runoff process. The shallow peat soils are poorly permeable, and precipitation extremes often cause soil erosion and even landslides. The KINFIL model in the version with parameter derivation of saturated hydraulic conductivity *Ks* and sorptivity *S* (at *FC*), as a simple three-parameter model (along with Manning roughness *n*), has proved not to be entirely reliable for simulating extreme runoff. The derived parameters from two calibration cases are applicable (Table 6), but only three out of four validated episodes are fully acceptable (Table 9).

Unlike a physically-based model, the mechanism of the artificial neural network ANN model involves approximating the relationship between rainfall (an input to the system) and runoff (an output from the system) represented by the available historical data. In our case, the calibration process is based on training the network on data from several episodes, irrespective of the physical system, the structure, and the governing equations. The robustness of the model is based on two important factors. The first factor is the reliability of data representing the rainfall-runoff relations, while the second factor is the leave-one-out approach. It means that each simulation is calibrated on several episodes, and is validated on one episode that has not been used for calibration. All possible combinations of calibration and validation splits of the episodes were tested.

The most important issue that we had to address when calibrating the ANN model was over-fitting of the training data. The obvious non-linearity of the problem, represented by the data, calls for a more complex network design with a larger number of units. This conflicts with the rather small sizes of the datasets describing the episodes by means of one hour-based data. Thus, the networks of dozens of units in two layers have a tendency to capture too many details (maybe including rainfall measurement errors). The network parameters and the length of the training episode were therefore verified by means of the validation set results. Since our goal is not the best-possible performance of the training set, but relevant performance of the validation data, the models typically show better validation results than calibration.

CONCLUSION

The rainfall-runoff processes in the Smědá basin are admittedly difficult to calibrate, especially in a model with a small number of parameters. Generally, the KINFIL model used here is a physically-based four-parameter 2D model (2 infiltration parameters and 2 transformations by a kinematic wave). When a version of the runoff *CN* curves was tested, the resulting values were used for deriving two parameters, *Ks* and *S*. Thus the four-parameter version was reduced to a three-parameter version. The selection of more recent calibration episodes (not from the 1960s and 1970s) would probably also help the simulation. We also assume that direct measurements of the soil hydraulic parameters using geo-statistical methods, instead applying *CN* methods to derive both infiltration parameters, would bring more relevant results. However, a method of that kind would be very laborious.

In the case of ANN models, it has been demonstrated that neural networks in general have the ability to capture the non-linear nature of the rainfall–runoff relationship, and the results are to a degree comparable with those obtained using hydrological models. The application of neural networks in this area raised several issues that needed to be dealt with. Due to the low statistical frequency of extreme episodes, the ANN model has to be trained on selected data where these episodes are present, and most of the data is not of interest and has to be abandoned. Unfortunately, the amount of available data from extreme episodes is relatively small, taking into account the complexity of the inherent nonlinear relationship of the model. We therefore have to address the issue of a suitable network size. It has to be large enough for the problem to be modelled faithfully, but at the same time it should be small enough to generalize well. Our solution to this problem was to use the validation data performance as a stopping criterion during the calibration phase. This allowed us to stop the calibration before the algorithm started to over-fit the data. This problem should be further investigated in future, and several other methods for improving generalization should be employed. Ensembles of ANNs are a promising approach.

Acknowledgement. The authors gratefully acknowledge the financial support provided by Technology Agency of the Czech Republic (Project TA02020402 “Water regime optimalisation to mitigate the impact of hydrological extremes”).

References

Andréassian V. (2004): Water and forests: from historical controversy to scientific debate. Journal of Hydrology, 291: 1–27.

Beven K.J. (1979): On the generalized kinematic routing method. Water Resources Research, 15: 1238–1242.

Beven K.J. (2001): Rainfall-Runoff Modelling: The Primer. Chichester, John Wiley & Sons.

Čamrová L., Jílková J. (2006): Flood Damages and Tools for their Mitigation. Praha, IEEP, VŠE. (in Czech)

Kibler D.F., Woolhiser D.A. (1970): The Kinematic Cascade as a Hydrologic Model. Hydrology Paper No. 39. Fort Collins, Colorado State University.

Kirchner J.W. (2009): Catchments as simple dynamical systems: Catchment character ization, rainfall-runoff modelling, and doing hydrology backward. Water Resources Research, 45: W02429.

Kovář P. (1992): Possibilities of design floods assessment using model KINFIL. Journal of Hydrology and Hydromechanics, 40: 197–220.

Kovář P., Křovák F. (2002): Torrent Control. Praha, FLE ČZU. (in Czech)

Kovář P., Vaššová D. (2012): The KINFIL Model Manual. Praha, FŽP ČZU. (in Czech)

Kovář P., Pelikán M., Heřmanovská D., Vrana I. (2014): How to reach a compromise solution on technical and non-structural flood control measures. Soil and Water Research, 9: 143–152.

Lax P.D., Wendroff B. (1960): Systems of conservation laws. Communications on Pure and Applied Mathematics, 13: 217–237.

Lippmann R.P. (1987): An introduction to computing with neural nets. IEEE ASSP Magazine, 4: 4–22.

Morel-Seytoux H.J., Verdin J.P. (1981): Extension of the Soil Conservation Service Rainfall-Runoff Methodology for Ungauged Watersheds. Fort Collins, Colorado State University.

Nash J.E., Sutcliffe J.V. (1970): River flow forecasting through conceptual models. Part I, A discussion on principles. Journal of Hydrology, 10: 282–290.

Neruda M., Neruda R., Kudová P. (2005): Forecasting runoff with artificial neural networks. Progress in surface and subsurface water studies at plot and small basin scale. In: 10th Conf. Euromediterranean Network of Experimental and Representative Basins (ERB), Turin, Oct 13–17, 2004: 65–69.

Perrin C., Michel C., Andréassian V. (2001): Does a large number of parameters enhance model performance? Comparative assessment of common catchment model structures on 429 catchments. Journal of Hydrology, 242: 275–301.

Ponce V.M., Hawkins R.H. (1996): Runoff curve number: Has it reached maturity? Journal of Hydrologic Engineering, 1: 11–19.

Rumelhart D.E., McClelland J.L. (1986): Parallel Distributed Processing: Explorations in the Microstructure of Cognition I&II. Cambridge, MIT Press.

Singh V.P. (1976): A note of the step error of some partial finite-difference schemes used to solve kinematic wave equations. Journal of Hydrology, 30: 247–255.

Singh V.P. (1996): Kinematic Wave Modelling in Water Resources: Surface Water Hydrology. New York, John Wiley&Sons.

US SCS (1986): Urban Hydrology for Small Watersheds. Technical Release 55. Washington D.C., USDA.

US SCS (1992): Soil Conservation. Program Methodology. Chapter 6.12: Runoff Curve Numbers. Washington D.C., USDA.

WMO (1984): Commission for Hydrology: Abridged Final Report of the Seventh Session. Geneva, Aug 27–Sept 7, 1984, Secretariat of the World Meteorological Organisation.

STUDIE 2: Mitigation of Surface Runoff and Erosion Impactson Catchment by Stone Hedgerows

Pavel Kovář, Darina Vaššová and Michaela Hrabalíková

Soil & Water Res., 6, 2011 (4): 153–164

Abstract: This paper presents the results of a study on the influence of hedgerows on the process of the surface runoff in the experimental catchment Verneřice 1, Ústí n. L. region, the Czech Republic. The influence of hedgerows on the surface runoff was simulated using the KINFIL rainfall-runoff model. The model parameters were assessed from the field measurements of the soil hydraulic parameters, in particular the saturated hydraulic conductivity and sorptivity. The catchment area is characterised by stone hedgerows constructed by land users throughout the past centuries, using stones collected from the adjacent agricultural fields. Presently, the hydraulic properties of these hedgerows reflect the characteristics of the mixture of stones, deposited soil, and vegetation litter, and they are more permeable than soil on the areas between them. Due to this fact, the permeability of the hedgerows produces a higher infiltration and a lower surface runoff. Therefore, the overland flow vulnerability and impact of water erosion decrease if they are situated in parallel to the contour lines system. The model was applied for two scenarios in the catchment – with and without hedgerows – to assess their effects on extreme rainfalls with a short duration. The surface runoff caused by extreme rainfall was simulated in order to show how hedgerows can mitigate the resultant flood and erosion. This paper provides relevant hydrological data and summarises the influence of man-made hedgerows on the overland flow control, i.e. on long and steep slopes surface runoff.

Keywords: extreme rainfall; infiltration intensity; rainfall-runoff model; soil erosion; stone hedgerows; surface runoff

INTRODUCTION

Landscape structures are significant factors affecting biodiversity and spatial variety, and they represent an important ecological value for the countryside (Langlois *et al*. 2001). Landscape

structures change in time and in space by natural influences and by agricultural practices of the land users.

In many parts of the Czech Republic, especially in the boarder regions, the landscape is characterised by systems of linear field margins, which at present are usually overgrown with hedgerows. Many of these systems date back to the late Middle Ages, when these highland areas were first colonised (Löw & Míchal 2003). They are called remnants of medieval "pluzina" (i.e. ploughed land) (Sklenička *et al.* 2009), and can be recognised by a characteristic comb-like or radial pattern of fields and field margins, radiating from a village, or a former village. The fields of a pluzina often have the characteristic shape of a flat letter S.

The earthworks of field margins can be of three types: a mound, a step, or a terrace (Černý 1973). Mounds (about 0.3–2.0 m in height and 2–4 m in width) are typical for milder slopes and were created by piling up stones collected from the fields. Steps (1.0–1.5 m in height and 1.5–3.0 m in width) are found in slightly hilly terrains, where the margins run horizontally or diagonally and were created by long-term ploughing. These two types of margins separated the fields of different land owners. Horizontal terraces (1.0–2.5 m in height) were usually created on steep slopes and several of the narrow fields were farmed by only one land owner.

Occasionally, systems of the field margins of a younger origin than Medieval can be found in the landscape. Unlike pluzinas, these margins often cannot be found in the Stable Cadastre maps system that was established in the 30's of the 19th century (Molnárová *et al.* 2008). They usually have different structures and do not have the characteristic spatial relationship to the settlement. Mounds are usually defined by stone hedgerows, composed of wood and herbs.

Extensive agriculture has had a long lasting tradition in North-Western parts of Bohemia. Whether a stone hedgerows axis was parallel to contour lines or down slope, or in any direction between, was not very important for growing crops or for animal husbandry. Constructing hedgerows was obviously part of good practice in cultivation. Of course, from the hydrological point of view, the longitudinal axis of stone hedgerows is very important as a stabilising factor in the direct runoff formation (Mérot 1999; Marshall & Moonen 2002). The best positioning is in the contour line direction. This can mitigate overland flow as an effective belt. This belt transforms part of the flow, and allows it to infiltrate. A description of differently situated stone hedgerows is given in Figure 1, where the well situated hedgerows have number 1, while those having numbers 2 and 3 are orientated down slope, without any runoff control effect. A detailed view of a typical stone hedgerow is provided in Figure 2.

Figure 1. The Verneřice region with different axis directions of stone hedgerows (1 – well situated, 2 and 3 – non effective, GPS 50°40'42.7''N, 14°14'24.9''E)

These hedgerow forms are effective obstacles to the overland flow, offering high water permeability and usually also a high diversity of vegetation species (Machová & Elznicová 2009, 2010). These landscape studies analyse the development of stone hedgerows from 1938 to the present days, with reference to their slopes, lengths, longitudinal and cross-section profiles and botanical diversity. The most frequent vegetation growing on these stone hedgerows belong to woody species (trees and shrubs), specifically *Fraxinus excelsior* (up to 60%), *Acer pseudoplatanus*, *Tilia cordata*, *Acer campestre*, *Corylus avellana*, *Prunus avium*, *Prunus spinosa*, and *Carpinus betulus.* The dominant herbs (59 species found) include mainly *Impatiens parviflora* and *Geranium robertianum* (Machová & Elznicová 2010). Figure 3 describes the scheme of

contour line orientated hedgerows with protective flood and erosion control on a mild slope catchment. A number of these landscape forms are characteristic for the area of the Ore Mountains (Krušné hory) (Adolfov, Fojtovice, Knínice, Libouchec) and for the northern part of the Central Bohemian Uplands (Oblík, Verneřice). Our case study is focused on the territory of Verneřice, and analyses the hydrological and erosion control functions of stone hedgerows as a biotechnical measure of historical importance. This case study follows up a paper, which has been published by Štibinger (2011).

Figure 2. Typical hedgerow made of stone deposition with three levels of vegetation (trees, shrubs and herbs)

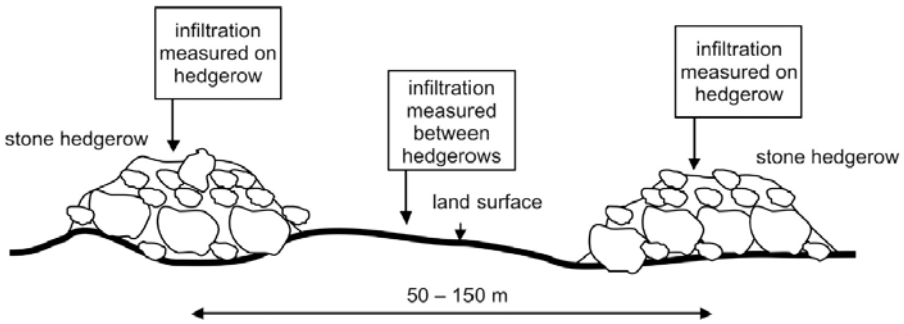

Figure 3. The scheme of contour lines orientated hedgerow protecting soil against surface runoff impact; infiltration intensity is measured on hedgerows and also on land between them

MATERIAL AND METHODS

The protective hydrological function of contour lines orientated stone hedgerows mitigates the negative impacts of extreme intensity rains, i.e. their runoff and soil erosion effects on the catchments. By using infiltrometer measurements, it has been determined that hedgerows and their subsoil are usually more permeable than the upper soil layers between them. Hence, a stone hedgerow can be considered as a biotechnical measure resulting in excellent infiltration properties. It has favourable deep-infiltration properties, which reduce the overland flow and replenish groundwater storage. It can operate as “a linear infiltration belt”. When directed parallel to the contour lines, it can be considered as a land management element and one of the catchment characteristics in Figure 4. However, the goal of our study is more pertinent. We want to find an answer to the question, to what extent can we mitigate the surface runoff from extreme rainfalls to prevent the damage caused by flooding and soil erosion.

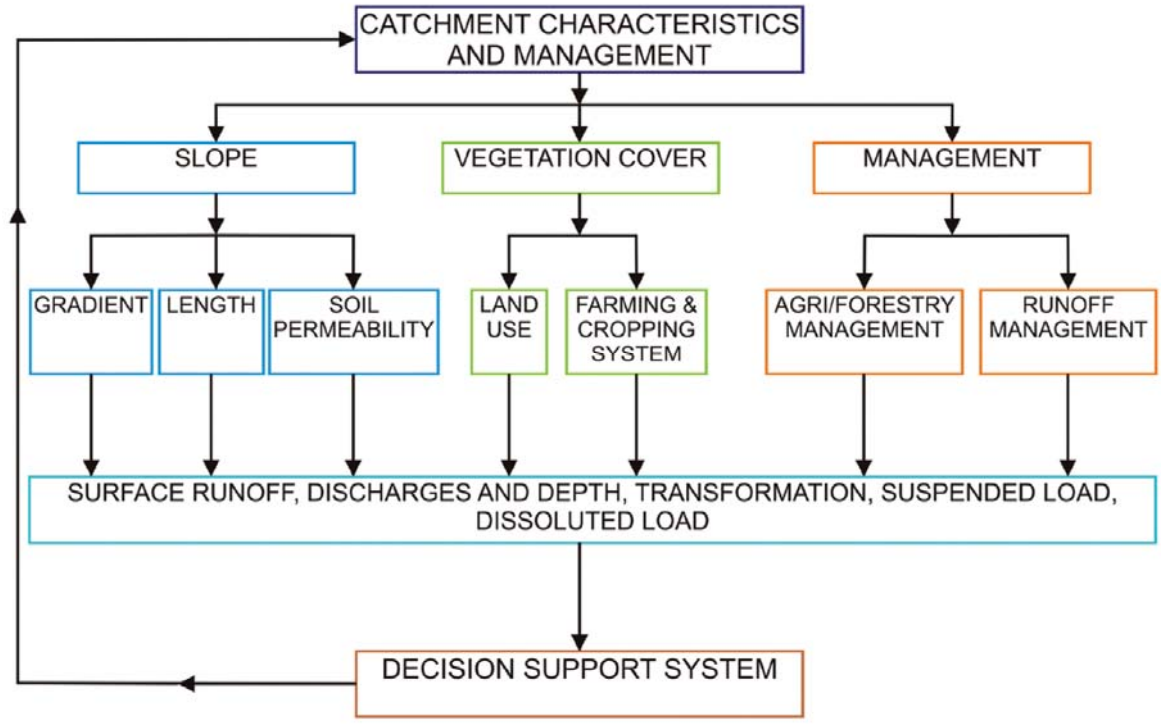

Figure 4. Catchment and management characteristics affecting surface runoff and sediment transport

Experimental area

Our experimental area is situated in the catchment area Verneřice 1 (Figure 1) in the Central Bohemian Uplands, district Ústí n. L. It is an ungauged catchment with the upper water divide on the southern side of the Verneřice 1 area. This catchment is 14 km from the raingauge station Ústí n. L.-Kočkov, where the data used in our study have been collected. The catchment altitude is about 410 m a.s.l. and does not differ significantly from the rain-gauge altitude (the difference is about 160 m). The catchment does not end with one outlet profile, but with an open contour line profile which is 475 m wide, transferring the sur face runoff down to the rest of the catchment. For practical reasons, the lower part of the catchment is not part of our analysis. The catchment area has a form of a non-regular hexagon, spreading over an area of 40.1 ha. The average slope is 0.08 (8%) with eight sub-catchments (DP1 to DP8), and with the same number of stone hedgerows. The width of the individual sub-catchments varies from 335 to 534 m, their length from 70 to 165 m, with permanent grassland use. The margins are composed of forested areas, the rest are hedgerow areas. More detailed information is given in Table 6; the overall situation is shown in Figure 5.

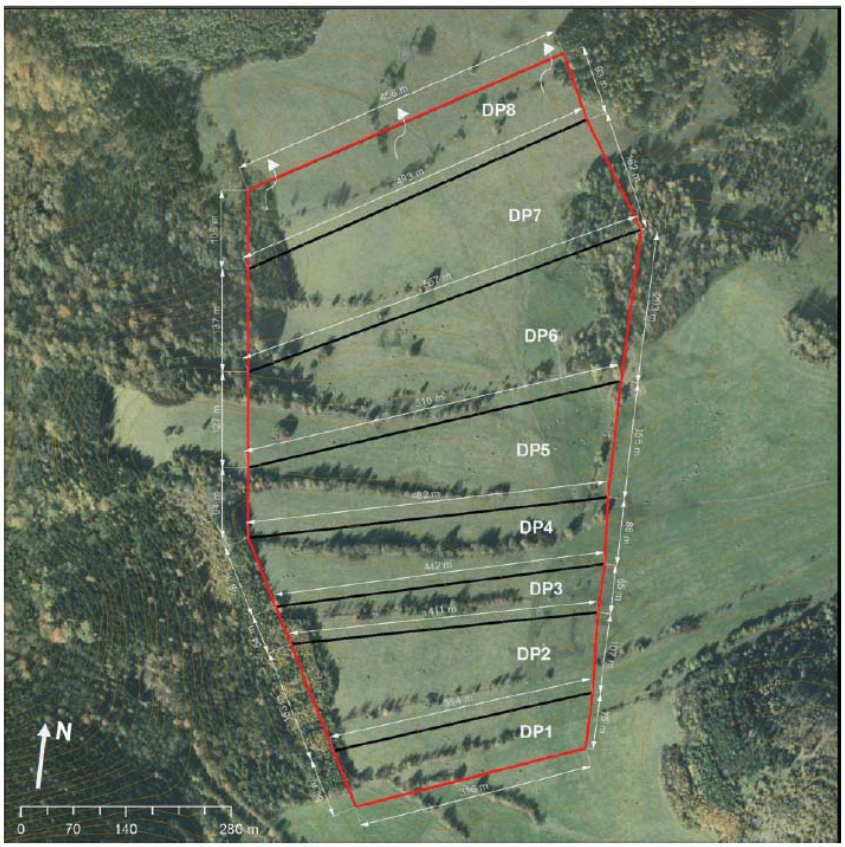

Figure 5. The catchment area Verneřice 1 with stone hedgerows

Table 1. The sub-catchment areas of the Verneřice 1 catchment (see Figure 5)

	Area No. DP							
	DP1	DP2	DP3	DP4	DP5	DP6	DP7	DP8
Area (ha)	2.524	4.840	2.419	4.210	5.959	8.167	7.608	4.345

Field measurements

The field measurements of the infiltration intensity in the catchment area Verneřice 1 were taken four times in the period from 2009 to 2010. The results were analysed statistically within the research project NAZV QH 82126/2008 "Harmonisation of landscape-stabilizing, hydrologic and production function of stone hedgerows and terraces for diversification activities in rural areas". The purpose of these measurements was to determine the values of the infiltration parameters and the soil hydraulic characteristics in the areas between the hedgerows, and also within these hedgerows. Such measurements have not yet been taken in this area, and thus our study offers unique findings (Cílek 2009). One of the specific outcomes of this study is the evaluation of the Richards' equation (Kutílek & Nielsen 1994) and the Philip's solution of non-steady infiltration

(Philip 1957). The shortened Philip equation for the vertical cumulative infiltration, *V* (m), into homogeneous soil with water ponded on the surface was applied for the determination of the saturated hydraulic conductivity *Ks* (m/s) and sorptivity *S* (m/s$^{1/2}$), which has the form:

$$V = S \times t^{1/2} + A_t \times t \quad (1)$$

where: A_t – soil parameter (m/s$^{1/2)}$

A_t is related to the saturated hydraulic conductivity *Ks*, and for the saturated soil surface is equal to it. Then, it can be written:

$$V = S \times t^{1/2} + K_s \times t \quad (1a)$$

The infiltration intensity $v(t)$ can be obtained by derivation of Eq. (1a) in time, when:

$$v(t) = \frac{1}{2} S \times t^{-1/2} + K_s \quad (2)$$

The non-linear regression was computed and, in order to collect the values by the field measurement in the Verneřice catchment area (Figure 1), the two-cylinder method of infiltration was used and all data were analysed. The measurement technique as well as its statistical analysis have been described in detail elsewhere (Štibinger 2011).

Subsequently, both parameters *S* and *Ks* were computed, applying the method of non-linear regression. The correlation coefficient *R* showed the best fit of the data series, when *R* = 0.999 and 0.970.

The final parameter values are given in Table 2. On the basis of the analysis of the data collected in the Verneřice 1 catchment, it became clear that the *Ks* permeabilities values of the hedgerows lines were about 4.5 times higher (*Ks* = 3.58 x 10^{-5} m/s) than those in the empty spaces lying between them (*Ks* = 8.10 x 10^{-6} m/s).

Table 2. Values of saturated hydraulic conductivity (*Ks*) and sorptivity (*S*) on the Verneřice 1 catchment

	Between hedgerows	On hedgerows
Ks (m/s)	8.10 × 10–6	3.58 × 10–5
S (m/s$^{1/2}$)	2.16 × 10–4	2.38 × 10–4
R	0.997	0.999

Extreme rainfall assessment

The catchment Verneřice 1 has a rainfall gauge in close vicinity, which provides daily rainfall data with a return period *N* = 2, 5, 10, 20, 50 and 100 years, as shown in Table 3. The length of the

data record was 90 years (1901 to 1990). These data were used for a shorter duration than one day (24 h), as the catchment area is relatively small (0.40 km^2). Therefore, the periods of critical rainfalls duration were selected for time t = 10, 20, 30, 60, 90, 120 and 300 min. For this computation, the RAIN_red procedure (Kovar & Hradek 1994) was used, according to the relations (Hrádek & Kovář 1994):

$$P_{t,N} = P_{1d,N} \times a + t^{1-c} \quad (3)$$

$$i_{t,N} = P_{1d,N} \times a + t^{c} \quad (4)$$

where:

$P_{t,N}$ – maximum extreme rainfall depth (mm) of duration t and return period N

$i_{t,N}$ – maximum extreme rainfall intensity (mm/min) of duration t and return period N

$P_{1d,N}$ – maximum extreme rainfall depth (mm) of one day duration and return period N

t – time

a, c – regional parameters

The regional parameters for the extreme rainfall reduction a and c were derived by means of the methodology used by Hrádek and Kovář (1994). The return period (N years) for extreme rainfall is assumed to be the same as the return period for runoff. These extreme rainfalls are used also for the design purposes, with planning flood or erosion control measures. Such "design" rainfalls were used with a constant intensity. Table 4 provides the $P_{t,N}$ rainfall depth values needed for the design input hydrograph computation, using the RAIN_red procedure, as already mentioned. Similarly, Table 5 gives the $i_{t,N}$ rainfall intensity values of a short duration, as estimated from daily values. These short duration extreme rainfalls were tested using the KINFIL rainfall-runoff model in the experimental catchment, to simulate the runoff. Due to the small catchment area and thus a short concentration time, a particular expectation was put on the short time extreme rainfall of duration t = 10 to 30 min.

Table 3. One day extreme rainfalls $P_{1d,N}$ at the Ústí n. L.-Kočkov station*

	Return period N (years)					
	2	5	10	20	50	100
Daily extreme rain P1d,N (mm)	30.6	41.8	49.0	56.5	65.7	79.2

Table 4. Maximum extreme rainfall depths $P_{t,N}$ of short duration for the station Ústí n. L. (in mm)

N (years)	*P*1d,*N*	*t* (min)						
	(mm)	10	20	30	60	90	120	300
2	30.6	10.1	12.4	14.0	16.3	17.6	18.6	22.4
5	41.8	14.7	18.2	20.7	24.8	26.9	28.4	32.8
10	49.0	17.6	22.4	25.7	30.7	33.3	35.2	39.8
20	56.5	21.5	27.4	31.6	38.0	41.1	43.5	47.9
50	65.7	26.3	33.8	39.2	47.5	51.5	54.6	58.5
100	79.2	32.5	42.1	49.1	59.4	64.4	68.1	72.0

Table 5. Maximum extreme rainfall intensities $i_{t,N}$ of short duration for the station Ústí n. L. (in mm/min)

N (years)	*P*1d,*N*	*t* (min)						
	(mm)	10	20	30	60	90	120	300
2	30.6	1.01	0.62	0.47	0.27	0.2	0.16	0.07
5	41.8	1.47	0.91	0.69	0.41	0.3	0.24	0.11
10	49.0	1.76	1.12	0.86	0.51	0.37	0.29	0.13
20	56.5	2.15	1.37	1.05	0.63	0.46	0.36	0.16
50	65.7	2.63	1.69	1.31	0.79	0.57	0.45	0.19
100	79.2	3.25	2.11	1.64	0.99	0.72	0.57	0.24

KINFIL rainfall-runoff model

The KINFIL model is based on the combination of infiltration (1st part) and direct runoff transformation processes (2nd part). This model (2D) is physically based and it has been used for the reconstruction of many historical rainfall-runoff events and also for various scenario simulations on gauged or ungauged catchments (Kovář 1992; Heřman *et al.* 2001; Kovář *et al.* 2002). It requires physiographical parameters of the catchment, which can be determined from maps and field survey. It is often used for the design discharge determination and also for scenario situations, e.g. when the effects of the climate change are simulated. The first part of the KINFIL model computes infiltration rates $v_f(t)$ for each interval of duration t and subtracts them from the extreme rainfall intensities $i(t)$ (of return period N) in order to get the effective rainfall hyetograph $r_e(t)$:

$$r_e(t) = i(t) - v_f(t) \tag{5}$$

This infiltration part of the KINFIL model is based on the infiltration theory of Green and Ampt applying the concept of the ponding time and storage suction factor S_f by Morel-Seytoux and Verdin (1981) and by Morel-Seytoux (1982):

$$v_f = (\theta_s - \theta_t)\frac{dz_f}{dt} = K_s\left[\frac{z_f + H_f}{z}\right] \quad (6)$$

The left side of Eq. (6) expresses the Darcy principle of an infiltration process, while its right side reflects the Green-Ampt theory (Rawls & Bra-kensiek 1983). It has been used by many authors (e.g. Morel-Seytoux & Verdin 1981).

The ponding time is expressed as:

$$t_p = \frac{S_f}{i\left(\frac{i}{K_s} - 1\right)} \quad (7)$$

and the storage suction factor as:

$$S_f = H_f\,(\theta_s - \theta_t) = \frac{S^2(\theta_i)}{2K_s} \quad (8)$$

where:

ϑ_s – saturated soil water content (–)

ϑ_i – initial soil water content (–)

z_f – depth of infiltration front (m)

z – vertical ordinate (m)

H_f – capillary suction on infiltration front (m)

K_s – saturated hydraulic conductivity (m/s)

i – constant rate of design rainfall (m/s)

S_f – storage suction factor (m)

S (ϑ_s) – sorptivity at initial soil water content (m/s$^{1/2}$)

t_p – ponding time (s)

When we know the parameters such as the saturated conductivity *Ks* and sorptivity *S*, we can use the equations needed for the KINFIL model to compute Eqs. (5) to (8) and to receive the effective rainfall ordinates $r_e(t)$ to be further used for the surface runoff component computed in the second part (KIN).

The second part of the KINFIL model is the surface runoff component, using the kinematic equation of flow over a catchment (Kibler & Woolhiser 1970; Beven 2006):

$$r_e(t) = \frac{\delta y}{\delta t} + \alpha \times m \times y^{m-1} \times \frac{\delta y}{\delta x} \quad (9)$$

where:

$r_e(t)$ – effective rainfall intensity (m/s)

y, t, x – ordinates of depth, time, and position (m, s, m)

α, m – hydraulic parameters

This equation describes the non-steady flow, approximated, after neglecting the velocity terms of St. Venant's equation, by kinematic wave on a plane or a cascade of planes or segments.

Eq. (9) is computed, using the finite differences method and implementing the explicit numerical scheme (Lax & Wendroff 1960). The upper boundary condition of the Lax-Wendroff scheme is $y(x, 0) = 0$ for all x. For the practical application of the KINFIL model, the catchment was divided into a cascade of planes, with the same slopes and different lengths and widths.

The present version of the KINFIL model assumes that the individual small sub-catchments are substituted by a system of planes, arranged according to the flow direction, i.e. from 1 to 8. This system puts emphasis on the geometry of planes, their slopes and roughness conditions. Therefore, the KINFIL model requires geometric parameters of planes, slopes, soil hydraulic parameters *Ks* and *S*, Manning roughness *n,* and flow pattern system.

RESULTS AND DISCUSSION

The topographic fragmentation of the experimental catchment Verneřice 1 was implemented through GIS ArcInfo with respect to the hedgerows system. The topology-vector data ZABADEG 1:10 000, including planimetry and hypsography, was the basis of the study. The demarcation of the experimental catchment and partial sub-catchments DP1–DP8 were designed from the geographic data, using the ArcInfo programme in the ESRI system. The land slope is almost the same for all sub-catchments (0.08). The fragmentation of the experimental catchment is presented in Figure 5, the geometric and land use data are given in Table 6. Its use had been tested in several locations, i.e. in catchments with rainfall and overland flow observation (Kovář *et al*. 2002, 2006). The determination of the Manning roughness *n* value is usually difficult. In our study, we used the values recommended in relevant literature (Fread 1989; Maidment 1992), i.e. $n = 0.100$ for grassland, and $n = 0.150–0.200$ for forests. The value for hedgerows was estimated at $n = 0.300$. We assume that for extreme discharge from extreme rainfall events with a return period $N = 20–100$ years, the roughness and turbulent flow correspond to reality. Due to the short runoff lengths (see runoff lengths in Table 6: 60.0–165.0 m) and the homogenous slope of

a meadow, it was not necessary to subdivide the partial catchment into more detailed cascades of planes for simulation by the KINFIL model.

Table 6. Fragmentation of the Verneřice 1 catchment area for the KINFIL model

Sub-catchment DP	Area (ha)	Average slope (–)	Average width (m)	Average length (m)	Land use (%)		
					grassland	forest	hedgerow
DP1	2.524	0.080	335	70	90.2	3.2	6.6
DP2	4.840	0.080	383	130	91.3	4.8	3.9
DP3	2.419	0.080	426	60	87.5	3.7	8.8
DP4	4.210	0.080	462	93	93.4	0	6.6
DP5	5.959	0.080	496	125	96.2	0	3.8
DP6	8.167	0.080	534	165	87.1	9.6	3.3
DP7	7.608	0.080	525	150	85.8	12.5	1.7
DP8	4.345	0.080	475	99	91.0	3.5	5.5

Table 7. Major rainfall parameters and runoff hydrograph peaks on the Verneřice 1 catchment without hedgerows and with hedgerows as computed with the KINFIL model

Design rainfall			Effective rainfall		Peak discharges	
Return period N (years)	duration time t (min)	depth P (mm)	without hedgerows R_e	With hedgerows R_{eh}	without hedgerows Q	With hedgerows Q_h
			(mm)		(m3/s)	
2	10	10.1	1.26	–	–	–
2	20	12.4	0.33	–	–	–
2	30	14.0	–	–	–	–
2	60	16.3	–	–	–	–
2	120	18.6	–	–	–	–
5	10	14.7	4.93	0.12	0.206	–
5	20	18.2	2.85	–	0.086	–
5	30	20.7	1.60	–	0.032	–
5	60	24.8	0.27	–	–	–
5	120	28.4	–	–	–	–
10	10	17.6	7.54	0.85	0.419	0.011
10	20	22.4	6.52	0.14	0.329	0.001
10	30	25.7	4.77	–	0.192	–
10	60	30.7	1.43	–	–	–
10	120	35.9	–	–	–	–
20	10	21.5	11.24	3.09	0.818	0.096

Design rainfall			Effective rainfall		Peak discharges	
Return period N (years)	duration time t (min)	depth P (mm)	without hedgerows R_e	With hedgerows R_{eh}	without hedgerows Q	With hedgerows Q_h
			(mm)		(m3/s)	
20	20	27.4	11.20	0.22	0.813	0.001
20	30	31.6	10.11	–	0.681	–
20	60	38.0	5.06	–	0.215	–
20	120	43.5	–	–	–	–
50	10	26.3	15.8	7.05	1.460	0.373
50	20	33.8	17.40	2.37	1.706	0.060
50	30	39.2	12.78	0.12	1.010	0.003
50	60	47.5	12.14	–	0.900	–
50	120	54.6	3.53	–	–	–
100	10	32.5	21.83	12.91	2.514	1.041
100	20	42.1	25.58	8.49	3.182	0.489
100	30	49.1	27.29	3.96	3.595	0.144
100	60	59.4	23.62	0.66	0.496	0.007
100	120	68.1	11.98	–	–	–

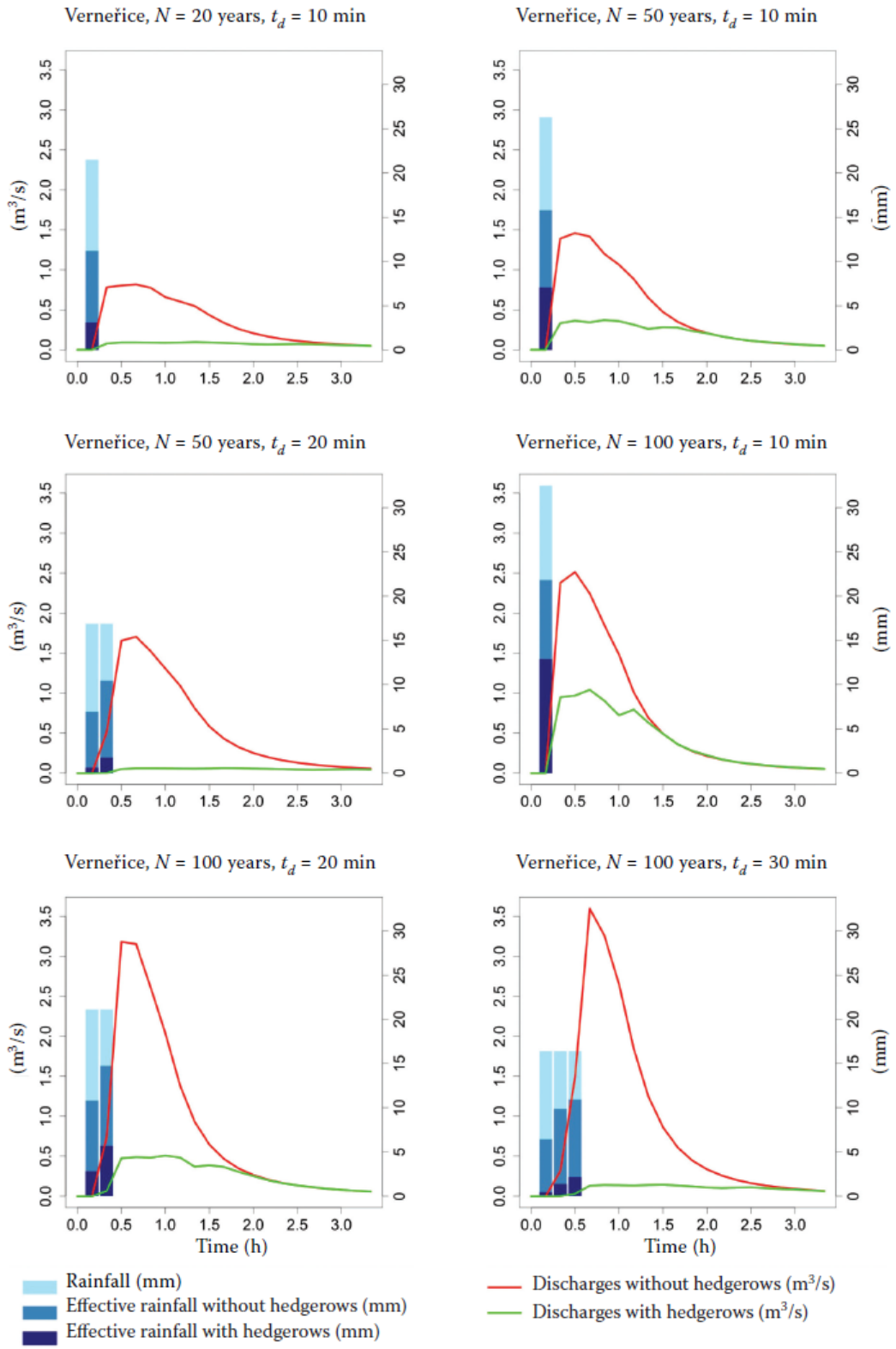

Figure 6. The hydrographs comparison on the Verneřice 1 catchment with a hedgerow infiltration function and without it, for extreme rainfalls of various return periods *N* and duration periods *t*

One of the important contributions of this paper was the comparison of the function of hedgerows during extreme rainfall-runoff events in various circumstances. A model simulation was implemented for all events of the return periods of extreme rainfalls N = 2 to 100 years and periods of their duration t = 10', 20', 30', 60', 90', 120' and 300' for the basic scenario without hedgerows and with hedgerows to see how much they reduce the surface runoff. By using GIS, the sub-catchment areas DP fragmentation was created, thus reflecting the fact that each DP sub-catchment had one protective biotechnical element in the form of a hedgerow. Their geometry dimension corresponded to the real situation.

The surface runoff simulation using the KINFIL model was applied in both scenarios, with and without hedgerows. Infiltration and the hyetographs of the effective rainfalls and their transformation in final hydrographs were then computed. It was assessed that in this particular catchment gross rainfalls, of the return periods N = 2, 5 and 10 years, create only small effective rainfalls. Their depths and rates are quite low, and therefore they can hardly form a significant surface runoff. More heavy rainfalls can create surface runoff only in scenarios without hedgerows, i.e. without their protection, when the return periods are N = 20, 50 and 100 years. Thus, the protection effect of hedgerows is relatively robust. The graphic representation in Figure 6 shows the most critical situations with heavy extreme rains, which cause a significant discharge. In our study, the discharges Q20 (10'), Q50 (10' and 20'), and Q100 (10', 20' and 30') have been found as the highest and they are highlighted in Table 7 and plotted in Figure 6.

Of course, we are aware of the fact that because the experimental catchment Verneřice 1 is ungauged, as is the case with all small catchments with hedgerow systems in the Czech territory, we cannot use the observed runoff data as the feedback for control. However, it is also the fact that the measured data on the infiltration parameters and extreme rainfall data were collected meticulously. Furthermore, the KINFIL model has been implemented successfully many times in other catchments, with acceptable degree of fit with the observed and computed discharges as the criterion of reliability. This fact seems to be a major source of uncertainty.

CONCLUSIONS

Following the previous analyses of the measurement results, obtained *in situ*, of infiltration and computational simulation by the KINFIL model in the Verneřice 1 catchment, the following conclusions may be drawn.

Hedgerows possess distinct hydro-physical characteristics which are different from the characteristics of permanent grassland growing between them. In particular, the latter have much higher infiltration intensity. As a result of favourable infiltration characteristics, they act as infiltration and erosion control biotechnical measures for decreasing surface runoff. Their influence on the water regimes may also be significant during dry seasons.

Simulations using the KINFIL model proved that, as a result of the favourable infiltration characteristics of the soils in the Verneřice 1 catchment, the depth of the surface runoff (i.e. the depth of effective rainfall) for gross rainfall with the return periods N = 2, 5 and 10 years is insignificant (see Table 5). The discharges caused by rainfall with the return period N = 20, 50, and 100 years could be dangerous in the absence of hedgerows. Due to their infiltration capacity and hydraulic roughness, the hedgerows effectively reduce such discharges. In the most critical $Q100$ (10'), the discharge from the extreme rainfall is reduced by hedgerows from a value of 2.5 to 1.0 m^3/s (i.e. by 60%).

Hydraulic variables, which are characteristic for the runoff formation process, i.e. the flow depth, velocity, and shear stress, indicate that for runoff with the return period exceeding N = 10 years, hedgerows obviously protect grassland against erosion. Model simulations, for the alternatives without hedgerows and with hedgerows, have shown that the non-scouring velocity and the critical shear stress on grassland are always resistant against water erosion. If these plots were again transformed in arable land for growing field crops (e.g. root crops, maize, sunflower, rape, etc.), this would surely not be the case, because of the changes in critical shear stress of soil that is not covered by permanent grassland. In our present times of hydrological extremes, such as rainstorms, research focusing on land and water regime protection is of course very relevant.

The next step in our research will be to install a pair of rainfall-runoff gauges in this catchment, in order to compare the observed and computed data. We assume that this will generate reliable data, which will highlight the positive hydrological impact of hedgerows in landscape during strong rainfall-runoff events.

References

Beven K.J. (2006): Rainfall-Runoff Modelling. The Primer. John Wiley & Sons, Chichester.

Cílek V. (2009): Interior and Exterior Landscapes. 2nd Ed., Dokořán, Prague. (in Czech)

Černý E. (1973): Exploration methodology of the extinct settlements and pluzinas on the Drahanska Highlands. Zprávy Československé Společnosti archeologické při ČSAV, Praha, XV. (in Czech)

Fread D.L. (1989): Flood routing models and the Manning n. In: Yen B.C. (ed.): Proc. Int. Conf. Centennial of Manning's Formula and Kuichling's Rational Formula. Charlottesville, 699–708.

Heřman M., Zemek F., Cudlín P., Kovář P. (2001): Landscape fragmentation for flood prevention: GIS and hydrological modelling approach assessing forested landscape. Ecology (Bratislava), 20: 149–157.

Hrádek F., Kovář P. (1994): Computation of the design torrential rainfalls. Vodní hospodářství, 11: 49–53. (in Czech)

Kibler D.F., Woolhiser D.A. (1970): The kinematic cascade as a hydrologic model. Hydrology paper No. 39, Colorado State University, Fort Collins.

Kovář P. (1992): Posibilities of design discharge determination on small catchments using the KINFIL model. Journal of Hydrology and Hydromechanics/Vodohospodářský časopis, 40: 197–220. (in Czech)

Kovar P., Hradek F. (1994): Design flood determination on small catchments using the KINFIL II model. In: Seuna P. *et al.* (eds): FRIEND: Flow Regimes from International Experimental and Network Data. IAHS Publication No. 221, Wallingford, 307–313.

Kovář P., Cudlín P., Heřman M., Zemek F., Korytář M. (2002): Analysis of flood events on small river catchments using the KINFIL model. Journal of Hydrology and Hydromechanics SAV Bratislava, 50: 157–171.

Kovář P., Dvořáková Š., Kubátová E. (2006): Possibilities of using the direct runoff model KINFIL for a road network design. Soil and Water Research, 1: 49–56.

Kutílek M., Nielsen D.R. (1994): Soil Hydrology. Geo-ecology Textbook. Catena Verlag, Cremlingen Destedt, 98–102.

Langlois J.P., Fahrig L., Merriam G., Artsob H. (2001): Landscape structure influences continental distribution of hantavirus in deer mice. Landscape Ecology, 16: 255–266.

Lax P.D., Wendroff B. (1960): Systems of conservation laws. Communications on Pure and Applied Mathematics, 13: 217–237.

Löw J., Míchal I. (2003): Landscape Character. Lesnická práce, Kostelec n. Černými Lesy. (in Czech)

Machová I., Elznicová J. (2009): Identification of hedgerows changes. In: MU Brno Conference Geospheric Aspects of Mid-European Space. Masaryk University, Brno. (in Czech)

Machová I., Elznicová J. (2010): Identification of hedgerows changes. Studia Oecologica, 4: 10.

Maidment D.R. (1992): Handbook of Hydrology. McGraw-Hill, Inc., New York.

Marshall E.J.P., Moonen A.C. (2002): Field margins in Northen Europe: their functions and interactions with agriculture. Agriculture, Ecosystems and Environment, 89: 5–21.

Mérot P. (1999): The influence of hedgerow systems on the hydrology of agricultural catchments in a temperate climate. Agronomie, 19: 655–669.Molnárová K., Šímová P., Kotaška J., Ešnerová J., Škvárová Š. (2008): Hedgerow-defined medieval field patterns in the Czech Republic: a case study of the dendrological and dendrochronological structure of hedgerows of varying ages in Northern Moravia. Journal of Landscape Studies, 1: 1802–4416.

Morel-Seytoux H.J. (1982): Analytical results for predictions of variable rainfall infiltration. Journal of Hydrology, 59: 209–230.

Morel-Seytoux H.J., Verdin J.P. (1981): Extension of the Soil Conservation Service. Rainfall-runoff Methodology for Ungauged Watersheds. Colorado State University, Fort Collins.

Philip J.R. (1957): Numerical solution of equations of the diffusion type with diffusivity concentration-dependent. II. Australian Journals of Physics, 10: 29–42.

Rawls W.J., Brakensiek D.L. (1983): A procedure to predict Green and Ampt infiltration parameters. In: ASCE Proc. Conf. Advance in Infiltration. Chicago.

Sklenička P., Molnárová K., Brabec E., Kumble P., Pittnerová B., Pixová K., Šálek M. (2009): Remnants of medieval field patterns in the Czech Republic: Analysis of driving forces behind their disappearance with special attention to the role of hedgerows Agriculture Ecosystems & Environment, 129: 465–473.

Štibinger J. (2011): Infiltration capacities. Stavební Obzor, 2: 78–83. (in Czech)

3 Časové a prostorové měřítko v modelování

Podle literatury (Karydas et al., 2014) hraje časové a prostorové měřítko (např. rozlišení DMR) významnou roli v modelování. Např. Yin et al. (2007) nebo Williams a Sheridan (1991) uvádí, že se s klesajícím časovým krokem výpočtu výsledná hodnota R-faktoru podhodnocuje. Toto tvrzení dokládají i výsledky obsažené v následujících dvou studiích a graf hodnot R-faktoru vypočítaného na základě různého časového kroku na obr. 4

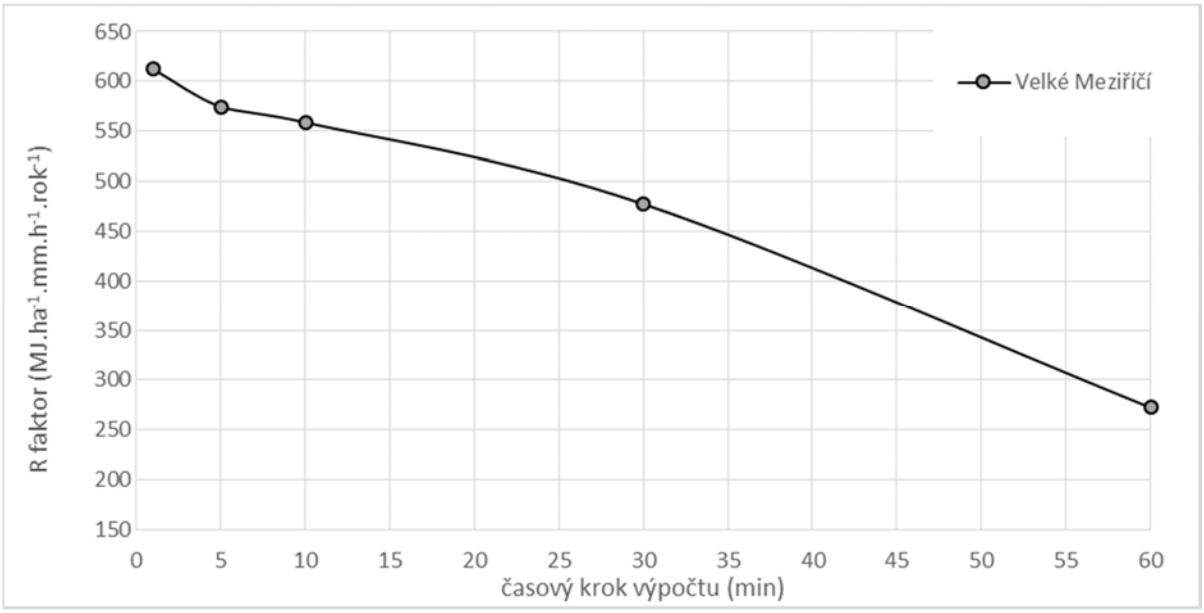

Obr. 4: R-faktor pro stanici Velké Meziříčí vypočítaný v časovém kroku: 1 min, 5 min, 10 min, 30 min a 60 min

Studie 3 a 4 se zabývá výpočtem R-faktoru pro celou EU, kdy v rámci spolupráce mezi dalšími státy a jako jeden z cílů této práce se za Českou republiku:

- Vypočítal R faktor pro 32 stanic
- Data ze stanic převážně pokrývala období 1961 – 1999

Vzhledem prostorovému měřítku (EU) a množství vstupujících dat bylo třeba homogenizovat časový krok výpočtu pro všechny státy, které použily jiný časový krok. Stejnou homonegizaci dat v rámci USA provedl i Renard et al. (1997), kdy se na základě doplňujících výpočtů v různém časovém kroku stanoví přepočítávací koeficient. Konverze 60-min dat např. na 10-min data v sobě zahrnuje poměrně velkou chybovost (nejistoty) a tak bylo zvoleno jako jednotný časový krok 30 min. Regresní funkcí se stanovil koeficient pro přepočet (viz obr. 5)

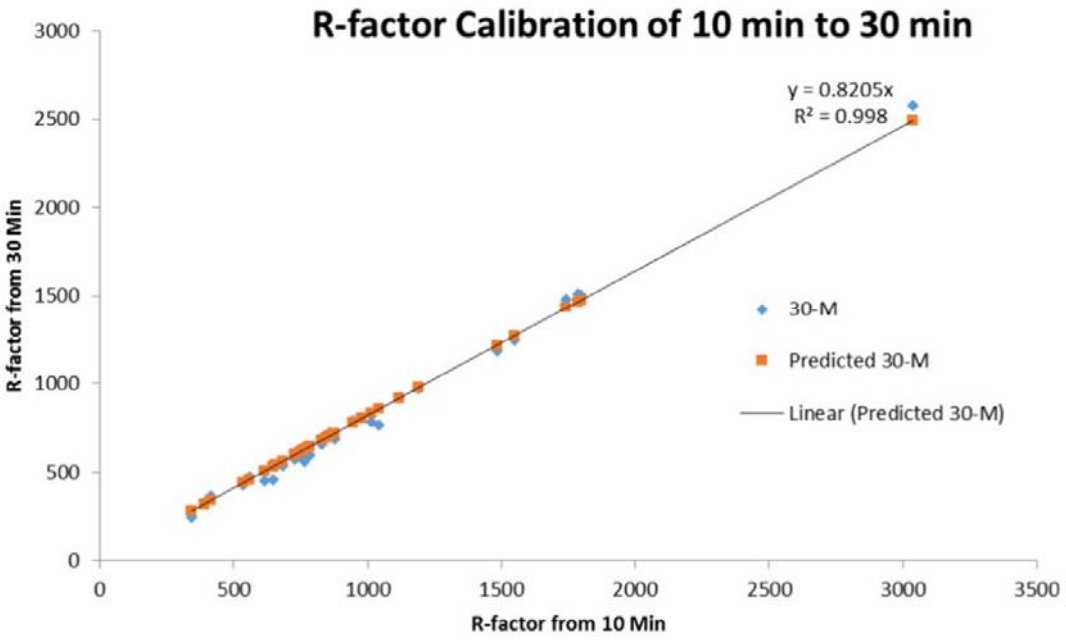

Obr. 5: Kalibrace dat pro přepočet R faktoru z 10 min kroku na 30 min časový krok

Faktor pro přepočet časového rozlišení dat

Časový krok zdrojových dat	Počet stanic	Země	Regresní funkce	R^2
60-min	82	BE, CZ, CH, CY, DE, EE, FR, IT, LU, RO	$R_{30\,min} = 1.5597 \cdot R_{60\,min}$	0.994
15-min	31	BE, ES	$R_{30\,min} = 0.8716 \cdot R_{15\,min}$	0.998
10-min	31	CZ, CY, CH, DE, EE, HR, HU, LU, RO	$R_{30\,min} = 0.8205 \cdot R_{10\,min}$	0.998
5-min	12	CZ, CY, FR, HR, LU	$R_{30\,min} = 0.7984 \cdot R_{5\,min}$	0.998

Jak již bylo zmíněno v úvodu, R faktor je jedním z faktorů rovnice USLE, který s sebou nese jistá úskalí v podobě nedostatku dat. Podle literatury je minimální délka časové řady pro reprezentativní odhad R faktoru:

- Foster et al. (2003): 15 let
- Wishmeier, Smith (1978): 22 let
- Verstraeten et al. (2006): 22 let a více

STUDIE 3: Rainfall erosivity in Europe

Panos Panagos, Cristiano Ballabio, Pasquale Borrelli, Katrin Meusburger, Andreas Klik, Svetla Rousseva, Melita Perčec Tadić, Silas Michaelides, Michaela Hrabalíková, Preben Olsen, Juha Aalto, Mónika Lakatos, Anna Rymszewicz, Alexandru Dumitrescu, Santiago Beguería, Christine Alewell

Science of the Total Environment 511 (2015) 801–814

Abstract: Rainfall is one the main drivers of soil erosion. The erosive force of rainfall is expressed as rainfall erosivity. Rainfall erosivity considers the rainfall amount and intensity, and is most commonly expressed as the R-factor in the USLE model and its revised version, RUSLE. At national and continental levels, the scarce availability of data obliges soil erosion modellers to estimate this factor based on rainfall data with only low temporal resolution (daily, monthly, annual averages). The purpose of this study is to assess rainfall erosivity in Europe in the form of the RUSLE R-factor, based on the best available datasets. Data have been collected from 1541 precipitation stations in all European Union (EU) Member States and Switzerland, with temporal resolutions of 5 to 60 min. The R-factor values calculated from precipitation data of different temporal resolutions were normalized to R-factor values with temporal resolutions of 30 min using linear regression functions. Precipitation time series ranged from a minimum of 5 years to a maximum of 40 years. The average time series per precipitation station is around 17.1 years, the most datasets including the first decade of the 21st century. Gaussian Process Regression (GPR) has been used to interpolate the R-factor station values to a European rainfall erosivity map at 1 km resolution. The covariates used for the R-factor interpolation were climatic data (total precipitation, seasonal precipitation, precipitation of driest/wettest months, average temperature), elevation and latitude/longitude. The mean R-factor for the EU plus Switzerland is 722 MJ mm ha^{-1} h^{-1} yr^{-1}, with the highest values (> 1000 MJ mm ha^{-1} h^{-1} yr^{-1}) in the Mediterranean and alpine regions and the lowest (< 500 MJ mm ha^{-1} h^{-1} yr^{-1}) in the Nordic countries. The erosivity density (erosivity normalized to annual precipitation amounts) was also the highest in Mediterranean regions which implies high risk for erosive events and floods.

Keywords: RUSLE; R-factor; Rainstorm; Rainfall intensity; Modelling; Erosivity density; Precipitation; Soil erosion

INTRODUCTION

Soil erosion by water affects soil quality and productivity by reducing infiltration rates, water-holding capacity, nutrients, organic matter, soil biota and soil depth (Pimentel et al., 1995). Soil erosion also has an impact on ecosystem services such as water quality and quantity, biodiversity, agricultural productivity and recreational activities (Dominati et al., 2010 and Dale and Polasky, 2007).

Since soil erosion is difficult to measure at large scales, soil erosion models are crucial estimation tools at regional, national and European levels. The high heterogeneity of soil erosion causal factors, combined with often poor data availability, is an obstacle to the application of complex soil erosion models. The empirical Revised Universal Soil Loss Equation (RUSLE) (Renard et al., 1997), which predicts the average annual soil loss resulting from raindrop splash and runoff from field slopes, is still most frequently used at large spatial scales (Kinnell, 2010 and Panagos et al., 2014a). In RUSLE, soil loss may be estimated by multiplying the rainfall erosivity factor (*R*-factor) by five other factors: Soil erodibility (*K*-factor), slope length (*L*-factor), slope steepness (*S*-factor), crop type and management (*C*-factor), and supporting conservation practices (*P*-factor).

Among the factors used within RUSLE and its earlier version, the Universal Soil Loss Equation (USLE) (Wischmeier and Smith, 1978), rainfall erosivity is of high importance as precipitation is the driving force of erosion and has a direct impact on the detachment of soil particles, the breakdown of aggregates and the transport of eroded particles via runoff. Rainfall erosivity is the kinetic energy of raindrop's impact and the rate of associated runoff (Wischmeier and Smith, 1978). The *R*-factor is a multi-annual average index that measures rainfall's kinetic energy and intensity to describe the effect of rainfall on sheet and rill erosion. However, the erosive forces of runoff due to snowmelt, snow movement, rain on frozen soil, or irrigation are not included in this factor. Besides (R)USLE, the rainfall erosivity can be used as input in other models such as USPED, SEMMED and SEDEM. Further, this dataset could also be interesting for natural hazard predictions such as landslide and flood risk assessment that are mainly triggered by high intensity events.

A precise assessment of rainfall erosivity requires recordings of precipitation at short time intervals (1–60 min) for a period of at least several years. The rainfall erosivity is calculated by multiplying the kinetic energy by the maximum rainfall intensity during a period of 30-minutes for each rainstorm. The *R*-factor accumulates the rainfall erosivity of individual rainstorm events and averages this value over multiple years.

Field experiments using plot-sized rainfall simulators provide precise results of rainfall erosivity (Marques et al., 2007). However, since field experiments are expensive and often not easily transferable to large scales, researchers develop models for estimating rainfall erosivity. Two approaches are used to model rainfall erosivity: a) calculate the R-factor based on high-temporal-resolution precipitation data, and b) develop functions that correlate the R-factor with more readily available (daily, monthly, annual) rainfall data (Bonilla and Vidal, 2011). Only a few studies in Europe have determined the R-factor directly from high-temporal-resolution data (the first approach), including those carried out in Slovenia (Mikos et al., 2006), the Ebro catchment in Spain (Angulo-Martinez et al., 2009), Switzerland (Meusburger et al., 2012), and one of the federal states of Germany, North Rhine Westphalia (Fiener et al., 2013). At the continental scale, a recent study has accounted for the rainfall erosivity in Africa based on time series of 3-hours precipitation data (Vrieling et al., 2014).

In most soil erosion studies, the calculation of rainfall erosivity is limited due to the lack of long-term time series rainfall data with high temporal resolution (< 60 min). Following the second approach (called the empirical approach), equations have been developed to predict R-factor based on rainfall data with lower temporal resolution (Loureiro and Coutinho, 2001, Marker et al., 2007, Diodato and Bellocchi, 2007 and Panagos et al., 2012a). In those cases, expert knowledge of local conditions and seasonal characteristics plays an important role in estimating rainfall erosivity. Authors have suggested that rainfall erosivity equations should be used with caution in different applications, as the empirical relationships are location dependent and, in most cases, cannot be applied to larger areas (Oliveira et al., 2013). Moreover, those empirical equations cannot capture the high rainfall intensities which have significant influence on the average rainfall erosivity. *R*-factor equations developed for a specific region cannot be applied to the whole of Europe.

The main objective of this study is to estimate rainfall erosivity based on high-temporal-resolution precipitation data in Europe. It aims to:

a) present the spatial and temporal extent of high-resolution precipitation data available in Europe,
b) compute rainfall erosivity for 1541 precipitation stations in Europe, and propose a pan-European database of stations with *R*-factor data,
c) produce a European *R*-factor map based on a regression approach,
d) identify spatial patterns and map the relationship of the *R*-factor to precipitation (erosivity density), and

e) identify the possible use of the final *R*-factor dataset in situations beyond soil erosion monitoring.

DATA COLLECTION

The geographical extent of this study includes the 28 Member States of the European Union (EU) plus Switzerland. High-resolution precipitation data were also available for the Swiss territory, which permitted us to avoid the "white lake" effect in the European rainfall erosivity map.

Given the growing concerns about climate change, climatic data is particularly important for the scientific community and society in general, as decisions of individuals, business and governments are dependent on available meteorological data (Freebairn and Zillman, 2002). More than 15 years ago, Peterson et al. (1998) recognized that data infrastructures hosting climatic data are becoming more important and that their contributions are becoming more valuable to policy making.

The present data collection exercise is based on an initiative to develop a network of high-temporal-resolution precipitation stations, which could also be useful for other research purposes such as climate change studies. Generally, climatic data of high temporal resolution are not easily accessible in Europe, or are only available for a fee.

The data collection exercise began in March 2013 and was concluded in May 2014. Previous attempts to collect soil erosion data from Member States used a top-down approach, and the response from countries was rather limited. In a recent top-down data collection exercise, only 8 Member States from a network of 38 countries provided estimates on soil loss (Panagos et al., 2014a). For the present rainfall erosivity data collection exercise, a participatory approach has been followed in order to collect data from all Member States.

The participatory data collection approach followed the steps listed below. Each step was followed in a sequential manner in case the preceding step was not successful:

a) High-temporal-resolution precipitation data are publicly available for download. This was the case for data from the Royal Netherlands Meteorological Institute (Netherlands) only.
b) The European Soil Data Centre (ESDAC) contacted the national meteorological services calling for precipitation data at high temporal resolution. Meteorological services such as Meteo-France, the Deutscher Wetterdienst — DWD (Germany), the Flemish Environmental Agency and the Service Public de Wallonie (Belgium), the Estonian

Environment Agency, the Latvian Meteorology Centre and the Agrarmeteorologisches Messnetz (Luxembourg) responded to this request as some of them have bilateral agreements with the Joint Research Centre, which hosts ESDAC.

c) If the data were not available to ESDAC, recognised scientists of the various meteorological services were invited to participate in this project. Meteorologists from Cyprus, Finland, Croatia, Hungary and Romania participated in estimating the rainfall erosivity of their respective countries, based on their datasets.
d) By means of a literature review, scientists who have developed similar research activities in their countries and have access to or have developed their own R-factor datasets (based on high-temporal-resolution precipitation data) were identified and contacted.
e) High-resolution precipitation datasets were identified in research project databases such as Hydroskopio (Greece) and Sistema National de Recursos Hidricos (Portugal).
f) A review of the 'grey' literature and searches with national language terms led to the discovery of data sources in Lithuania, Slovakia and Poland.

In Italy and Spain, high-resolution precipitation data were collected at the regional level from regional meteorological authorities (Italy) and water agencies (Spain).

The conditions set for the data collection exercise were:

- Continuous records for at least 10 years. If such data were not available, data collected over a period of at least five years were included. Vrieling et al. (2014) also stated that the R-factor may be cumulated for shorter timespans in calculating rainfall erosivity trends.
- Preference was given to datasets that cover the last decade. Where this was not possible, older time series were also included, e.g., for Bulgaria, Greece, the Czech Republic, Poland and Slovakia. As the priority of this study was to capture the spatial trends of rainfall erosivity by averaging erosive events over several years, we consider this time discrepancy to be of minor importance (Table 1).
- Data of up to 60 minute resolution were included.
- In Italy, which has a larger pool of available stations (> 500), 251 stations were selected in order not to bias the pan-European results. A stratified random sample of the Italian stations were selected, covering all climatic conditions (Mediterranean, Continental and Alpine) and all elevation levels.

Table 1. Overview of the precipitation data collected in the presented study for R-factor estimation.

Country		No. of stations	(Main) period covered	Years per station (average)	(Main) temporal resolution: 5 min, 10 min, 15 min, 30 min, 60 min	Source of data
AT	Austria	31	1995–2010	21	12 stations: 10 min 19 stations: 15 min	Hydrographic offices of Upper Austria, Lower Austria, Burgenland, Styria, Salzburg
BE	Belgium	20 29	2004–2013 2004–2013	10 10	Flanders (20 stations): 30 min Wallonia (29 stations): 60 min	Flemish Environmental Agency (VMM), Service Public de Wallonie
BG	Bulgaria	84	1951–1976	26	30 min	Rousseva et al. (2010)
CY	Cyprus	35	1974–2013	39	30 min	Cyprus Department of Meteorology
CZ	Czech Republic	32	1961–1999	35	30 min	Research Institute for Soil and Water Conservation (Czech Republic)
CH	Switzerland	71	1988–2010	22	10 min	Meusburger et al. (2012)
DE	Germany	148	1996–2013	18	60 min	Deutscher Wetterdienst (DWD)
DK	Denmark	30	1988–2012 2004–2012	15	60 min	Danish Meteorological Institute (DMI), Aarhus University
EE	Estonia	20	2007–2013	7	60 min	Estonian Environment Agency
ES	Spain	113	2002–2013	12	14 stations: 10 min, 81 stations: 15 min 18 stations: 30 min	Regional water agencies
FI	Finland	64	2007–2013	7	60 min	Finnish Climate Service Centre (FMI)
FR	France	60	2004–2013	10	60 min	Météo-France DP/SERV/FDP
GR	Greece	80	1974–1997	30	30 min	Hydroskopio
HR	Croatia	42	1961–2012	40	10 min	Croatian Meteo & Hydrological Service
HU	Hungary	30	1998–2013	16	10 min	Hungarian Meteorological Service

Country		No. of stations	(Main) period covered	Years per station (average)	(Main) temporal resolution: 5 min, 10 min, 15 min, 30 min, 60 min	Source of data
IE	Ireland	13	1950–2010	56	60 min	Met Éireann — The Irish National Meteorological Service
IT	Italy	251	2002–2011	10	30 min	Regional meteorological services, Regional agencies for environmental protection (ARPA)
LT	Lithuania	3	1992–2007	16	30 min	Mazvila et al. (2010)
LU	Luxembourg	16	2000–2013	11	60 min	Agrarmeteorologisches Messnetz
LV	Latvia	4	2007–2013	7	60 min	Latvian Environment, Geology and Meteorology Centre
NL	Netherlands	32	1981–2010	24	60 min	Royal Netherlands Meteorological Institute
PL	Poland	9	1961–1988	27	30 min	Banasik et al. (2001)
PT	Portugal	41	2001–2012	11	60 min	Agência Portuguesa do Ambiente
RO	Romania	60	2006–2013	8	10 min	Meteorological Administration
SE	Sweden	73	1996–2013	18	60 min	Swedish Meteorological and Hydrological Institute (SMHI)
SI	Slovenia	31	1999–2008	10	5 min	Slovenian Environment Agency, Petan et al. (2010)
SK	Slovakia	81	1971–1990	20	60 min	Malíšek (1992)
UK	United Kingdom	11	1993–2012	20	60 min	NERC & UK Environ. Change Network (ECN)
		27	2001–2013	11	60 min	British Atmospheric Data Centre (BADC)

Priority was given to datasets with high temporal resolution, independent of the period covered, because the objective of this data collection exercise was to capture the spatial trends of rainfall erosivity. In the majority (> 75%) of countries, the time-series include the first decade of the 21st century, except for Bulgaria, Greece, the Czech Republic, Poland and Slovakia. However, the time-series for those five countries are long enough (> 25 years) to capture the average rainfall erosivity.

Data have been collected from all EU Member States except Malta (the smallest EU Member State). In Malta, precipitation data were available only at a daily time step and, as they do not satisfy the criteria requirement of high temporal resolution, could not be used for *R*-factor estimation. However, Malta is only 80 km distant from the southern Italian island of Sicily, where a very dense network of stations is able to capture the spatial variability of rainfall erosivity. High-temporal-resolution data was available for Poland, but only against payment. In this case, data from literature sources were used.

METHODS

Besides the high-temporal-resolution precipitation data collection, the estimation of the *R*-factor in Europe includes three further steps: a) The calculation of the *R*-factor for each precipitation station, b) the normalisation of *R*-factor values calculated using rainfall data with different time steps (5 min to 60 min), and c) the spatial interpolation of *R*-factor point values.

R-factor calculation

The erosive power of precipitation is accounted for by the rainfall erosivity factor (R-factor), which gives the combined effect of the duration, magnitude and intensity of each rainfall event. In this study, the original RUSLE R-factor equation was used to create an R-factor database of 1541 precipitation stations in Europe.

The R-factor is the product of kinetic energy of a rainfall event (E) and its maximum 30-min intensity (I_{30}) (Brown and Foster, 1987):

$$R = \frac{1}{n}\sum_{j=1}^{n}\sum_{k=1}^{mj}(EI_{30}) \quad (1)$$

where *R* = average annual rainfall erosivity (MJ mm ha^{-1} h^{-1} yr^{-1}), n is the number of years covered by the data records, m_j is the number of erosive events of a given year *j*, and EI_{30} is the rainfall erosivity index of a single event *k*.

The event erosivity EI_{30} (MJ mm ha^{-1} h^{-1}) is defined as:

$$EI_{30} = (\sum_{r=1}^{0} e_r v_r) I_{30} \quad (2)$$

where e_r is the unit rainfall energy (MJ ha^{-1} mm^{-1}) and v_r is the rainfall volume (mm) during a time period r. I_{30} is the maximum rainfall intensity during a 30-min period of the rainfall event (mm h^{-1}). The unit rainfall energy (e_r) is calculated for each time interval as follows (Brown and Foster, 1987):

$$e_r = 0.29[1 - 0.72exp(-0.05i_r)] \quad (3)$$

where i_r is the rainfall intensity during the time interval (mm h^{-1}).

The *R*-factor calculation requires the identification of erosive rainfall events (m_j) for each station. Three criteria for the identification of an erosive event are given by Renard et al. (1997): (i) the cumulative rainfall of an event is greater than 12.7 mm, or (ii) the event has at least one peak that is greater than 6.35 mm during a period of 15 min (or 12.7 mm during a period of 30 min). A rainfall accumulation of less than 1.27 mm during a period of 6 h splits a longer storm period into two storms. The 12.7-mm threshold defines precipitation events that have erosive power. Interestingly, a reduction of the threshold from 12.7 mm to 0 mm leads to an increase in the R-factor of no more than 3.5% (Lu and Yu, 2002).

The Rainfall Intensity Summarisation Tool (RIST) software (USDA, 2014) was used to calculate the R-factor. The RIST can be used for R-factor calculations using precipitation data that have the same temporal resolution (Klik and Konecny, 2013).

Normalization procedure for *R*-factors with different precipitation recording intervals

The precipitation data collected from the 28 countries across Europe have different temporal resolutions: 60-min, 30-min, 15-min, 10-min and 5-min. This variation in temporal resolutions is due to high numbers of data providers (minimum one per country; data from Spain, Italy, Austria, Belgium and the United Kingdom came from more than one data source, see Table 1).

According to the literature, the R-factor is underestimated as time steps increase from 5, 10, 15, 30 to 60 min (Yin et al., 2007 and Williams and Sheridan, 1991). In order to homogenise the R-factor results calculated using different time-step data, conversion factors were established in the present study. The conversion of 60-min-resolution data to very fine resolution introduces quite a high level of uncertainty. As a compromise, the 30-min temporal resolution data was used, even though the most abundant time-step is 60 min. In addition, Yin et al. (2007) recommended that it is not needed to move towards time intervals of less than 30-min to obtain reliable erosivity estimations.

The data at very fine resolution were aggregated to coarse resolutions, and the *R*-factor was estimated for different temporal resolutions. For example, data of 30-min resolution were aggregated to 60-min resolution, and the *R*-factor was calculated both at 30-min and 60-min resolutions. Data of 10-min resolution were aggregated to 30-min resolution, and the *R*-factor was calculated using both 10-min and 30-min resolutions. Regression functions between R-factors based on high and low resolution data were established to normalize the *R*-factor values to 30-min resolution.

Spatial prediction of the *R*-factor

Given the relatively low observation density for the European continent and the huge climatic variability of the study area, interpolation by kriging was not expected to produce realistic results. Instead, given the likely correlation between the R-factor and climatic data, a regression approach was used to infer the distribution of rainfall erosivity from a series of related, but independent, climatic covariates (Goovaerts, 1998). Basically, this approach aims to find a statistical relationship between the property to be predicted and a set of spatially exhaustive covariates. Once this relationship is established, the dependent property, here the R-factor, can be estimated for the area of interest. Various covariates were considered for the regression model, but three main types were identified as being significant:

1. Climatic data: average monthly precipitation, average minimum & maximum monthly precipitation, average monthly temperature, precipitation of the wettest month, precipitation of the driest month and precipitation seasonality (variation of precipitation over seasons). The climatic data are derived from the WorldClim database (Hijmans et al., 2005), which reports monthly averages of precipitation and temperature for the period 1950–2000 at 1-km resolution.
2. Elevation derived from the Digital Elevation Model of the Shuttle Radar Topography Mission (SRTM).
3. Latitude and longitude spatial coordinates, derived from the measuring stations' location, were added explicitly to the regression model in order to model spatial correlation.

In the late 1990's, Goovaerts (1999) introduced the geostatistical interpolation method for calculating rainfall erosivity based on regionalized variables such as elevation. This linear model for spatial R-factor prediction has been widely used because it allows for non-biased estimation at non-sampled points with minimum variance. The high dimensionality (number of degrees of freedom) of the data used and the likely non-linear relation between the target variable and the covariates, discouraged the use of linear regression. Instead, this study

adopted Gaussian Process Regression (GPR) (Rasmussen and Williams, 2006 and Stein, 1999), a non-linear regression approach.

Compared to linear regression, GPR can model non-linear processes by projecting the inputs into some high dimensional space using basis functions and applying linear model in the said space. In this study the Radial Basis Function (RBF) Gaussian kernel has been used; this is a kernel commonly applied in machine learning (Hofmann et al., 2008). The kernel function is equivalent to a covariance function in kriging and its value is considered as a measure of similarity between the two feature vectors. In this respect, GPR is mathematically equivalent to kriging (Stein, 1999); however, while kriging is usually performed on two- or three-dimension geographical space, GPR can be performed over an arbitrary number of covariates, including terrain features and geographical coordinates. The main advantages of GPR are that it can model complex non-linear relations between covariates and the target variable, and directly model both average and variance estimations, thus providing information about prediction uncertainty.

Gaussian Process Regression was selected as the best performing model in terms of cross validation among a series of candidate models (including OLS, GLM, GAM, and Regression Kriging). The criteria chosen for the selection were the minimization of the root-mean squared error and the maximization of the R^2. The GPR model performance was tested for both a fitting and a cross-validation dataset. The cross-validation is carried out by random sampling with 10% replacement of the original dataset used for validation.

RESULTS AND DISCUSSION

Rainfall Erosivity Database on the European Scale (REDES)

In preparing the Rainfall Erosivity Database on the European Scale (REDES), high temporal resolution precipitation data were collected from 1541 precipitation stations within the European Union (EU) and Switzerland, covering a territory of 4,422,661 km^2. The average density of the precipitation stations is one in every 53.5 km × 53.5 km (or 2869 km^2). The variability is quite high, with a dense network of stations in Cyprus and Luxembourg, and a sparse network in Poland and some regions of Spain (Figure 1).

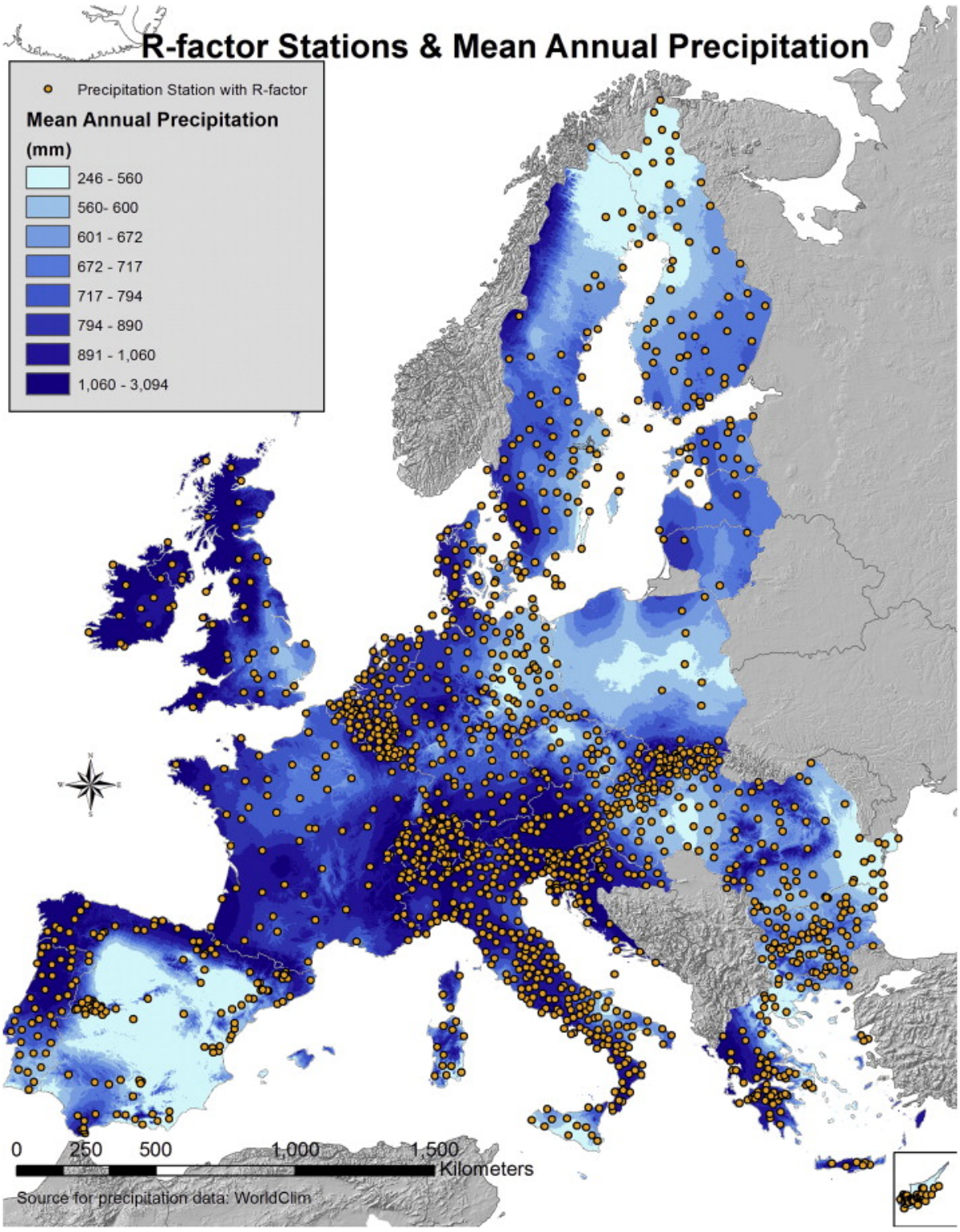

Figure 1. Spatial distribution of precipitation stations used for the R-factor calculation.

Since erosivity varies significantly from year to year, at least 15 years of data are required to obtain representative estimates of annual erosivity (Foster et al., 2003). Oliveira et al. (2013) carried out an extensive literature review (ISI Web of Science, Scopus, SciELO, and

Google Scholar databases) of rainfall erosivity studies using different time series. They identified 35 studies, but only 15% of these used data covering more than 20 years. The Rainfall Erosivity Database on the European Scale (REDES) of precipitation stations is the result of calculating the R-factor for a total of 26,394 years with a mean value of 17.1 years per station (Table 1). In almost all countries, the average time-series per station is more than 10 years, except in Estonia, Finland, Latvia and Romania, where the average recorded period was 7 years.

REDES, with its 1541 precipitation stations, covers all elevation levels. 106 of the stations are at an altitude of more than 1000 m above sea level (asl), in order to reflect the fact that around 6.5% of the total study area has an elevation greater than 1000 m asl. The majority of the stations at high elevations are located in the Alps (Switzerland, Italy, France, Slovenia and Croatia), the Apennines (Italy), Troodos (Cyprus) and Spain.

In terms of the time resolution of precipitation data, 42.3% of the stations (in 13 countries) make hourly recordings, 34.4% make recordings every 30 min (in 8 countries), 6.5% record their data at 15-minute intervals (major part of Spain and Austria), 14.9% make recordings every 10 min (4 countries) and only 2% (in Slovenia) of the data records are at a 5-minute time step.

The availability of data is not scarce in the domain of rainfall intensity. During the past decade (2004–2013), the development of automatic weather stations in many European countries (Belgium, Germany, France, Denmark, Estonia, Finland, Hungary, Italy, Luxembourg, Latvia, Portugal and Romania) led to the generation of more high resolution precipitation data. Besides the data availability, the data quality is considered sufficient for this study as the main source of the high resolution precipitation datasets were the official meteorological services or environmental agencies of the Member States (Table 1). The main limitation was the non-availability of high resolution precipitation data from some Meteorological services (Poland, Slovakia and UK). This limitation will be bypassed by the INSPIRE directive which foresees the data sharing between public authorities. Following the experience of REDES, this data collection can potentially be extended to Norway, Turkey and Balkan states in a later phase.

Conversion factors for different temporal resolutions

Using a very representative pool of stations (in terms of geographical coverage, R-factor values), regression functions have been developed to convert the *R*-factor from different temporal resolutions to 30-min resolutions (Table 2). According to the conversion factors (Table 2), there is a strong underestimation of the *R*-factor (circa 56%) whenever 60-min data are used. The results are in accordance with previous literature findings (Yin et al.,

2007 and Williams and Sheridan, 1991). However, the R^2 values for the regression between *R*-factors calculated using precipitation data with different temporal resolutions show that 60-min data in combination with a conversion factor can be successfully used to estimate the *R*-factor where fine-resolution data are not available (Table 2). The conversion factors for recording time-steps of < 30 min are less than 1, which implies that the homogenised 30-min-based *R*-factor dataset slightly underestimates the "real" rainfall erosivity.

Table 2. Conversion factors for the calibration of temporal resolutions.

Source data resolution	No. of stations	Countries covered	Regression function	R^2 Coefficient of determination
60-min	82	BE, CZ, CH, CY, DE, EE, FR, IT, LU, RO	$R_{30\ min} = 1.5597 \cdot R_{60\ min}$	0.994
15-min	31	BE, ES	$R_{30\ min} = 0.8716 \cdot R_{15\ min}$	0.998
10-min	31	CZ, CY, CH, DE, EE, HR, HU, LU, RO	$R_{30\ min} = 0.8205 \cdot R_{10\ min}$	0.998
5-min	12	CZ, CY, FR, HR, LU	$R_{30\ min} = 0.7984 \cdot R_{5\ min}$	0.998

Unfortunately, in Ireland, UK and Scandinavian countries, no data were available at both resolutions (30-min and 60-min) necessary to contribute to the calibration of temporal resolutions.

Rainfall erosivity in Europe

The mean R-factor of the 1541 precipitation stations included in REDES is 911.3 MJ mm ha^{-1} h^{-1} yr^{-1} with a high standard deviation of 844.9 MJ mm ha^{-1} h^{-1} yr^{-1}as expected due to the high climate variability in Europe. The smallest R-factors were calculated for two stations of the Ebro catchment (Spain), two stations in Slovakia (Gabcikovo, Komarno), and the stations in Tain Range (UK) and Inari Kaamanen (Finland) with values less than 100 MJ mm ha^{-1} h^{-1} yr^{-1}. The maximum values were calculated for five stations in Slovenia (Kneške Ravne, Vogel, Kal Nad Kanalom, Log Pod Mangartom and Lokvein) and one station in north-eastern Italy (Tramonti di Sotto, close to Slovenia) with values greater than 5000 MJ mm ha^{-1} h^{-1} yr^{-1}.

The map of rainfall erosivity in Europe (Figure 2) gives a spatial overview of the erosive energy of rain. The Gaussian Process Regression (GPR) model used to interpolate the R-factor point values to a map showed a good performance for both the cross-validation dataset (R^2 = 0.63) and the fitting dataset (R^2 = 0.72). From the large pool of parameters used in calculating the

R-factor, the precipitation seasonality (coefficient of the variation of seasonal precipitation), latitude and elevation were found to have the strongest influence.

The *R*-factor map (Figure 2) of the 28 European Union Member States and Switzerland has an average value of 722 MJ mm ha^{-1} h^{-1} yr^{-1} and a standard deviation of 478.6 MJ mm ha^{-1} h^{-1} yr^{-1}. The range of R-factor in Europe is 51.4–6228.7 MJ mm ha^{-1} h^{-1} yr^{-1}. The distribution of R-factor values is skewed to the right, with 610 MJ mm ha^{-1} h^{-1} yr^{-1} in the 50th percentile, which implies that a few extremely high values increase the overall mean. The 25% of the study area with the lowest R-factor values (< 410 MJ mm ha^{-1} h^{-1} yr^{-1}) is located in Scandinavia, western UK and eastern Germany (Figure 2). As the definition of high rainfall erosivity depends on the study location, we adopt a statistical approach to define the values in the 4th quartile as high R-factors. The 25% of the study area shows high R-factor values exceeding 900 MJ mm ha^{-1} h^{-1} yr^{-1}. In a quantitative comparison, the rainfall erosivity spatial pattern (Figure 2) is similar to the results produced by Diodato and Bosco (2014). Both studies predicted rainfall erosivity higher than 1000 MJ mm ha^{-1} h^{-1} yr^{-1} in Italy, southern France, Switzerland, Slovenia, western Croatia, Pyrenees, Andalusia, Galicia (Spain) and North Portugal.

The regions found to have the highest rainfall erosivity levels are in line with the three major regions identified by van Delden (2001) as having the highest frequency of thunderstorms. The first region includes the Southern Alps, the Apennines, Istria and Slovenia. The second region includes the gulf of Liguria and Corsica. In both regions the rainfall erosivity exceeded the 1500 MJ mm ha^{-1} h^{-1} yr^{-1} in agreement also with the findings of Diodato and Bosco (2014). The third region expands (in an arch form) from the higher parts of Bavaria in southern Germany, to cross the Swiss plateau and the area close to Dijon, and ends in the Lyon valley. All of those regions have the three characteristics likely to produce thunderstorms: potential instability of atmospheric pressure (indicated by a decrease of the equivalent potential temperature with increasing height), high levels of moisture in the atmospheric boundary layer, and forced lifting (McNulty, 1995). Little thunderstorm activity was found in the Scandinavian countries studied (Finland and Sweden) by van Delden (2001).

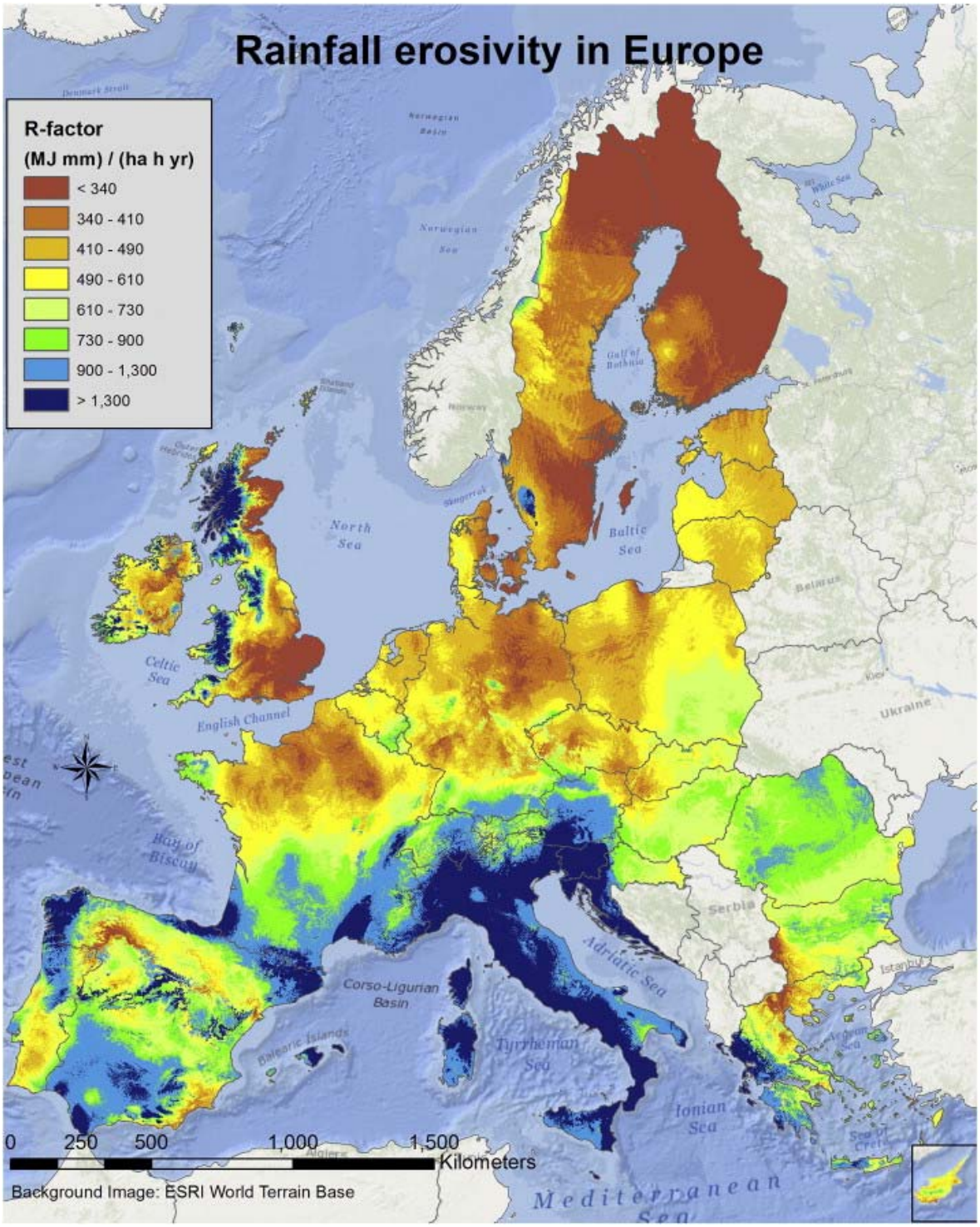

Figure 2. High-resolution (1-km grid cell) map of rainfall erosivity in Europe.

At country level, the highest levels of rainfall erosivity (R-factor) are found in Italy and Slovenia, while Croatia and Austria also have mean values that are greater than 1000 MJ mm ha^{-1} h^{-1} yr^{-1} (Table 3). The lowest values were identified in Sweden and Finland followed by Denmark, the Netherlands and the three Baltic states (EE, LT, LV). The mean R-factor values of all of those North European countries are less than 500 MJ mm ha^{-1} h^{-1} yr^{-1} (Table 3).

Table 3. R-factor descriptive statistics per country.

Country		Mean	Standard deviation	Minimum	Maximum	Coefficient of variation
		MJ mm ha^{-1} h^{-1} yr^{-1}				
AT	Austria	1075.5	517.1	346.9	4345.7	0.48
BE	Belgium	601.5	106.6	412.7	1253.8	0.18
BG	Bulgaria	695.0	151.8	79.8	1447.1	0.22
CH	Switzerland	1039.6	449.3	367.2	4249.6	0.43
CY	Cyprus	578.1	115.1	223.6	1353.5	0.20
CZ	Czech Republic	524.0	118.5	218.0	1093.5	0.23
DE	Germany	511.6	160.9	262.3	1489.3	0.31
DK	Denmark	433.5	93.6	143.8	800.5	0.22
EE	Estonia	444.3	33.2	330.1	568.3	0.07
ES	Spain	928.5	373.0	164.8	3071.2	0.40
FI	Finland	273.0	67.0	65.5	555.6	0.25
FR	France	751.7	353.5	235.2	2661.1	0.47
GR	Greece	827.7	387.6	152.0	2728.5	0.47
HR	Croatia	1276.2	633.5	523.4	3522.7	0.50
HU	Hungary	683.3	73.1	361.4	1000.8	0.11
IE	Ireland	648.6	389.6	205.1	3403.3	0.60
IT	Italy	1642.0	598.0	477.6	6228.8	0.36
LT	Lithuania	484.2	32.6	371.5	605.3	0.07
LU	Luxembourg	674.5	97.6	436.8	1002.8	0.14
LV	Latvia	480.4	42.1	373.9	602.4	0.09
MT	Malta	1672.4	65.6	1491.4	1869.2	0.04
NL	Netherlands	473.3	46.1	348.3	646.0	0.10
PL	Poland	537.1	100.0	247.7	1055.3	0.19
PT	Portugal	775.1	317.5	226.4	2758.1	0.41
RO	Romania	785.0	95.6	462.2	1150.1	0.12
SE	Sweden	378.1	152.6	51.4	2033.8	0.40
SI	Slovenia	2302.0	954.6	757.0	5655.8	0.41
SK	Slovakia	579.7	93.6	330.8	1111.2	0.16
UK	United Kingdom	746.6	604.9	78.1	4107.4	0.81

The coefficient of variation (CV) is used as an indicator to identify the degree of variability of the *R*-factor inside a country. The Netherlands and Baltic States show a very smooth distribution of the *R*-factor, with a CV of less than 10% (Table 3). By contrast, the United Kingdom has a very pronounced erosivity gradient with a CV of more than 81%, with extremely high *R*-factors in Western Wales and Scotland and very low *R*-factors in the eastern parts of England and Scotland. Medium to high variability is found in Croatia (Adriatic coast–

inland), France (north–south gradient) and Greece (west–east gradient). The distribution of the R-factor values in the countries is skewed to the right with the exception of Baltic States, Hungary, Netherlands and Romania (normal).

The rainfall erosivity was further evaluated in the context of climatic zones. The official Biogeographical regions dataset (EEA, 2011) delineates the main climatic zones in Europe, and is independent of political boundaries. The Mediterranean climatic zone, which has hot summers and mild winters, has the highest mean rainfall erosivity, followed by the Alpine zone, which covers the Alps and the Pyrenees (Table 4). The Atlantic zone, which has a humid climate, has a high variability with high erosivity values in northern Spain, western France and western UK, and relatively low R-factor values in the Netherlands, eastern UK and northern France. The highest spatial variability is noticed in Alpine and Continental zones mainly due to orographic effect. The Continental zone, which is characterized by warm summers and cold winters, is the largest climatic zone and also has a high variability of rainfall erosivity. The Boreal zone (which is dominated by forests) includes the greater part of Scandinavia and the Baltic states, and has the lowest R-factor. The Boreal zone has a relatively low variability of rainfall erosivity considering its spatial extent. The mean R-factor of the Pannonian zone, also known as the central Danubian basin, is similar to that of Hungary. Finally, the Black Sea and Steppic zones have a relatively minor spatial extent in the study area, covering the eastern parts of Bulgaria and Romania. The third highest R-factors were mapped for this climatic zone.

Table 4. R-factor descriptive statistics per biogeographical region.

Climatic zone	Proportion of the study area	Mean	Standard deviation	Coefficient of variation
	%	MJ mm ha^{-1} h^{-1} yr^{-1}		
Alpine	9.2	932.3	666.9	0.72
Atlantic	17.7	678.2	446.7	0.66
Black Sea	0.2	702.1	144.8	0.21
Boreal	19.1	359.5	126.6	0.35
Continental	29.7	695.7	394.3	0.57
Mediterranean	20.4	1050.6	502.0	0.48
Pannonian	2.9	660.1	100.5	0.15
Steppic	0.8	729.8	91.0	0.12

The *R*-factor map (Figure 2) and the related statistics (Table 3 and Table 4) can be used for soil erosion modelling at European and national scale. At regional or local scale, it is recommended to modellers to use REDES plus local high resolution data for making their interpolations. Combining the relatively high *R*-factor values with the relatively high *K*-factor

values (> 0.038 t ha h ha^{-1} MJ^{-1} mm^{-1}) of the soil erodibility dataset (Panagos et al., 2014b), the modellers may identify the areas at high risk of soil erosion. The development of the remaining factors (topography, support practices, land use and management practices) will contribute to the perfecting of soil erosion modelling at the European scale. Furthermore, the calculation of monthly R-factor values in REDES will contribute to the seasonal estimation of rainfall erosivity in Europe.

Erosivity density

In the present study, the erosivity density is used for a post-assessment of rainfall erosivity patterns and type of precipitation involved in erosive events in Europe. Annual erosivity density is the ratio of the mean annual erosivity to the mean annual precipitation (Kinnell, 2010). In practice, erosivity density (ED) measures the erosivity per rainfall unit (mm), and is expressed as MJ ha^{-1} h^{-1}.

$$ED = R/P \quad (4)$$

where R is the average annual rainfall erosivity (MJ mm ha^{-1} h^{-1} yr^{-1}) and P is the average annual rainfall (mm yr^{-1}) according to the WorldClim database (Hijmans et al., 2005).

According to WorldClim statistics, the mean annual precipitation in the study area is 788.4 mm with a range from 246 to 3094 mm and a standard deviation of 253 mm (Figure 1). High erosivity density areas indicate that the precipitation is characterised by high intensity events of short duration (rainstorms). Particularly high erosivity density is observed in Italy, Slovenia and Spain (Figure 3), where the R-factor is 2–3 times higher than the amount of precipitation. By contrast, the rain distribution is much smoother in the northern parts of Europe (northern Germany, France, and the Netherlands), where relatively high amounts of precipitation have a smaller erosive effect (Figure 3).

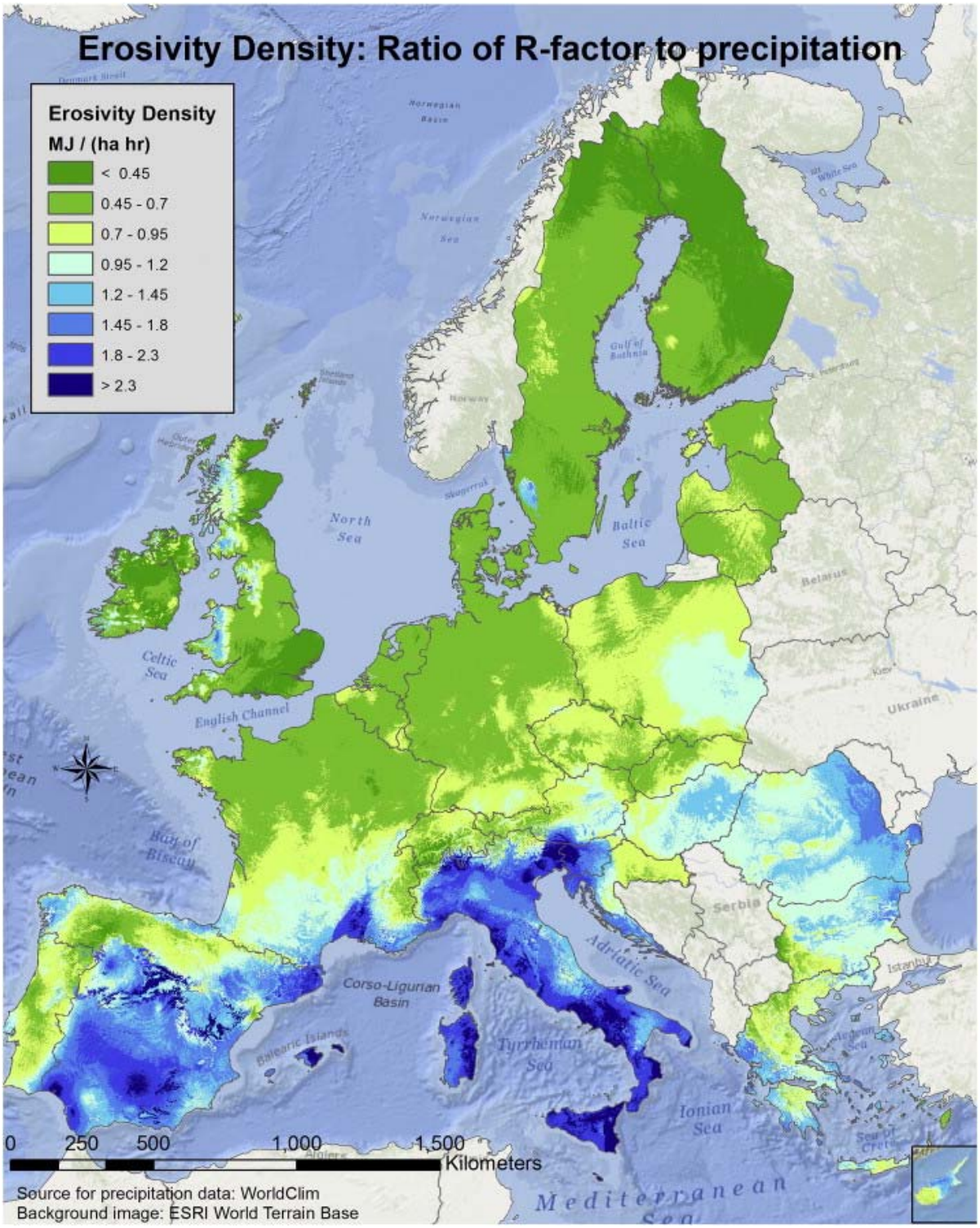

Fig. 3. Erosivity density (rainfall erosivity per mm of precipitation).

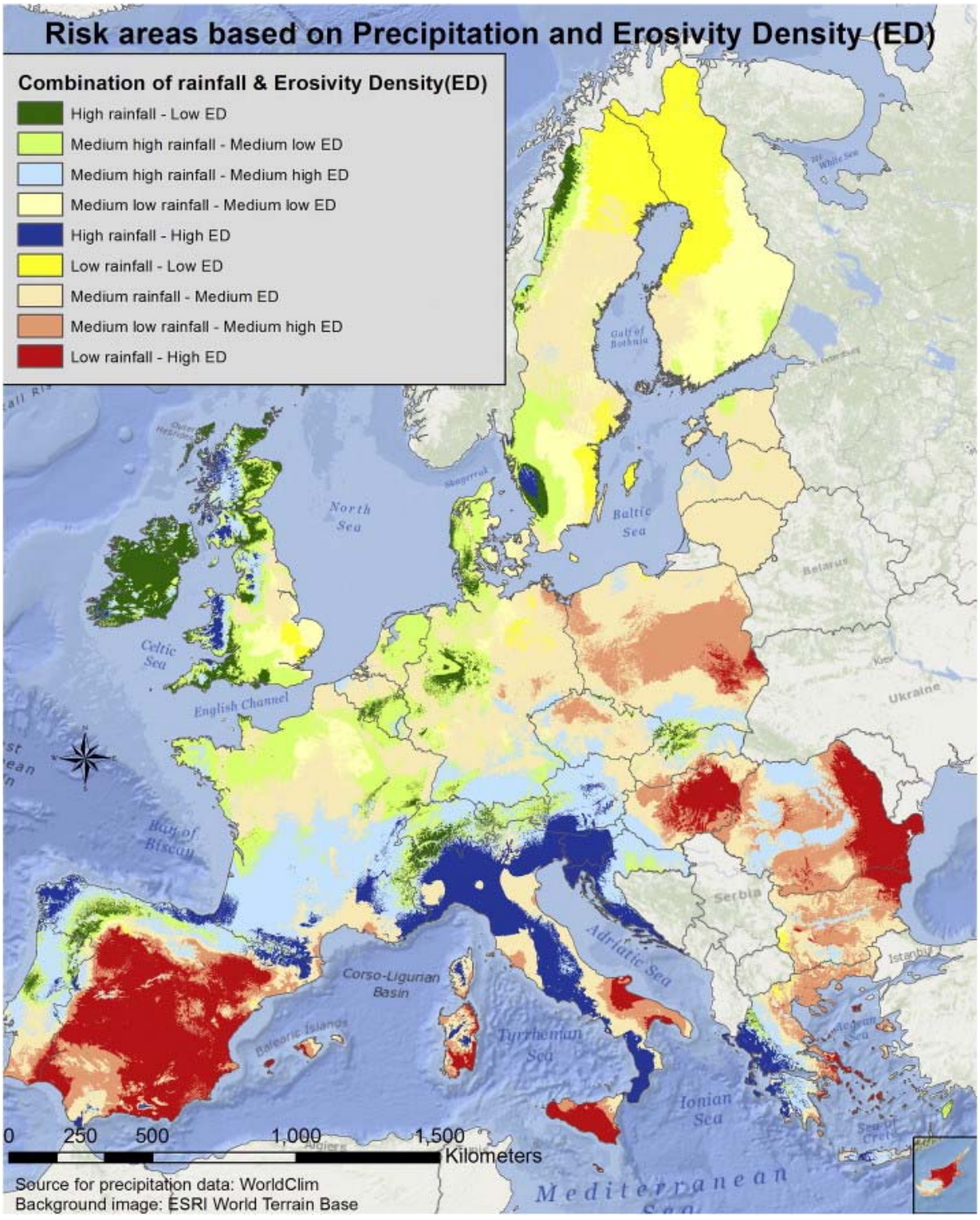

Figure 4. Risk areas based on precipitation and erosivity density.

The erosivity density has a mean value of 0.92 MJ ha^{-1} h^{-1}, with high variability ranging from 0.1 to 4.47 MJ ha^{-1} h^{-1}. This high variability highlights the fact that rainfall erosivity is not solely dependent on the amount of precipitation. Consequently, it is impossible to predict the R-factor in Europe exclusively based on precipitation levels. Regional patterns can be identified, and although regression functions may be developed, they cannot be extrapolated to other regions with different climatic characteristics.

The erosivity density may contribute to the identification of risk areas, taking into account the precipitation volume. The precipitation (Figure 1) and erosivity density (Figure 3) datasets have been classified in nine combined categories that represent the four quartiles of each parameter. The highest risk is identified in areas where low annual mean precipitation is accompanied by high erosivity. Thus, highly erosive rainfall hits long-period dry soils which usually causes great damage and is connected to a very high flood risk (Diodato et al., 2011).

We define this category as the highest overall risk (1st quartile of precipitation volume which is less than 600 mm annually) with values of erosivity density higher than 1.2 MJ ha^{-1} h^{-1} (4th quartile). The lowest risk is identified in those areas where, even though annual precipitation levels are high, the precipitation is relatively homogenously distributed and therefore has low erosivity (green in Figure 4). Dry soils, which account for 9.6% of the study area, are identified in central and southern Spain, Sicily, Sardinia and Puglia (IT), the Greek islands, Cyprus, western Romania and central Hungary (Figure 4). Most of Ireland, the northern United Kingdom and small parts of Germany were found to have the lowest risk (4th quartile of precipitation which is higher than 890 mm annually), with erosivity density values that are lower than 0.55 (1st quartile). The combination of high levels of rainfall and high erosivity densities (blue areas in Figure 4) may also be associated with some risk: high rainfall amounts falling on moist or even saturated soils could trigger landslides or wetland erosion.

Mapping of rainfall erosivity and related uncertainties

Catari et al. (2011) identified the following main sources of uncertainty in estimating rainfall erosivity:

1) measurement errors of precipitation stations,
2) the efficiency of the equation used (methodology) to derive the kinetic energy of rainfall from its intensity,
3) the efficiency of regressions obtained between daily precipitation (or even annual precipitation) levels and the R-factor,
4) the temporal variability of annual rainfall erosive values, and
5) the spatial variability.

The third point is not addressed here, as the R-factor values were calculated based on high temporal resolution precipitation data. While the calibration of different temporal resolutions could be considered to be a source of uncertainty, this source of uncertainty is minimised by the amount of experimental data and the excellent performance of the regression functions used (Table 4).

With respect to instrumental errors, the participatory approach of involving the major meteorological services in Europe has a high likelihood of yielding high data quality. In addition, the RIST software calculates all the individual erosive events. Possible outliers (single events of > 1000 MJ mm ha^{-1} h^{-1}) were verified with the source data. The RUSLE R-factor equation used to derive rainfall kinetic energy from intensity (see Eq. (3)) is empirical and was derived from long-term experiments (Brown and Foster, 1987). It is applied in the majority of studies worldwide.

In the present study, the uncertainty due to temporal variability is lessened by averaging long-term time-series (average 17.1 years per station). Regarding the spatial uncertainty, the extensive data collection exercise was carried out on a dense network with good geographical coverage. Furthermore, the dataset is representative of all possible elevation and climatic levels covered in the regression analysis.

The application of the Gaussian Process Regression (GPR) spatial interpolation model allowed us to derive not only the R-factor but also the standard error of the estimate. In this study, the map of standard error (Figure 5) was directly used to estimate the uncertainty of the prediction model. Using the standard error to estimate the dispersion of prediction errors, the highest uncertainty was found to be in north-western Scotland, north-western Sweden and northern Finland due to the relatively small number of precipitation stations and high diversity of environmental features (Figure 5). The model prediction was also found to have increased uncertainty levels in the southern Alps and the Pyrenees. Medium uncertainty is noticed in Spain, northern Poland, the west of Ireland, North Cyprus and the Aegean islands due to a lack of stations. In general, the model had a good prediction rate with low standard errors in the majority of the study area.

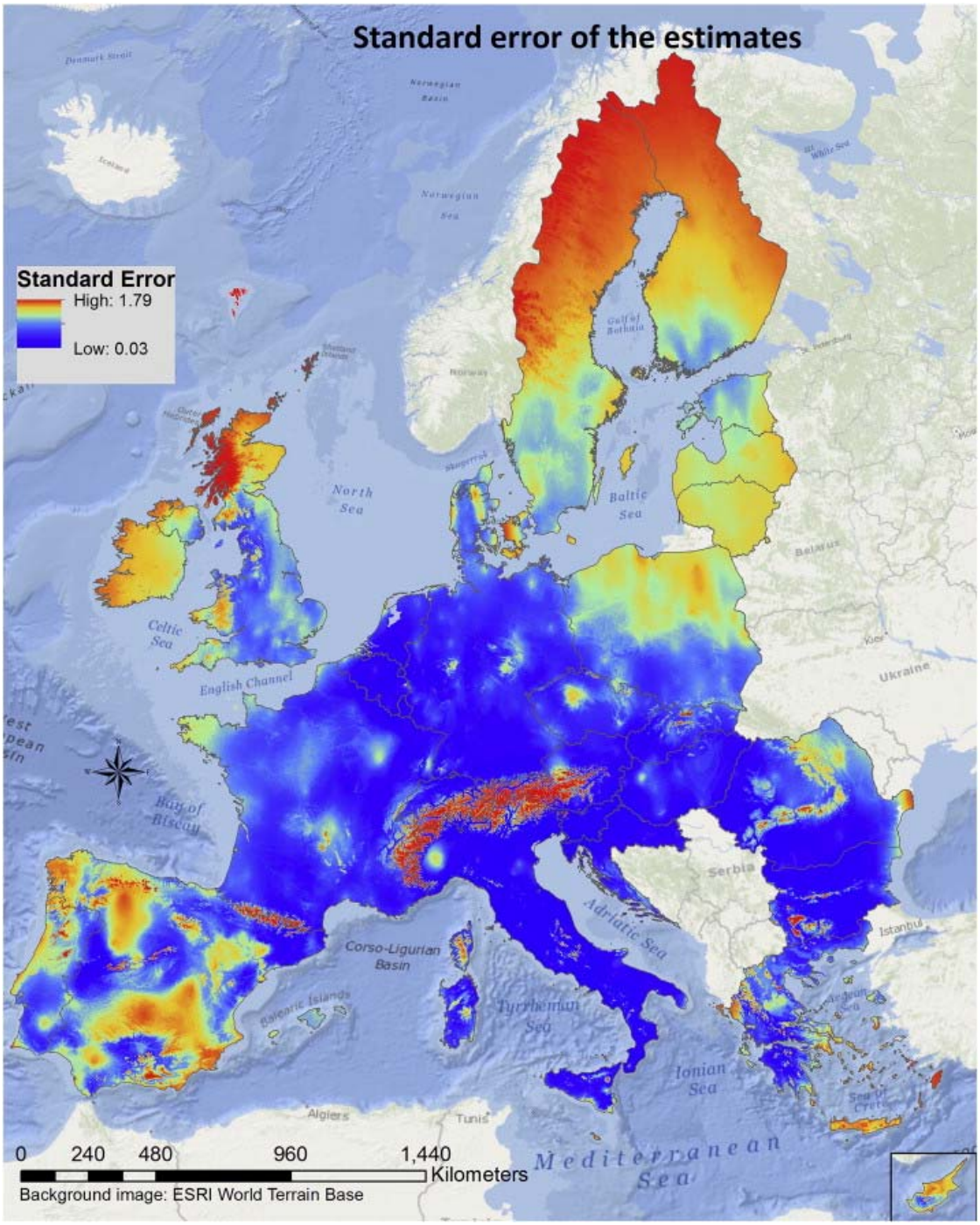

Fig. 5. Uncertainty of the R-factor prediction calculated with the GPR spatial interpolation model.

Potential applications of *R*-factor dataset

Rainfall erosivity (*R*-factor) in Europe is a key parameter for estimating soil erosion loss and soil erosion risk, but the use of this dataset can be widely extended to other applications. The R-factor dataset can be used by landslide experts as a predictor to improve landslide susceptibility assessment in Europe (Günther et al., in press). The landslide susceptibility map

is the spatial probability of generic landslide occurrence based on topographic and climatic conditions.

Flood risk is of crucial importance for civil protection, due to the large numbers of people affected and the related economic costs. According to Barredo (2007), 40% of the flood-related casualties in Europe during the period 1950–2006 were due to flash floods. Flash floods are associated with short and high-intensity rainfall events, and their likelihood of occurrence increases exponentially when such rainfall events occur on dry and hydrophobic soils (see Figure 4). Flash flood occurrence is generally more intense in Mediterranean countries than in continental areas (Marchi et al., 2010), in line with the rainfall erosivity pattern. Differences in the spatial and temporal scales of the rainfall events (and rainfall erosivity) should be taken into account in the design of flash flood forecasting and warning systems.

Most forest fires in Europe occur in the south — 75% of the total area burnt every year in the European Union is located in Portugal, Spain, the south of France, Italy, Greece and Cyprus (European Commission, 2009). The post-fire effect in areas that are susceptible to highly erosive events may accelerate the risk of flash floods and soil loss due to lack of vegetative protection. The rapid damage assessment carried out by the European Forest Fire Information System (EFFIS) (San-Miguel-Ayanz et al., 2012) generates burnt area maps at 250-m spatial resolution. In combination with the R-factor dataset, such maps can help identify areas that are at high risk of soil erosion, in order to decide where critical prevention measures should be swiftly applied so as to avoid further disasters.

In the context of the European Common Agricultural Policy (CAP), sustainable agricultural practices should take into account the soil and water resources and specific local or regional conditions such as climate. As an example, Renschler et al. (1999)showed the high impact of rainfall erosivity in evaluating the vulnerability of different crop rotation scenarios in Andalusia. It has been found that extreme rainfall events and high erosivity can reduce or completely destroy yields of permanent crops (olives, vineyards, fruit trees), which are of particular importance in the Mediterranean (Maracchi et al., 2005). The R-factor dataset should therefore be taken into account in the application of crop-rotation scenarios, agricultural management, and conservation policies.

REDES can also be used to identify the trends and threats of climate change. It was found that the increase of extreme rainfall events between 1960 and 2001 in the Carpathian region (Romania, Slovakia, Czech Republic, Hungary, southern Poland) was coupled with a lower frequency, leading to constant precipitation totals (Bartholy and Pongrácz, 2007). On the other hand, Fiener et al. (2013) and Verstraeten et al. (2006) have reported higher erosivity

values in their areas of study (North Rhine Westphalia, Ukkel) after the 1990s. Also, Diodato et al. (2011) have found increased erosive events in low Mediterranean latitudes in the last 50 years. Future research will focus on subset of REDES precipitation stations with high temporal scale (< 30 min) and long continuous records (> 20 years) well distributed in Europe. The objective will be to identify trends of rainfall erosivity in Europe and incorporate them in future climatic scenarios for predicting soil loss.

The R-factor data availability is a key issue for modellers who have no access to high temporal resolution data. With the publication of this study, modellers and in general scientists will be able to download the R-factor dataset from the European Soil Data Centre (Panagos et al., 2012b). Besides the application for soil erosion modelling, the European rainfall erosivity dataset can be used in different areas such as landslide risk assessment, flood risk forecasting, post-fire conservation measures, agricultural management and design of crop rotation scenarios.

CONCLUSIONS

The R-factor was successfully mapped at 1-km grid cell resolution for the European Union and Switzerland, applying the Gaussian Process Regression model. The spatial interpolation model showed a very good performance (R^2 = 0.62 for the cross validation, R^2 = 0.73 for the fitting dataset). The low number of stations and the high diversity of environmental features resulted in high prediction uncertainty in North Scandinavia, West Ireland, Scotland, high Alps and parts of Spain. The high variability of climatic and terrain conditions in an area of more than 4.4 million km^2 resulted in a broad spectrum of rainfall erosivity, ranging from 51.4 to 6228.7 MJ mm ha^{-1} h^{-1} yr^{-1}, with a mean value of 722 MJ mm ha^{-1} h^{-1} yr^{-1}. The Mediterranean and Alpine regions were found to have the highest R-factor values, while Scandinavia countries were found to have the lowest.

There is a large amount of data available regarding rainfall intensity. The inclusive participatory data collection approach applied in this study showed that high temporal precipitation data is available free of charge for the European Union. Even though the selected approach was time-consuming and requested laborious pre-processing, it has resulted in Rainfall Erosivity Database at European Scale (REDES), with R-factor estimations for 1541 stations across Europe.

Due to different temporal resolutions of input data, the proposed conversion to 30-min based R-factor was an important step towards a homogeneous database. Comparisons between different temporal resolutions showed that the use of 60-min precipitation data for the

calculation of the R-factor results in a strong underestimation (56%) compared to the use of 30-min data.

Using the large number of R-factor stations available on a large scale (Europe), it was found that R-factor does not solely depend on precipitation. The erosivity density indicator showed that the R-factor per unit of precipitation is highly variable. Therefore, the choice of regression equations should be made with caution and should be based on local climate studies and high temporal resolution data. The Mediterranean countries and the Alpine areas have a relatively high erosivity density and high rainstorm frequency compared to northern Europe, where the erosivity density is much lower. Furthermore, an assessment of the erosivity density and the risk areas which combine low amounts of precipitation with high erosivity density demonstrates that the Mediterranean regions have the highest risk not only of erosive events, but also of floods and/or water scarcity.

Conflict of interest

The authors confirm and sign that there is no conflict of interests with networks, organizations, and data centers referred in the paper.

Acknowledgements

The authors would like to thank Gráinne Mulhern for the revision of the article from a linguistic point of view. The authors would also like to acknowledge the following services for providing access to their data:

Austria: Hydrographic offices of Upper Austria, Lower Austria, Burgenland, Styria, Salzburg

Belgium-Flanders: Flemish Environmental Agency (VMM), Operational Water Management

Belgium-Wallonia: Service public de Wallonie, Direction générale Mobilité et Voies hydrauliques, Direction de la Gestion hydrologique intégrée, Namur

Bulgaria: Rousseva et al. (2010)

Cyprus: Cyprus Department of Meteorology.

Germany: Deutscher Wetterdienst (DWD), WebWerdis Service

Denmark: Aarhus University, Department of Agroecology

Estonia: Client service department, Estonian Environment Agency, Tallinn

Spain: Confederaciones Hidrográficas del Ebro, Tajo, Duero, Guadalquivir, Segura, Júcar, Miño-Sil, Cantábrico and Sur, Servei Meteorològic de Catalunya, and Meteo Navarra

France: Météo-France DP/SERV/FDP, Division Fourniture de Données Publiques

Greece: Hydroskopio

Croatia: Meteorological and Hydrological Service

Hungary: Hungarian Meteorological Service

Ireland: Data from Met Éireann, financial support from Irish EPA STRIVE Programme-SILTFLUX (2010-W-LS-4) and UCD Earth Institute

Italy: the Servizio Idrografico Abruzzo, Protezione Civile Regione Basilicata, Ufficio idrografico Bolzano, Servizio Idrografico Friuli-Venezia Giulia, Centro funzionale regione Lazio, Meteotrentino, Agenzia Regionale per lo Sviluppo e l'Innovazione dell'Agricoltura nel Molise, Servizio Meteo-Idro-Pluviometrico Marche, Associazione Regionale dei Consorzi di Difesa della Puglia, Osservatorio delle Acque Sicilia, Servizio Idrologico Regionale Toscana, Servizio Risorse idriche e rischio idraulico Umbria, Diodato Nazzareno from Regione Campagna, Centro funzionale regionale Valle d'Aosta and the Hydro-Meteo-Climate Service of the Environmental Agency ARPA Calabria, ARPA Emilia Romagna, ARPA Liguria, ARPA Lombardia, ARPA Piemonte, ARPA Veneto

Latvia: Latvian Environment, Geology and Meteorology Centre, Riga

Lithuania: Mazvila et al. (2010)

Luxembourg: Agrarmeteorologisches Messnetz Luxembourg

Netherlands: KNMI, Royal Netherlands Meteorological Institute

Portugal: Agência Portuguesa do Ambiente, Departamento de Monitorização de Recursos Hídricos

Poland: Banasik et al. (2001)

Romania: National Meteorological Administration

Slovakia: Malíšek (1992), Jan Styk and Jozef Kobza from Soil Science and Conservation Research Institute Bratislava

Slovenia: Slovenian Environment Agency, Petan et al. (2010)

Sweden: Swedish Meteorological and Hydrological Institute (SMHI)

United Kingdom: NERC & UK Environmental Change Network (ECN), and British Atmospheric Data Centre (BADC).

References

Angulo-Martinez, M., Lopez-Vicente, M., Vicente-Serrano, S.M., Begueria, S., 2009. Mapping rainfall erosivity at a regional scale: a comparison of interpolation methods in the Ebro Basin (NE Spain). Hydrol. Earth Syst. Sci. 13, 1907–1920.

Banasik, K., Górski, D., Mitchell, J.K., 2001. Rainfall erosivity for east and central Poland. Soil Erosion Research for the 21st Century Proceedings. Amer Soc Agr. Engineers, pp. 279–282.

Barredo, J.I., 2007. Major flood disasters in Europe: 1950–2005. Nat. Hazards 42 (1), 125–148.

Bartholy, J., Pongrácz, R., 2007. Regional analysis of extreme temperature and precipitation indices for the Carpathian Basin from 1946 to 2001. Glob. Planet. Chang. 57 (1), 83–95.

Bonilla, C.A., Vidal, K.L., 2011. Rainfall erosivity in Central Chile. J. Hydrol. 410 (1–2), 126–133.

Brown, L.C., Foster, G.R., 1987. Storm erosivity using idealized intensity distributions. Trans. ASAE 30, 379–386.

Catari, G., Latron, J., Gallart, F., 2011. Assessing the sources of uncertainty associated with the calculation of rainfall kinetic energy and erosivity — application to the Upper Llobregat Basin, NE Spain. Hydrol. Earth Syst. Sci. 15, 679–688.

Dale, V.H., Polasky, S., 2007. Measures of the effects of agricultural practices on ecosystem services. Ecol. Econ. 64 (2), 286–296.

Diodato, N., Bellocchi, G., 2007. Estimatingmonthly (R)USLE climate input in aMediterranean region using limited data. J. Hydrol. 345 (3–4), 224–236.

Diodato, N., Bosco, C., 2014. Spatial pattern probabilities exceeding critical threshold of annual mean storm-erosivity in Euro-Mediterranean areas. In: Diodato, N., Bellocchi, G. (Eds.), Storminess and Environmental Change: Climate Forcing and Responses in the Mediterranean Region. Springer, Dordrecht, pp. 79–99.

Diodato, N., Bellocchi, G., Romano, N., Chirico, G.B., 2011. How the aggressiveness of rainfalls in the Mediterranean lands is enhanced by climate change. Clim. Chang. 108 (3), 591–599.

Dominati, E., Patterson,M.,Mackay, A., 2010. A framework for classifying and quantifying the natural capital and ecosystem services of soils. Ecol. Econ. 69 (9), 1858–1868.

EEA, 2011. Biogeographical Regions Dataset of European Environment Agency. Accessed from, http://www.eea.europa.eu/data-and-maps/data/biogeographical-regionseurope (June 2014).

European Commission, 2009. Forest Fires in Europe 2008. Office for Official Publications of the European Communities, Luxemburg, EUR 23971 ENp. 77.

Fiener, P., Neuhaus, P., Botschek, J., 2013. Long-term trends in rainfall erosivity-analysis of high resolution precipitation time series (1937–2007) fromWestern Germany. Agric. For. Meteorol. 171–172, 115–123.

Foster, G.R., Yoder, D.C., Weesies, G.A., McCool, D.K., McGregor, K.C., Bingner, R.L., 2003. Draft User's Guide, Revised Universal Soil Loss Equation Version 2 (RUSLE-2). USDA-Agricultural Research Service, Washington, DC.

Freebairn, J.W., Zillman, J.W., 2002. Economic benefits of meteorological services. Meteorol. Appl. 9 (1), 33–44.

Goovaerts, P., 1998. Geostatistical tools for characterizing the spatial variability of microbiological and physico-chemical soil properties. Biol. Fertil. Soils 27 (4), 315–334.

Goovaerts, P., 1999. Using elevation to aid the geostatistical mapping of rainfall erosivity. Catena 34, 227–242.

Günther, A., Van Den Eeckhaut, M., Malet, J.-P., Reichenbach, P., Hervás, J., 2015. Climate-physiographically differentiated Pan-European landslide susceptibility assessment using spatial multi-criteria evaluation and transnational landslide information. Geomorphology http://dx.doi.org/10.1016/j.geomorph.2014.07. 011 (in press).

Hijmans, R.J., Cameron, S.E., Parra, J.L., Jones, P.G., Jarvis, A., 2005. Very high resolution interpolated climate surfaces for global land areas. Int. J. Climatol. 25, 1965–1978.

Hofmann, T., Schölkopf, B., Smola, A.J., 2008. Kernel methods in machine learning. Ann. Stat. 1171–1220.

Kinnell, P.I.A., 2010. Event soil loss, runoff and the Universal Soil Loss Equation family of models: a review. J. Hydrol. 385, 384–397.

Klik, A., Konecny, F., 2013. Rainfall erosivity in northeastern Austria. Trans. ASABE 56 (2), 719–725.

Loureiro, N.D., Coutinho, M.D., 2001. A new procedure to estimate the RUSLE EI30 index, based on monthly rainfall data and applied to the Algarve region, Portugal. J. Hydrol. 250, 12–18.

Lu, H., Yu, B., 2002. Spatial and seasonal distribution of rainfall erosivity in Australia. Aust. J. Soil Res. 40, 887–991.

Malíšek, A., 1992. Optimal slope length in accordance with soil erosion (in Slovak). VÚPÚ Bratislava.

Maracchi, G., Sirotenko, O., Bindi,M., 2005. Impacts of present and future climate variability on agriculture and forestry in the temperate regions: Europe. Clim. Chang. 70 (1–2), 117–135.

Marchi, L., Borga, M., Preciso, E., Gaume, E., 2010. Characterisation of selected extreme flash floods in Europe and implications for flood risk management. J. Hydrol. 394 (1–2), 118–133.

Marker, M., et al., 2007. Assessment of land degradation susceptibility by scenario analysis: a case study in Southern Tuscany, Italy. Geomorphology 93, 120–129.

Marques, M.J., Bienes, R., Jimenez, L., Perez-Rodriguez, R., 2007. Effect of vegetal cover on runoff and soil erosion under light intensity events. Rainfall simulation over USLE plots. Sci. Total Environ. 378 (1–2), 161–165.

Mazvila, J., Staugaitis, G., Kutra, G.J., Jankauskas, B., 2010. Empirinių modelių panaudojimas dirvožemių erozingumo įvertinimui Lietuvoje. Agric. Sci. 17 (3–4), 69–78.

McNulty, R.P., 1995. Severe and convective weather: a central region forecasting challenge. Weather Forecast. 10, 187–202.

Meusburger, K., Steel, A., Panagos, P., Montanarella, L., Alewell, C., 2012. Spatial and temporal variability of rainfall erosivity factor for Switzerland. Hydrol. Earth Syst. Sci. 16. http://dx.doi.org/10.5194/hess-16-1-2012.

Mikos, M., Jost, D., Petkovsek, G., 2006. Rainfall and runoff erosivity in the alpine climate of north Slovenia: a comparison of different estimation methods. Hydrol. Sci. J. 51, 115–126.

Oliveira, P.T.S.,Wendland, E., Nearing, M.A., 2013. Rainfall erosivity in Brazil: a review. Catena 100, 139–147.

Panagos, P., Karydas, C.G., Gitas, I.Z., Montanarella, L., 2012a. Monthly soil erosion monitoring based on remotely sensed biophysical parameters: a case study in Strymonas river basin towards a functional pan-European service. Int. J. Digit. Earth 5 (6), 461–487.

Panagos, P., Van Liedekerke,M., Jones, A.,Montanarella, L., 2012b. European soil data centre: response to European policy support and public data requirements. Land Use Policy 29 (2), 329–338.

Panagos, P., Meusburger, K., Van Liedekerke,M., Alewell, C., Hiederer, R., Montanarella, L., 2014a. Assessing soil erosion in Europe based on data collected through a European Network. Soil Sci. Plant Nutr. 60 (1), 15–29.

Panagos, P., Meusburger, K., Ballabio, C., Borrelli, P., Alewell, C., 2014b. Soil erodibility in Europe: a high-resolution dataset based on LUCAS. Sci. Total Environ. 479–480 (2014), 189–200.

Petan, S., Rusjan, S., Vidmar, A., Mikos,M., 2010. The rainfall kinetic energy-intensity relationship for rainfall erosivity estimation in the Mediterranean part of Slovenia. J. Hydrol. 391 (3–4), 314–321.

Peterson, T.C., Vose, R., Schmoyer, R., Razuvaev, V., 1998. Global historical climatology network (GHCN) quality control of monthly temperature data. Int. J. Climatol. 18 (11), 1169–1179.

Pimentel, D., Harvey, C., Resosudarmo, P., Sinclair, K., Kurz, D., McNair, M., Crist, S., (…), Blair, R., 1995. Environmental and economic costs of soil erosion and conservation benefits. Science 267 (5201), 1117–1123.

Renschler, C.S., Mannaerts, C., Diekkruger, B., 1999. Evaluating spatial and temporal variability in soil erosion risk - Rainfall erosivity and soil loss ratios in Andalusia, Spain. Catena 34 (3–4), 209–225.

Rasmussen, C.E., Williams, C.K.I., 2006. Gaussian Processes for Machine Learning. MIT Press.

Renard, K.G., et al., 1997. Predicting Soil Erosion by Water: A Guide to Conservation Planning with the Revised Universal Soil Loss Equation (RUSLE) (Agricultural Handbook 703). US Department of Agriculture, Washington, DC, p. 404.

Rousseva, S., Lozanova, L., Nekova, D., Stefanova, V., Ch, Djodjov, Tsvetkova, E., Malinov, I., Kroumov, V., Chehlarova-Simeonova, S., 2010. Soil Erosion Risk in Bulgaria and Recommendations for Soil Protective Use of Agricultural Land. Part I: Northern Bulgaria (304 pp) & Part II Southern Bulgaria (320 pp).

San-Miguel-Ayanz, J., Schulte, E., Schmuck, G., Camia, A., et al., 2012. Comprehensive monitoring of wildfires in Europe: the European Forest Fire Information System (EFFIS). In: Tiefenbacher, John (Ed.), Approaches to Managing Disaster — Assessing Hazards, Emergencies and Disaster Impacts. InTech http://dx.doi.org/10.5772/28441.

Stein, M.L., 1999. Interpolation of Spatial Data: Some Theory for Kriging. Springer.

USDA, 2014. United States Department of Agriculture. Rainfall Intensity Summarization

Tool (RIST). Accessed from, http://www.ars.usda.gov/News/docs.htm?docid=3251 (Jun 2014).

van Delden, 2001. The synoptic setting of thunderstorms in western Europe. Atmos. Res. 56, 89–110.

Verstraeten, G., Poesen, J., Demaree, G., Salles, C., 2006. Long-term (105 years) variability in rain erosivity as derived from 10-min rainfall depth data for Ukkel (Brussels, Belgium): implications for assessing soil erosion rates. J. Geophys. Res. 111, D22.

Vrieling, A., Hoedjes, J.C.B., van der Velde,M., 2014. Towards large-scale monitoring of soil erosion in Africa: accounting for the dynamics of rainfall erosivity. Glob. Planet. Chang. 115, 33–43.

Williams, R.G., Sheridan, J.M., 1991. Effect of measurement time and depth resolution on EI calculation. Trans. ASAE 34 (2), 402–405.

Wischmeier, W., Smith, D., 1978. Predicting rainfall erosion losses: a guide to conservation planning. Agricultural Handbook No. 537. U.S. Department of Agriculture, Washington DC, USA.

Yin, S., Xie, Y., Nearing,M.A.,Wang, C., 2007. Estimation of rainfall erosivity using 5- to 60-minute fixed-interval rainfall data from China. Catena 70, 306–312

STUDIE 4: Monthly rainfall erosivity: conversion factors for different time resolutions and regional assessments

Panos Panagos, Pasquale Borrelli, Jonathan Spinoni, Cristiano Ballabio, Katrin Meusburger, Andreas Klik, Svetla Rousseva, Melita Perčec Tadić, Silas Michaelides, Michaela Hrabalíková, Preben Olsen, Juha Aalto, Mónika Lakatos, Anna Rymszewicz, Alexandru Dumitrescu, Santiago Beguería, Julia Kostalova, Sašo Petan, Kazimierz Banasik, Christine Alewell

Science of the Total Environment (accepted manuscript, under revision)

Abstract: Recently a Rainfall Erosivity Database at European Scale (REDES) has been established and a mean annual R-factor map based on high temporal resolution data was created. This study deals with the expansion of REDES by 140 rainfall stations, covering areas where monthly R-factor values were missing (Slovakia, Poland) or where former data density was low (Austria, France, and Spain). The different time resolutions (5 minutes, 10 minutes, 15 minutes, 30 minutes and 60 minutes) of high temporal data require a conversion of monthly R-factor based on a pool of stations with available data at all-time resolutions. On average, the R-factor at 5-minutes is 10% higher than the one estimated at 15-minutes and 95% higher than the one estimated with hourly data. However, those factors have a monthly variability as the smoother differences are found in winter months (January: 1.54) and the sharper ones in summer months (August: 2.13). The estimated monthly conversion factors allow transferring the measured R-factor to the desired time resolution. After the normalization of the monthly R-factor values at a 30- min temporal resolution, it is possible to estimate the monthly rainfall erosivity values in Europe. The June to September period contributes to around 53% of the annual rainfall erosivity in Europe with different spatial and temporal patterns depending on the region. The study has also identified the seasonal patterns in different regions of Europe (Mediterranean, Alpine, North/West Europe, and Central/North). There are heterogeneous patterns in seasonal rainfall erosivity in Europe. On average, the Northern and Central European countries exhibit the highest R-factor values in summer, while the Southern European countries from October to January. In almost all countries (excluding Ireland, United Kingdom and North France), the seasonal variability of rainfall erosivity is high. Very few areas and stations showed the highest erosivity during late winter to early spring period (February – April). In the majority of the stations, the rainfall erosivity is higher during summer and lower in autumn.

Keywords: REDES, R-factor, seasonality rainfall intensity, modelling, soil erosion, monthly erosion rate

INTRODUCTION

Soil erosion is mostly taking place in steep areas, when rainfall (and consequently surface runoff) falls on soils poorly covered with vegetation and without protection measures (Lal, 2001). In Europe soil loss is mostly modelled adopting the Revised Universal Soil Loss Equation (RUSLE) (Panagos et al., 2014a) which includes 5 factors: rainfall erosivity, soil erodibility, slope steepness and length, cover-management, and support practices. These factors are characterized by large spatial variability across the European Union resulting in very heterogeneous spatial patterns of soil loss. Among the five factors, rainfall erosivity and cover-management have in addition a high temporal variability during the different months of the year. Thus, an evaluation of rainfall erosivity in combination with vegetation cover and support management practices can provide a useful tool for monitoring soil erosion from local/regional scales (Panagos et al., 2014b) to large scales (Vrieling et al., 2014). Further, the intra-annual changes in rainfall erosivity affect agriculture, forestry, hydrology, water management, and ecosystem services. Consequently neglecting the seasonal variability of rainfall erosivity and as a result the intra-annual soil loss variability, may lead to improper decision making (Wang et al., 2002).

Rainfall erosivity -measured with R-factor in RUSLE- accounts for the erosive power of rainfall and the subsequent runoff. The erosivity results in detachments of soil particles and their transport by runoff. R-factor is calculated from a series of single storm events by multiplying the total storm kinetic energy (calculated by an empirical relationship) with the measured maximum 30-minutes rainfall intensity (Wischmeier and Smith, 1978). The R-factor of the erosive events is summed up for long-time periods (more than 22 years recommended) and then annual R-factor values can be calculated (Renard et al., 1997).

By definition, the rainfall erosivity should be calculated using the breakpoint data (Wischmeier and Smith, 1978; Istok et al., 1986). However, it is not always possible to have available recordings at very high temporal resolution (1-min, 5-min) due to the setup of rainfall stations. The availability of high temporal resolution data (30-min, 60-min) has been increasing during the last decades due to the large number of rainfall stations and the technological advancements. During the last decade, data from high temporal resolution rainfall stations are available in Belgium, France, Germany, Luxembourg, Estonia, Latvia, Finland, Romania, Italy and Portugal (Panagos et al., 2015a). The rainfall erosivity much depends on the time-interval that this is measured. Depending on the resolution of rainfall data, Renard et al. (1997) have developed regression equations that 'transfer' the R-factor values from coarse resolution (e.g., 60 minutes) to higher resolution(s) (e.g., 15 minutes).

In this study, we present the functions for calibrating rainfall erosivity at different resolutions and on a monthly basis. Based on these calibration functions, the measured monthly R-factor values have been processed to produce the monthly erosivity datasets at the common denominator of 30 minutes. In a second phase, the calibrated monthly R-factor values are used for the first assessment of seasonal rainfall erosivity at European scale.

Rainfall Erosivity Database at European Scale (REDES) and 2015 updates

The first version of the Rainfall Erosivity Database on the European Scale (REDES) (2014) included 1,541 rainfall stations within the European Union (EU) and Switzerland (Panagos et al., 2015a). The rainfall erosivity has been calculated in REDES by using high temporal resolution data (5-min, 10-min, 15-min, 30-min and 60-min) for periods ranging from 7 to 56 years (average length 17.1 years) and applying the equations proposed by Brown and Foster (1987).

In 2015, REDES has been updated by adding 134 rainfall stations (8.5% increase). In Austria, 53 stations have been added mainly covering southern regions of the country (Tyrol and Carinthia), where R-factor has been measured to be higher than 4,000 MJ mm ha^{-1} h^{-1} yr^{-1} (Nassfeld station) contributing also to reply on the Auerswald et al. comment (Panagos et al., 2015b). In Slovakia, 22 stations have been added in REDES, as the existing 81 stations had no monthly erosivity values. Finally, 21 stations (well distributed in the country) have been added in France, 4 stations in Poland and 33 stations in 4 Spanish catchments (Galicia, Jucar, Ebro and Hidrosur) (Fig .1)

The main objective of the REDES update (during 2015) was to cover areas with data gaps (Poland, Spain, South Austria, and France) and to insert new data where seasonal R-factor values were not available (Slovakia). The updated REDES included 1,675 rainfall stations with high resolution rainfall data. Monthly R-factor values have been calculated for the 1,568 stations out of 1,675 as the rest of the stations (107) have only annual R-factor values retrieved from the literature.

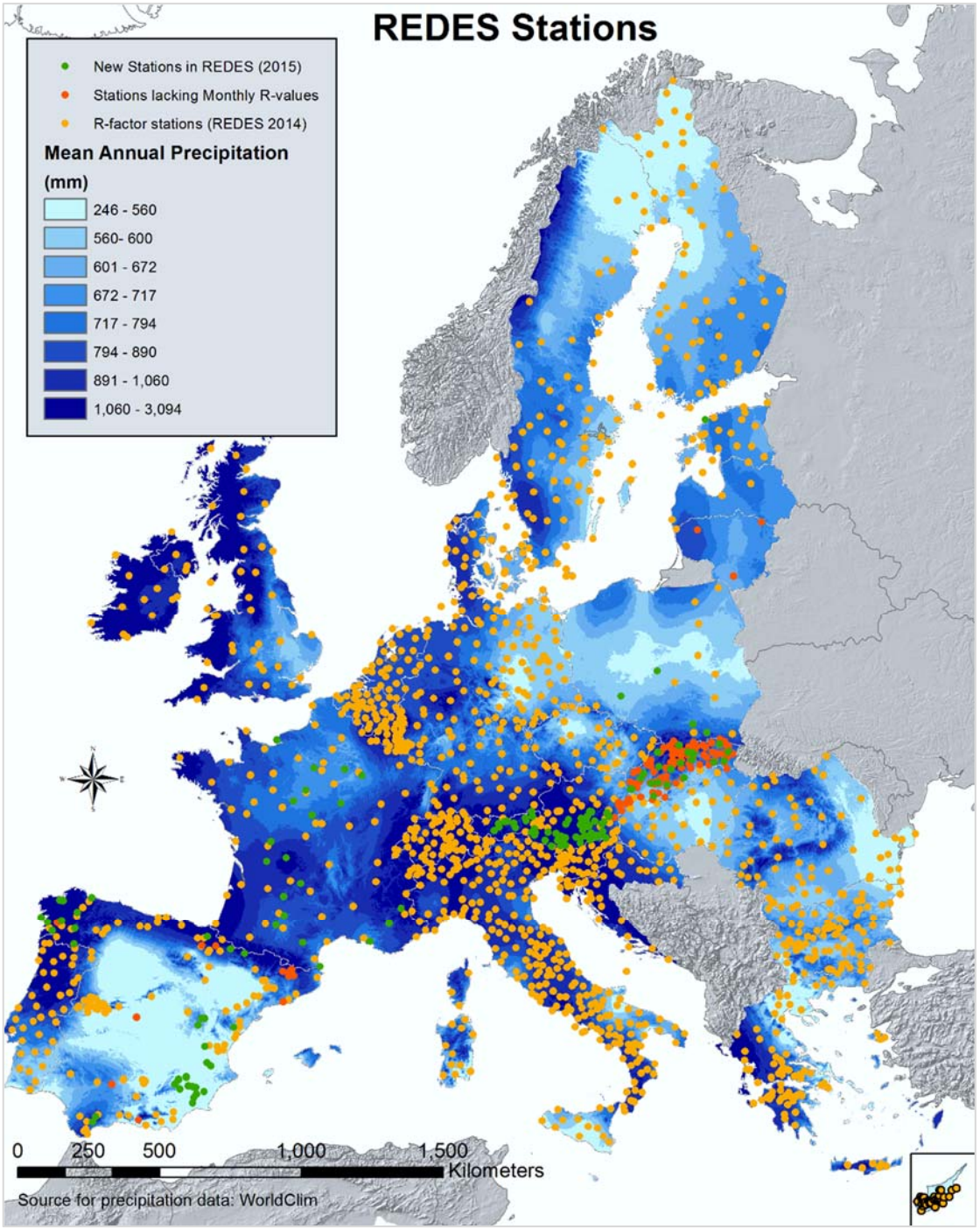

Fig. 1: Rainfall stations included in the Rainfall Erosivity Database on the European Scale (REDES) (In green colour, the new stations added in REDES (2015); in red colour, the stations lacking monthly R-factor values, in yellow colour REDES (2014)).

METHODOLOGY

The data collection of the high-temporal-resolution rainfall records has been explained in Panagos et al. (2015a). After the recent REDES update with the new 134 records, the methods include three further steps: a) The calculation of the monthly erosivity per station; b) the

normalisation of R-factor values calculated using rainfall data with different time steps (5-min to 60-min); c) the spatial analysis of intra-annual (monthly) rainfall erosivity and erosivity density.

Monthly R-factor calculation

Despite the high importance of seasonal rainfall erosivity, few studies have analysed the inter-annual and spatial variability (Diodato, 2006; Meusburger et al., 2012; Mannaerts and Gabriels, 2000; Sadeghi and Hazbavi, In Press). In the calculation of REDES values and in the present paper we have applied the equations proposed by Brown and Foster (1987) for the R-factor calculation and followed the criteria for the identification of an erosive events (Renard et al. 1997).

The rainfall kinetic energy (e_r) is calculated per rainfall depth (mm) and per unit area (ha) for each time interval as follows (Brown and Foster, 1987):

$$e_r = 0.29[1-0.72\exp(-0.05i_r)] \quad (1)$$

where, i_r is the rainfall intensity during the time interval (mm h^{-1}).

The single storm event erosivity multiplies the kinetic energy of this event (e_r expressed as MJ ha^{-1} mm^{-1}) with its maximum amount of rain falling in the 30 minutes v_r (expressed as mm h^{-1}):

$$EI_{30} = \left(\sum_{r=1}^{0} e_r v_r\right) I_{30} \quad (2)$$

The R-factor is the product of the kinetic energy of a rainfall event (E) and its maximum 30-minutes intensity (I_{30}) (Brown and Foster, 1987):

$$R = \frac{1}{n}\sum_{j=1}^{n}\sum_{k=1}^{mj}(EI_{30})_k \quad (3)$$

where, R is the average monthly rainfall erosivity (MJ mm ha^{-1} h^{-1} $month^{-1}$), n is the number of years recorded, m_j is the number of erosive events during a given month j, and EI_{30} is the rainfall erosivity index of a single event k.

The sums of EI_{30} and the average R-factor have been calculated on a monthly basis. To compute the R-factor, the erosive rainfall events (m_j) for each station has to be defined. The erosive events have been selected based on thresholds set by Renard et al. (1997) followed by Panagos et al. (2015a). It has been demonstrated that the selection of unit energy equation

(see Eq.1) and the application of thresholds do not significantly affect the computation of the R-factor (Lu and Yu, 2002).

The Rainfall Intensity Summarisation Tool (RIST) software (Klik and Konecny 2013) has been used to calculate the R-factor. Moreover, this tool derives also the monthly R-factor values, allowing us to build the monthly 'dimension' in REDES. Our database with monthly erosivity values is made up of 12 monthly values per 1,567 stations (i.e., 18,804 records).

Calibration of monthly R-factors calculated from different rainfall recording intervals

The objective of this calibration is to account for the impact of the rainfall measurement breakpoint on rainfall erosivity results and furthermore develop calibration functions to make the REDES homogeneous at a common denominator of 30-minutes resolution. The issue of different time resolutions for R-factor estimation has been faced in the past as well. Weiss (1964) has estimated the conversion factor between EI_{30} and EI_{15} to 1.0667. In the United States, Renard et al. (1997) developed a range of coefficients varying from 1.08 – 3.16 in order to 'transfer' hourly R-factor to 30-minutes erosivity based on measurements from 713 stations. Yin et al. (2007) have calculated the conversion factors between different resolutions based on measurements of 5 stations in China. Agnese et al. (2006) have also estimated the R-factor in 3 different resolutions (5-min, 15-min, and 60-min) for 7 stations in Sicily (Italy). In the European Union, Panagos et al. (2015a) have developed calibration functions based on R-factor estimations at 5 different resolutions (60-min, 30-min, 15-min, 10-min, and 5-min). According to the REDES statistics, 23.4% of the European stations have rainfall data at very high resolution (< 15 minutes). Taking into account this fact and assuming that few stations are recording data at the very high resolution, the calibration functions are necessary to provide reliable estimations of the R-factor for a wide area such as Europe.

The REDES database includes stations which have different recording intervals: 60-min, 30-min, 15-min, 10-min and 5-min. A calibration procedure has been followed for bringing the R-factor values at a common denominator of 30-min. In this way, the REDES becomes homogenous in terms of time resolution and allowing to make assessments of monthly erosivity. Using a geographically representative pool of rainfall stations with different time resolutions, four calibration functions have been produced in order to 'bring' the R-factor values at 30-minutes resolution (Panagos et al., 2015a). The calibration process included the following steps:

- R-factor was calculated at the highest available resolution (e.g. <30 minutes) for a number of stations (86 stations well distributed in Europe).

- Data have been aggregated to coarser resolution(s) and R-factor was calculated at the coarser resolution for the same stations.
- Calibration function (derived from regression analysis) has been developed based on the R-factor results at the highest possible resolution and the coarser resolution(s).

The four calibration functions were derived from the annual R-factor values and are applicable for the normalization of annual erosivity. Since R-factor has different monthly regimes, the annual regression functions would be inappropriate for the calibration of monthly R-factor values. Thus, we decided to develop calibration functions per month, following the same procedure as in the calibration of annual R-factor values. Those calibration functions have been developed per month and resolution. The pool of rainfall stations is well representing the European Union as stations from 14 countries (BE, CZ, CH, CY, DE, EE, ES, FR, HR, HU, IT, LU, RO, SI) have been involved in this calibration exercise.

RESULTS AND DISCUSSION

Calibration Curve for annual R-factor values

In addition to the calibration proposed by Panagos et al. (2015a), stations with data at very high resolution (1-min) from the Czech Republic and Slovakia have been used. The scale factor between R-factor at 1-minute and the 30-minutes is 0.7496. Based on the six scale factors at the corresponding time resolutions (1, 5, 10, 15, 30 and 60-min), a regression function has been developed (Fig. 2). This power function has a very good coefficient of determination (R^2) and may allow estimating scale factors at every temporal resolution between 1 and 60 minutes. If data are collected at 20-minute resolution, the calculated R-factor can be scaled at 30 minutes by multiplying it with the constant 0.9332. Similarly, the R-factor at 40 minutes has a scale factor of 1.1911.

The results of the annual calibration showed that the scaling factors in Europe are closer to the lowest values obtained by Renard et al. (1997). The estimated scaling factors are matching well with the findings in Sicily (Agnese et al., 2006), United States (Istok et al., 1986; Williams and Sheridan, 1991) and they are by 10-20% higher than the ones estimated in China (Yin et al., 2007). However, the precipitation regimes of China (e.g., Wang et al., 2005; Zhai et al., 2005) are remarkably different from the corresponding European ones (Pauling et al., 2006), so we did not expect similar scaling factors.

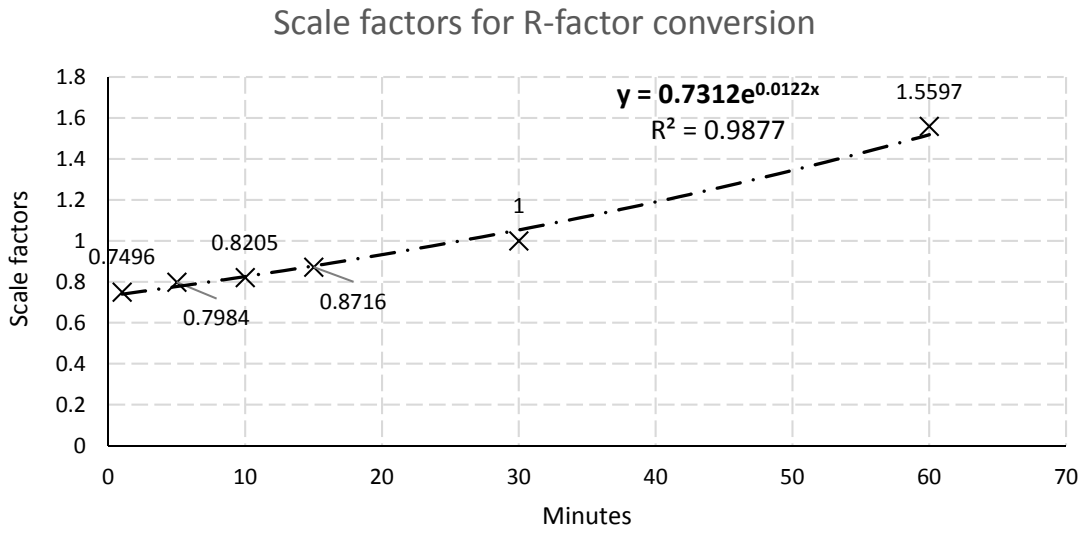

Fig. 2: Calibration curve for R-factor values at different time resolutions in Europe.

Monthly calibration factors for different temporal resolutions

The annual calibration factor for the R-factor estimation using the 60-minutes data has been estimated to be 1.5597, ranging from 1.2974 (January) to 1.6995 (August). The lowest calibration factors are estimated in winter months and the highest ones in summer months (Fig. 3). The smoothest calibration takes place in winter period compared to the summer period. The option to apply monthly calibration factors is recommended as there is 25% variability in the monthly conversion factors.

The annual calibration factor for estimating annual R-factor by using 10-min data has been estimated to be 0.8205, ranging from 0.7986 (July) to 0.8951 (January). The smoothest calibration factors (close to 1) are estimated in winter. The monthly conversion factors allow us to reallocate the R-factor at the desired resolution even if the data are available at coarser resolution. For example, the August R-factors at 60-min can be converted to 5-minutes by a factor 2.13, while the January ones by a factor 1.54 (Fig. 3). Also, the calibration factors between very high resolution (e.g., between 15-minutes and 5-minutes) are low varying between 1.05-1.12 for the different month.

The good performance of coefficient of determination both in the annual calibration functions and in the monthly ones permitted us to develop general pan-European calibration functions which can be used in all the European climatic zones.

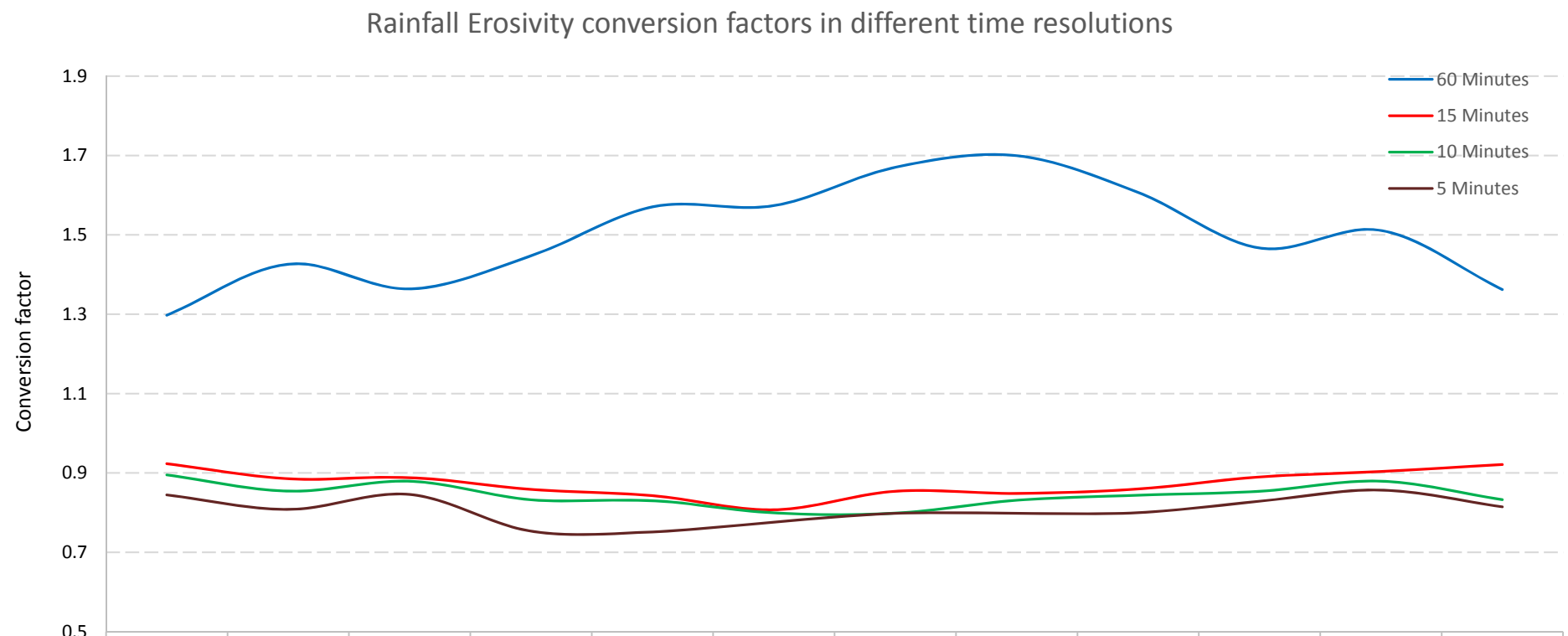

	Jan	Feb	Mar	Apr	May	Jun	Jul	Aug	Sep	Oct	Nov	Dec
60 Minutes	1.2974	1.4262	1.3636	1.4471	1.5705	1.5735	1.6702	1.6995	1.6069	1.4668	1.5112	1.3621
15 Minutes	0.9233	0.8854	0.8883	0.8586	0.8428	0.8072	0.8539	0.8484	0.8596	0.89	0.9036	0.9212
10 Minutes	0.8951	0.8542	0.8792	0.8324	0.8301	0.7993	0.7986	0.8312	0.8439	0.8538	0.8793	0.8326
5 Minutes	0.8447	0.8081	0.8459	0.7533	0.7514	0.7762	0.7984	0.7984	0.7999	0.8286	0.8568	0.8146

Figure 3: Monthly Rainfall erosivity calibration factors for different resolutions (5-min, 10-min, 15-min, 60-min) compared to the R-factor base resolution of 30-min.

Seasonal and monthly rainfall erosivity

The annual R-factor map of Europe (Panagos et al., 2015a) gives a spatial overview of the impact of rain to cause erosion and allow the identification of hotspots where intervention is needed. However, the control measures (agricultural, crop management and support practices) can be more efficient if the temporal distribution of the erosivity risk is known. The interaction of the two dynamic factors (rainfall erosivity and cover-management) is the key point to take control measures against erosion. Most of the RUSLE applications worldwide do not take into account the temporal variability of the two dynamic factors (Vrieling et al., 2014). The monthly R-factor in combination with forthcoming modelling of seasonal cover-management represent a relevant step ahead in the framework of soil loss monitoring activities at a European scale (Panagos et al., in Press). This can be achieved by modifying the classical RUSLE approach to estimate average annual soil loss and propose the seasonal erosivity (Hoyos et al., 2005) in combination with intra-annual land cover variability and closer monitoring of management practices. The increased availability of remote sensing data on land cover and vegetation (e.g., COPERNICUS programme; see Panagos et al., 2015c) can contribute to the seasonal estimation of a cover-management factor.

The mean R-factor of the updated REDES (1,675 stations) is with 906 MJ mm ha^{-1} h^{-1} yr^{-1} close to the one estimated in 2014. The monthly R-factor was calculated for 1,568 stations due to lack of monthly R-factor values of 107 stations whose annual R-factor values have been retrieved from the literature. The stations excluded are mainly located in Slovakia (81 stations), Spain and Lithuania and have low rainfall erosivity values. Those excluded low values have a small effect in aggregating slightly higher mean monthly R-factors values (Fig. 4).

July and August are the months in which the highest number of intense erosive events happen in Europe. More than 40% of total rainfall erosivity in the European Union and Switzerland is taking place in the summer period and more than 53% is noticed during the period June – September. According to the monthly distribution of rainfall erosivity in Europe, the mean R-factor does not show significant variations during the first four months (January to April) of the year followed by a remarkable linear increase till July/August (Fig. 4). Finally, a smoother decrease - compared to the summer increase- is noticed during autumn and continues till February.

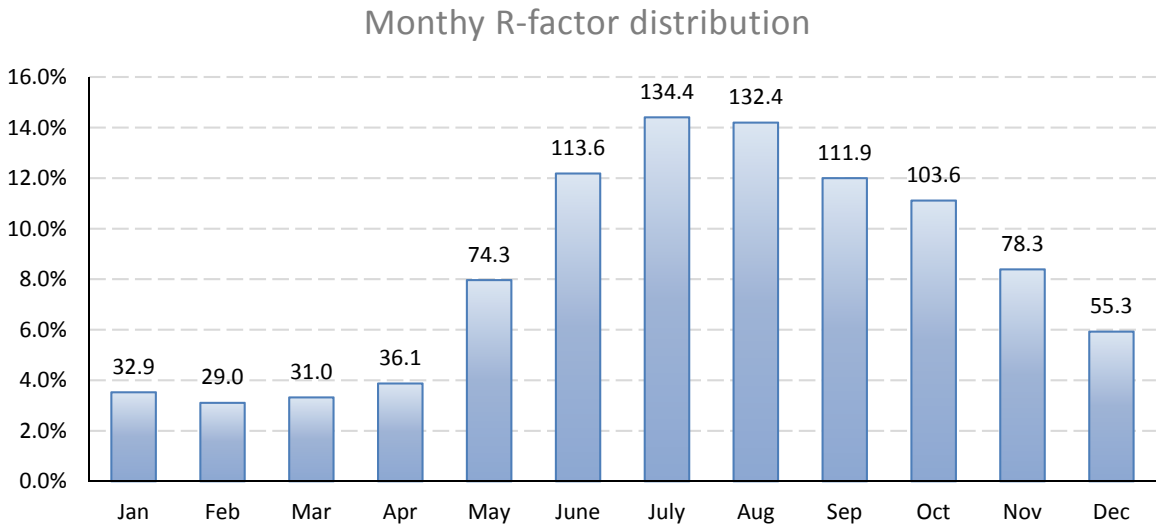

Fig. 4: Mean monthly R-factor (MJ mm ha^{-1} h^{-1} yr^{-1}) of REDES stations and their contribution (%) to the annual R-factor.

However, there are different patterns of the rainfall erosivity distribution during the year. The stations with highest R-factor in a single month (for instance July, August, September or October) are located mostly in Italy and Slovenia. For each REDES station, the season with the highest R-factor has been selected (Fig. 5). For 94% of the REDES stations, the most erosive period is either summer (68%) or autumn (26%). For only 22 REDES stations, mainly located in South Spain and France, the most erosive period is spring (Fig .5).

During summer, the R-factor exhibits its highest seasonal values for stations located in Northern European countries, i.e. the Baltic States, Central Europe, the Alpine region and the Apennines, as it can be seen from the distribution of the seasons with the highest R-factor values (Fig. 5). This zone covers the largest part of Europe. A second zone, where autumn is the most erosive period, includes parts of the Mediterranean basin (Western Greece, coastal Italy, south France, Portugal and major part of Spain, Croatia and coastal Slovenia). A third zone, where winter is the most erosive period is limited to Cyprus, Crete, part of Greece and Galicia. Finally, a mixed situation where summer and autumn are dominant erosive periods is noticed in United Kingdom, Ireland and part of North France. On average, more than 55% of the annual R-factor takes place in one season.

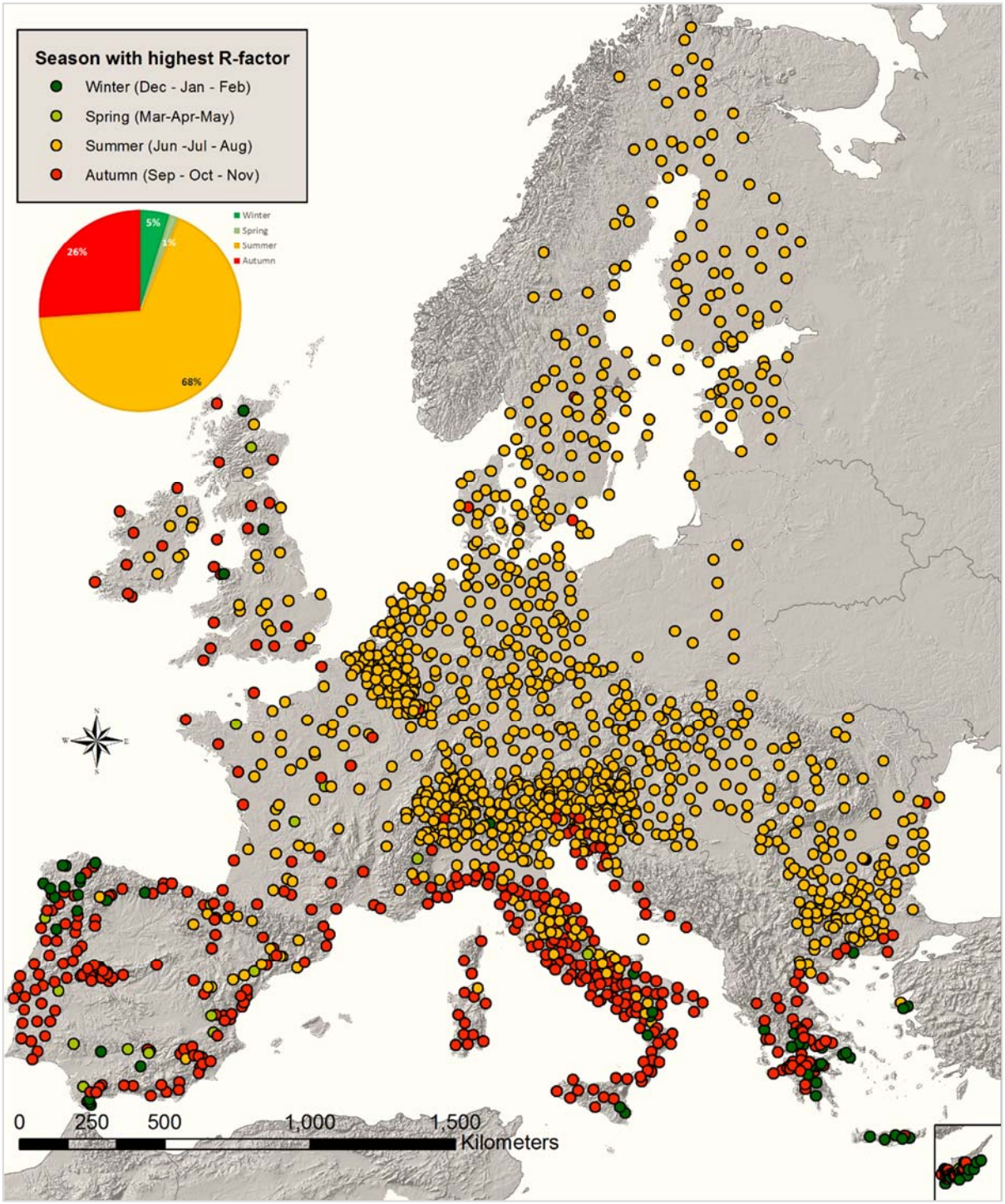

Fig. 5: Season with highest R-factor in REDES.

The R-factor shows the highest monthly values in autumn in most of the Mediterranean region, where the precipitation amount is generally higher in October-November (Klein Tank et al., 2002; Gonzalez-Hidalgo et al., 2011) and summers are frequently hot and dry (Hoerling et al., 2012). In the Mediterranean region, southern Greece and Cyprus can be considered to be an exception in R-factor patterns, as the rainfall erosivity peaks in winter and it is low in

spring even if those regions show similar rainfall amount compared to autumn (Xoplaki et al., 2014).

The Atlantic regions do not show distinctive patterns, probably because the monthly precipitation variability is lower than in the continental regions (Wibig, 1999), especially in the British Islands (Lloyd-Hughes and Saunders, 2003 and Haylock et al., 2008). The R-factor is highest in summer for Central Europe, Northern Europe, Eastern Europe and the Alps. This pattern might have different explanations, as Central Europe is generally affected by large-scale extreme precipitation events in summer (Frei et al., 2000), while the Alps are usually affected by local summer thunderstorms and rain showers, due to the high temperature gradient between hot and moist lowlands and cool and windy mountains (Peristeri et al., 2000; Christian et al., 2003; Meusburger et al., 2012). Similar patterns can be found in the Carpathians and Eastern Europe (Bartholy et al., 2007; Spinoni et al., 2015). Finally, Scandinavia shows higher variability in summer, but one should not forget that in winter the precipitation events at high-latitudes are often in the form of snowfall and so we expect low erosive events in winter compared to summer (Linderson, 2001). The stations with almost zero R-factor during winter months are located in Central and Eastern European countries (Czech Republic, Slovakia, Bulgaria, and Romania) and in the Northern ones (Sweden and Finland).

Regarding the most erosive months for single stations, we found that almost 30% of the REDES, the most erosive month is July, followed by August (23.7%) and June (12.7%). On the contrary, the months with the least number of stations having highest R-factor values are April and March. On average, the most erosive month of the year contains 28% of the annual erosivity. In Baltic and high-latitude regions, the most erosive month (either July or August) accounts for more than 38% of the annual R-factor (very sharp changes). Lastly, the situation is much smoother in Ireland where the most erosive month is not a peak as it contributes only with 16% to the total erosivity.

Besides the most erosive season or the most erosive month (in terms of R-factor), it is worth identifying the different intra-annual patters of the R-factor in the European continent. Most of the countries have been grouped based on their geographical position and their monthly patterns of rainfall erosivity (Fig. 6). The distribution of the monthly erosivity in the Mediterranean countries (Spain, Portugal, Greece and Cyprus) (Fig. 6a) follows a bathtub shaped curve (Klutke et al., 2003), as three periods can be identified. The rainfall erosivity is more or less stable in the period from February to June and then shows a decrease in July and August (second period). Finally, December is the most erosive in Greece and Cyprus while October has the highest values in the Iberian Peninsula (Fig. 6a).

The temporal distribution of rainfall erosivity is very similar in Switzerland and Austria (Fig. 6b) having the highest values in July and August. Instead, Northern Italy and Croatia show their peak values in September. These countries have the highest mean monthly values in REDES.

In Germany, Netherlands, Belgium and Denmark the rainfall erosivity is very limited during the winter months and early spring, then increases in May-June-July (and August in Denmark) followed by sharp falls in Autumn (Fig 6c). The monthly R-factor distribution is following the Gaussian shape (Sharma, 2000) in Germany, Netherlands, Belgium and Denmark. Contrary to three above mentioned regional patterns (Mediterranean, Alpine, North Europe), Ireland, United Kingdom and France show the smoothest distribution during the whole year (Fig 6d).

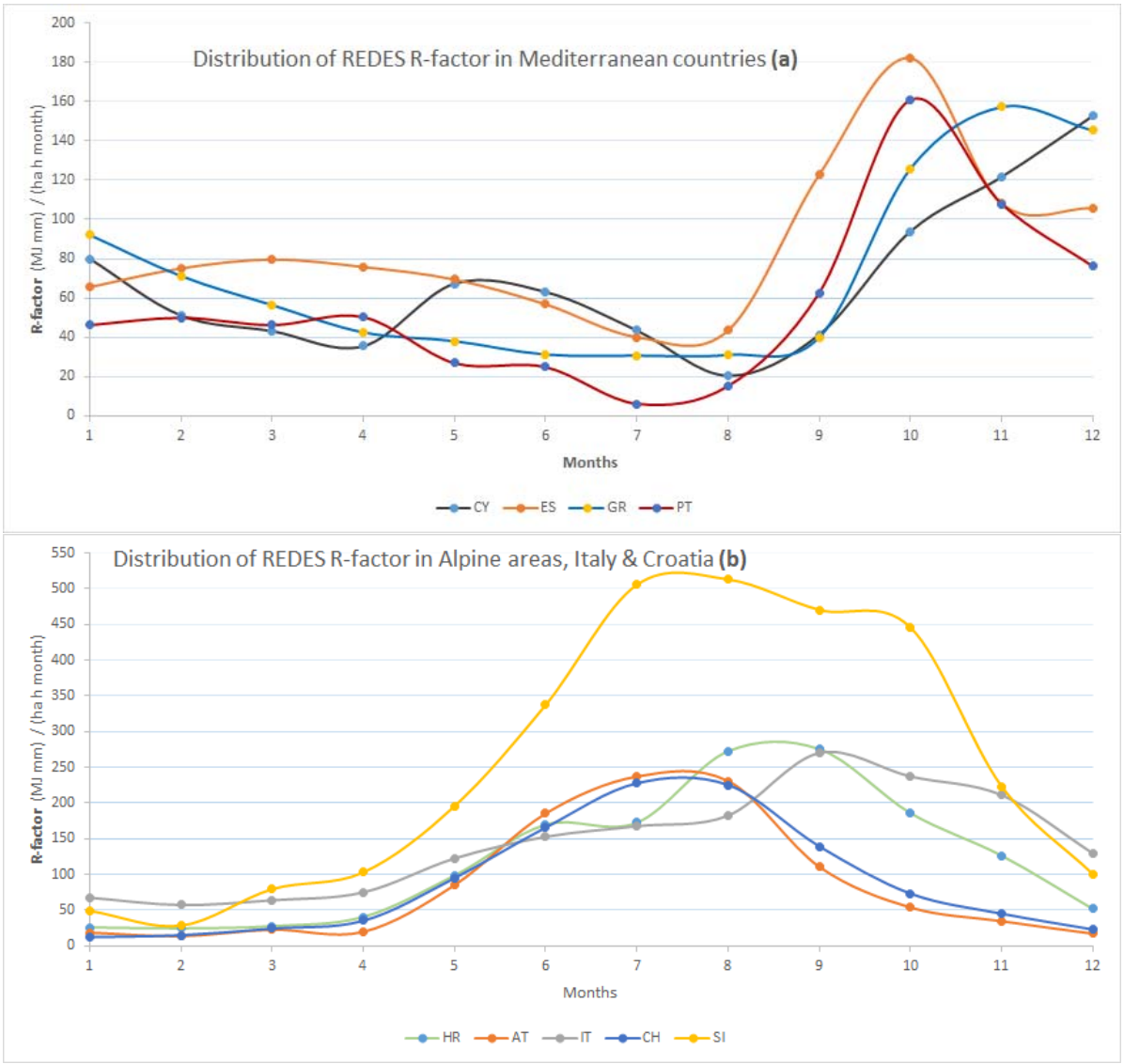

Fig. 6a, b: The main regional patterns of monthly rainfall erosivity in Europe (CY- Cyprus, GR – Greece, ES – Spain, PT – Portugal, IT – Italy, HR- Croatia, AT – Austria, DE – Germany, DK - Denmark, NL – The Netherlands, BE – Belgium, IE – Ireland, UK – United Kingdom, FR – France).

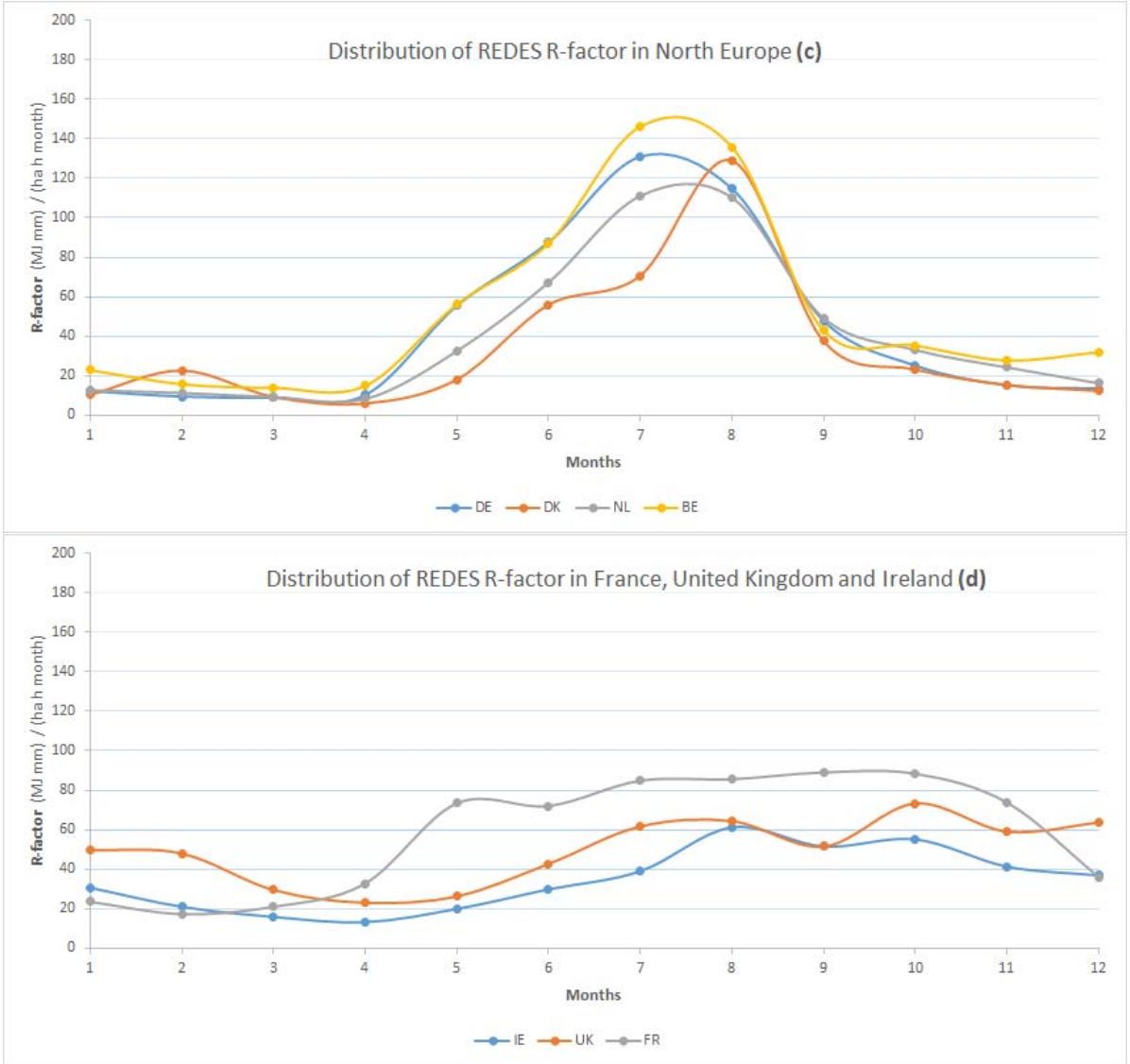

Fig. 6c, d : The main regional patterns of monthly rainfall erosivity in Europe (CY- Cyprus, GR – Greece, ES – Spain, PT – Portugal, IT – Italy, HR- Croatia, AT – Austria, DE – Germany, DK - Denmark, NL – The Netherlands, BE – Belgium, IE – Ireland, UK – United Kingdom, FR – France).

The rest of the countries (Scandinavia, Baltic States, and Central Europe) follow more the distribution identified in North Europe (Netherlands, Germany, Denmark), as shown in Fig. 6c.

The magnitude of the predicted climate change is likely to have different influence on soil erosion depending on regional conditions (Blanco and Lal, 2008; O'Neal, 2005). As the predictions in climate change scenarios are expected to increase the number of storms during summer months (Coumou and Rahmstorf, 2012; Orlowsky and Seneviratne, 2012), the countries with high erosivity during summer are projected to be more affected. However, the projected rainfall erosivity changes based on climatic scenarios are the subject of future studies.

Monthly rainfall erosivity density

Similar to annual erosivity density (Kinnell, 2010; Panagos et al., 2015a), the Monthly Erosivity Density (MED) expresses the rainfall erosivity per rainfall unit (mm) for each month. Dabney et al. (2011) used the monthly erosivity density to demonstrate the impact of climate change in increasing runoff and soil loss. For each station in REDES, the Monthly Erosivity Density (MED_i) for the i-th month is defined as the ratio of mean rainfall erosivity (R) for the i-th month divided by its mean precipitation (P):

$$MED_i = R_i / P_i \qquad (4)$$

High MED values suggest that the rainfall occurs in form of high intensity events (rainstorms) during the respective month. The distribution of MEDs in Europe is left skewed. Half of the monthly REDES records have erosivity density less than 0.45 while the 75th percentile is close to 1.

Some countries have similar characteristics regarding their MED and the corresponding monthly variability. For example, for all months the mean MED in Sweden, Finland, Denmark, Germany, Netherlands, France, Ireland and United Kingdom is less than 1. In these countries, MED is always lower than 0.40 in winter – early spring (December, January, February, March, April). For these eight countries the highest MED can be found either in July or August varying from 0.43 (Ireland) to 0.96 (France).

The Northern European countries show similar monthly variability regarding erosivity density (Fig 7a). The Gaussian distribution of mean monthly erosivity density is represented with the "bell-shaped curve", increasing during May-June and decreasing during early autumn. In France, the higher values of MED are due to higher R-factor values in the Alpine areas.

The mean MED reaches the highest values (close to 4.5 during summer) in the Eastern Alps (Slovenia, North-East Italy) and Croatia; in Central European countries (Austria, Slovakia, and Hungary) the mean MED is higher than 2.0 during summer months (Fig 7b). In all of these countries, the winter and early spring months are characterized by relatively low MED (< 0.80).

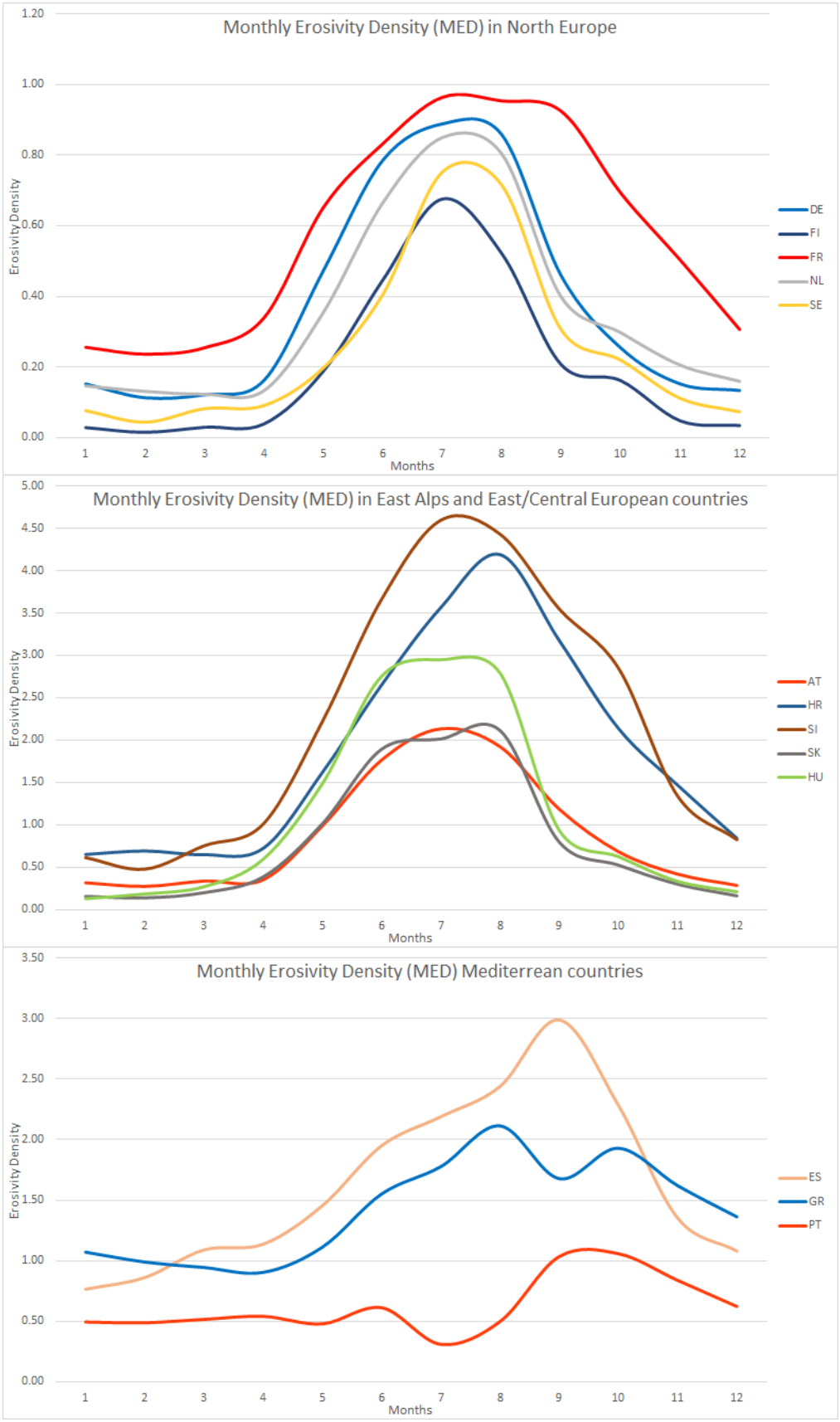

Fig. 7: The main regional patterns of Monthly Erosivity Density (MED) (CY- Cyprus, GR – Greece, ES – Spain, PT – Portugal, HR - , IT – Italy, HR- Croatia, AT – Austria, DE – Germany, DK - Denmark, NL – The Netherlands, BE – Belgium, IE – Ireland, UK – United Kingdom, FR – France).

In Ireland and the United Kingdom MEDs are very smooth compared with the rest of European countries and have values ranging between 0.15 (April) to 0.45 (July). The Mediterranean countries are quite different than the rest of the European countries, as their highest MED is noted during September and October (Fig. 7c). Moreover, the winter months in Spain and Greece have MEDs close to 1 which is not noted in any other country.

CONCLUSIONS

In this study, calibration factors for transferring the R-factor values between different time resolutions and on a monthly scale have been produced; these can be applied in case of monthly or annual estimation of R-factor in any part of Europe. As expected, the calculated rainfall erosivity values decrease as the rainfall measurement interval increases. However, the relationship between time resolution and conversion factors is exponential, contrary to past assessments, which have proposed linear functions. The coefficients of different resolutions for monthly rainfall erosivity contribute in normalizing the monthly R-factor values at the 30-min resolution for all the REDES stations. The development of the monthly dimension in REDES database allows the assessment and modelling of the R-factor at monthly and seasonal level.

The first rainfall erosivity assessment in Europe demonstrated when which regions suffer most from rainfall erosivity. The Alpine region is characterised by high erosivity during summer and early autumn (July to September) while the Mediterranean region has its highest peaks in late autumn and early winter.

The monthly rainfall erosivity assessment is of great help for soil erosion control. It can support management practice for soil conservation in agriculture. For instance, it is important to maintain vegetation coverage in Central and Northern European countries during summer months while October to December is the most critical season for Mediterranean countries. Identifying the most erosive season (month) per country (region) can contribute to mitigate soil erosion by protecting soil with vegetation coverage and applying appropriate management practices. As topography and soil properties are soil erosion drivers which are more constant in time, the vegetation coverage and crop management are the factors which can be primarily influenced by human intervention.

Finally, the new proposed monthly erosivity density index identifies the most risky seasons in terms of floods and erosive events as high monthly erosivity density values correspond to seasons and stations with high intensity of rainfall creating extreme erosive events. Based on this index, the erosive events in summer months in the Eastern Alps and Central Europe and

in autumn in the Mediterranean area may lead to R-factor values that range from two to four times the corresponding rainfall amounts.

Conflict of interest

The authors confirm and sign that there is no conflict of interest with networks, organisations and data centres referred to in this paper.

Acknowledgments

The authors would like to acknowledge the following services for providing access to their data:

Austria: Hydrographic offices of Upper Austria, Lower Austria, Burgenland, Styria, Salzburg, Carinthia, Vorarlberg and Tyrol.

Belgium - Flanders: Flemish Environmental Agency (VMM), Operational Water Management.

Belgium - Wallonia: Service public de Wallonie, Direction générale Mobilité et Voies hydrauliques, Direction de la Gestion hydrologique intégrée, Namur.

Bulgaria: Rousseva et al. (2010)

Cyprus: Cyprus Department of Meteorology.

Czech Republic: Faculty of Environmental Sciences, Czech University of Life Sciences Prague

Germany: Deutscher Wetterdienst (DWD), WebWerdis Service

Denmark: Aarhus University, Department of Agroecology

Estonia: Client service department, Estonian Environment Agency, Tallinn

Spain: Confederaciones Hidrográficas del Ebro, Tajo, Duero, Guadalquivir, Segura, Júcar, Miño-Sil, Cantábrico and Sur, Servei Meteorològic de Catalunya, and Meteo Navarra.

France: Météo-France DP/SERV/FDP, Division Fourniture de Données Publiques

Greece: Hydroskopio

Croatia: Meteorological and Hydrological Service

Hungary: Hungarian Meteorological Service

Ireland: Data from Met Éireann, financial support from Irish EPA STRIVE Programme - SILTFLUX (2010-W-LS-4) and UCD Earth Institute

Italy: the Servizio Idrografico Abruzzo, Protezione Civile Regione Basilicata, Ufficio idrografico Bolzano, Servizio Idrografico Friuli-Venezia Giulia, Centro funzionale regione Lazio, Meteotrentino, Agenzia Regionale per lo Sviluppo e l'Innovazione dell'Agricoltura nel

Molise, Servizio Meteo-Idro-Pluviometrico Marche, Associazione Regionale dei Consorzi di Difesa della Puglia, Osservatorio delle Acque Sicilia, Servizio Idrologico Regionale Toscana, Servizio Risorse idriche e rischio idraulico Umbria, Diodato Nazzareno from Regione Campagna, Centro funzionale regionale Valle d'Aosta and the Hydro-Meteo-Climate Service of the Environmental Agency ARPA Calabria, ARPA Emilia Romagna, ARPA Liguria, ARPA Lombardia, ARPA Piemonte, ARPA Veneto.

Latvia: Latvian Environment, Geology and Meteorology Centre, Riga

Luxembourg: Agrarmeteorologisches Messnetz Luxembourg

Netherlands: KNMI, Royal Netherlands Meteorological Institute

Portugal: Agência Portuguesa do Ambiente, Departamento de Monitorização de Recursos Hídricos

Poland: Warsaw University of Life Sciences

Romania: National Meteorological Administration

Slovakia: Slovak Hydrometeorological Institute, Climatological service

Slovenia: Slovenian Environment Agency, Hydrology and State of Environment Office

Sweden: Swedish Meteorological and Hydrological Institute (SMHI)

United Kingdom: NERC & UK Environmental Change Network (ECN), and British Atmospheric Data Centre (BADC)

References

Agnese, C., Bagarello, V., Corrao, C., D'Agostino, L., D'Asaro, F. 2006. Influence of the rainfall measurement interval on the erosivity determinations in the Mediterranean area. Journal of Hydrology, 329 (1-2), pp. 39-48.

Bartholy, J., & Pongrácz, R. (2007). Regional analysis of extreme temperature and precipitation indices for the Carpathian Basin from 1946 to 2001. Global and Planetary Change, 57(1), 83-95.

Bonilla C.A., Vidal K.L. Rainfall erosivity in Central Chile (2011) Journal of Hydrology, 410 (1-2) , pp. 126-133.

Blanco, H. Lal, R. 2008. Principles of Soil Conservation and Management. Springer Science - Business Media B.V. pp. 513-534

Brown, L.C., Foster, G.R., 1987. Storm erosivity using idealized intensity distributions. Transactions of the ASAE 30, 379–386.

Christian, H. J., Blakeslee, R. J., Boccippio, D. J., Boeck, W. L., Buechler, D. E., Driscoll, K. T., ... & Stewart, M. F. (2003). Global frequency and distribution of lightning as observed from space by the Optical Transient Detector. Journal of Geophysical Research: Atmospheres (1984–2012), 108(D1), ACL-4.

Coumou, D., & Rahmstorf, S. (2012). A decade of weather extremes. Nature Climate Change, 2(7), 491-496.

Dabney, S.M., Yoder, D.C., Vieira, D.A.N. 2012. The application of the Revised Universal Soil Loss Equation, Version 2, to evaluate the impacts of alternative climate change scenarios on runoff and sediment yield. Journal of Soil and Water Conservation, 67 (5) , pp. 343-353.

Diodato N. 2006 Predicting RUSLE (Revised Universal Soil Loss Equation) monthly erosivity index from readily available rainfall data in Mediterranean area. Environmentalist, 26 (1) , pp. 63-70.

Foster, G.R., Yoder, D.C., Weesies, G.A., McCool, D.K., McGregor, K.C., Bingner, R.L., 2003. Draft User's Guide, Revised Universal Soil Loss Equation Version 2 (RUSLE-2). USDA-Agricultural Research Service, Washington, DC.

Frei, C., Davies, H. C., Gurtz, J., & Schär, C. (2000). Climate dynamics and extreme precipitation and flood events in Central Europe. Integrated Assessment, 1(4), 281-300.

González‐Hidalgo, J. C., Brunetti, M., & de Luis, M. (2011). A new tool for monthly precipitation analysis in Spain: MOPREDAS database (monthly precipitation trends December 1945‐November 2005). International Journal of Climatology, 31(5), 715-731.

Haylock, M. R., Hofstra, N., Klein Tank, A. M. G., Klok, E. J., Jones, P. D., & New, M. (2008). A European daily high‐resolution gridded data set of surface temperature and precipitation for 1950‐2006. Journal of Geophysical Research: Atmospheres (1984‐2012), 113(D20).

Hoerling, M., Eischeid, J., Perlwitz, J., Quan, X., Zhang, T., & Pegion, P. (2012). On the increased frequency of Mediterranean drought. Journal of Climate, 25(6), 2146-2161.

Hoyos, N., Waylen, P.R., Jaramillo, A. 2005. Seasonal and spatial patterns of erosivity in a tropical watershed of the Colombian Andes. Journal of Hydrology, 314 (1-4) , pp. 177-191.

Istok, J.D., McCool, D.K., King, L.G., Boersma, L. 1986. Effect of rainfall measurement interval on EI calculation. Transactions of the American Society of Agricultural Engineers, 29 (3) , pp. 730-734.

Kinnell, P.I.A., 2010. Event soil loss, runoff and the Universal Soil Loss Equation family of models: a review. Journal of Hydrology 385, 384–397.

Klein Tank, A. M. G., Wijngaard, J. B., Können, G. P., Böhm, R., Demarée, G., Gocheva, A., ... & Petrovic, P. (2002). Daily dataset of 20th‐century surface air temperature and precipitation series for the European Climate Assessment. International journal of climatology, 22(12), 1441-1453.

Klik, A., Konecny, F. 2013. Rainfall erosivity in northeastern Austria. Transactions of the ASABE. 56(2): 719-725.

Klutke, G.A., Kiessler, P.C., Wortman, M.A. 2003. A critical look at the bathtub curve. IEEE Transactions on Reliability, 52 (1) , pp. 125-129.

Lal, R. 2001. Soil degradation by erosion. Land Degradation and Development, 12 (6) , pp. 519-539.

Linderson, M. L. (2001). Objective classification of atmospheric circulation over southern Scandinavia. International Journal of Climatology, 21(2), 155-169.

Lloyd‐Hughes, B., & Saunders, M. A. (2002). Seasonal prediction of European spring precipitation from El Niño‐Southern Oscillation and Local sea‐surface temperatures. International Journal of Climatology, 22(1), 1-14.

Lu, H., Yu, B., 2002. Spatial and seasonal distribution of rainfall erosivity in Australia. Aust. J. Soil Res. 40, 887–991.

Mannaerts, C.M., Gabriels, D. 2000. Rainfall erosivity in Cape Verde. Soil and Tillage Research, 55 (3-4) , pp. 207-212.

Meusburger, K., Steel, A., Panagos, P., Montanarella, L., and Alewell, C, 2012. Spatial and temporal variability of rainfall erosivity factor for Switzerland. Hydrology and Earth System Sciences, 16, 10.5194/hess-16-1-2012.

O'Neal Mr, Nearing, M, Vining R, South worth, J., Pfeifer, R. 2005. Climate change impacts on soil erosion in Midwest United States with changes in crop management. Catena 61:165-184.

Orlowsky, B., & Seneviratne, S. I. (2012). Global changes in extreme events: regional and seasonal dimension. Climatic Change, 110(3-4), 669-696.

Panagos, P., Meusburger, K., Van Liedekerke, M., Alewell, C., Hiederer, R., Montanarella, L. 2014a. Assessing soil erosion in Europe based on data collected through a European Network. Soil Science and Plant Nutrition, 2014, 60 (1): 15-29

Panagos P., Karydas C.G., Ballabio C., Gitas, I.Z. 2014b. Seasonal monitoring of soil erosion at regional scale: An application of the G2 model in Crete focusing on agricultural land uses. International Journal of Applied Earth Observation and Geoinformation, 27B, pp. 147–155.

Panagos, P., Ballabio, C., Borrelli, P., Meusburger, K., Klik, A., Rousseva, S., Tadic, M.P., Michaelides, S., Hrabalíková, M., Olsen, P., Aalto, J., Lakatos, M., Rymszewicz, A., Dumitrescu, A., Beguería, S., Alewell, C., 2015a. Rainfall erosivity in Europe. Sci. Total Environ. 511, 801–814

Panagos, P., Meusburger K., Ballabio C., Borrelli P., Begueria S., Klik A., Rymszewicz A., (...), Alewell C, 2015b. Reply to the comment on "Rainfall erosivity in Europe" by Auerswald et al. Science of the Total Environment, In Press. DOI:10.1016/j.scitotenv.2015.05.020.

Panagos, P., Borrelli, P., Meusburger, C., Alewell, C., Lugato, E., Montanarella, L., 2015c. Estimating the soil erosion cover-management factor at European scale. Land Use policy 48C: 38-50.

Panagos, P., Borrelli, P., Poesen, J., Ballabio, C., Lugato, E., Meusburger, K., Montanarella, L., Alewell, .C. The new assessment of soil loss by water erosion in Europe. Environmental Science & Policy. In Press. DOI: 10.1016/j.envsci.2015.08.012

Pauling, A., Luterbacher, J., Casty, C., & Wanner, H. 2006. Five hundred years of gridded high-resolution precipitation reconstructions over Europe and the connection to large-scale circulation. Climate Dynamics, 26(4), 387-405.

Peristeri, M., Ulrich, W., & Smith, R. K. (2000). Genesis conditions for thunderstorm growth and the development of a squall line in the northern alpine foreland. Meteorology and Atmospheric Physics, 72(2-4), 251-260.

Renard, K.G., et al., 1997. Predicting Soil Erosion by Water: A Guide to Conservation Planning with the Revised Universal Soil Loss Equation (RUSLE) (Agricultural Handbook 703). US Department of Agriculture, Washington, DC, pp. 404.

Sadeghi S.H.R., Hazbavi Z. 2015. Trend analysis of the rainfall erosivity index at different time scales in Iran. Natural Hazards, In Press.

Sharma A. 2000. Seasonal to interannual rainfall probabilistic forecasts for improved water supply management: Part 3 - A nonparametric probabilistic forecast model. Journal of Hydrology, 239 (1-4) , pp. 249-258.

Spinoni, J., Szalai, S., Szentimrey, T., Lakatos, M., Bihari, Z., Nagy, A., ... & Vogt, J. (2014). Climate of the Carpathian Region in the period 1961–2010: climatologies and trends of 10 variables. International Journal of Climatology.

Vrieling A., Hoedjes J.C.B., van der Velde M. (2014). Towards large-scale monitoring of soil erosion in Africa: Accounting for the dynamics of rainfall erosivity. Global and Planetary Change, 115 , pp. 33-43.

Wang, G., Gertner, G., Singh, V., Shinkareva, S., Parysow, P., Anderson, A. 2002. Spatial and temporal prediction and uncertainty of soil loss using the revised universal soil loss equation: A case study of the rainfall-runoff erosivity R factor. Ecological Modelling, 153 (1-2) , pp. 143-155.

Wang, Y., & Zhou, L. 2005. Observed trends in extreme precipitation events in China during 1961‐2001 and the associated changes in large‐scale circulation. Geophysical Research Letters, 32(9).

Weiss, 1964. Ratio of true to fixed-interval maximum rainfall. J. Hydreaul. Div. Proc. ASCE 90(1), 77-82.

Wibig, J. (1999). Precipitation in Europe in relation to circulation patterns at the 500 hPa level. International Journal of Climatology, 19(3), 253-269.

Williams, R.G., Sheridan, J.M., 1991. Effect of measurement time and depth resolution on EI calculation. Trans. ASAE 34 (2), 402–405.

Wischmeier, W., Smith, D. 1978. Predicting rainfall erosion losses: a Guide to conservation planning. Agricultural Handbook No. 537 U.S. Department of Agriculture, Washington DC, USA.

Yin, S., Xie, Y., Nearing, M.A, Wang, C. 2007. Estimation of rainfall erosivity using 5- to 60-minute fixed-interval rainfall data from China. CATENA 70, pp. 306-312.

Xoplaki, E., Gonzalez-Rouco, J. F., Luterbacher, J. U., & Wanner, H. (2004). Wet season Mediterranean precipitation variability: influence of large-scale dynamics and trends. Climate dynamics, 23(1), 63-78.

Zhai, P. M., & Pan, X. H. 2003. Change in extreme temperature and precipitation over northern China during the second half of the 20th century. *Acta Geographica Sinica*, *58*(S1), 1-10.

4 Modelování ztráty půdy v prostředí GIS

Digitální model reliéfu (DMR) je základním vstupem prostorově distribuovaných modelů, jako je například TOPMODEL, TOPOG a Model Erozního indexu nebezpečnosti (BEHI). DMR může být integrován do sub-povodí a modelovat dopady změn parametrů sub-povodí na erozi půdy v rámci celého povodí. Výhoda prostorově distribuovaného přístupu v modelování přístupů spočívá v tom, že může být rozšířena i do 3-D prostoru (Hengl and Reuter, 2008).

Zásadním zlomem v hydrologickém a erozním modelování v prostředí GIS bylo vytvoření konceptu „Specific catchment area“ (specifické přispívající plochy) v 70 letech minulého století (Speight, 1974). Na základě tohoto konceptu autoři jako např. Moore a Wilson (1992), Desmet a Govers (1996) Mitášová et al. (1997) odvodili platné vztahy pro výpočet LS faktoru modelu USLE v prostředí GIS. Moore a Wilson (1992) odvodili vztah pro LS faktor v prostředí GIS na základě „unit stream teorie“ z operativních rovnic pro model WEPP. Studie 5 se zabývá porovnání několika přístupů k výpočtu LS faktoru. Pro výpočet ztráty půdy v GIS je třeba také vzít v úvahu nejen použitou rovnici pro LS faktor, ale také jaký algoritmus byl zvolen pro výpočet:

1) „Specific catchment area“: zde existuje hned několik přístupů, které popisuje Hengl a Reuter (2008), Desmet a Govers (1996) nebo Wilson a Galant (2000)
2) Sklonitosti: Florinsky (1998) shrnuje, že k výpočtu rastru sklonitosti z DMR je k dispozici 6 přístupů. Dunn a Hickey (1998) provedli porovnání několika algoritmů pro výpočet sklonu a orientace ke světovým stranám a došli k závěru, že výsledné rastry se významně od sebe neliší.
3) Směr odtoku: na základě tohoto algoritmu se modelují všechny hydrologické parametry v GIS, tedy i LS faktor. V současné době existuje hned několik přístupů
   - Jednosměrný odtok: D8 (O'Callaghan a Mark, 1984), Rho8 (Fairfield a Leymarie, 1991),
   - Více-směrný odtok:
     - MFD8 – tato skupina algoritmů je souhrnně nazývána buď jako MFD (Holmgern, 1994), nebo algoritmus implementovaný v TOPMODEL (Quinn et al., 1991), nebo také jako FD8 (Freeman, 1991).
     - D-infinity (D∞): vytvořen Tarbotnem (1997)

STUDIE 5: Comparison of different approaches of LS factor calculations based on measured soil loss under simulated rainfall

Michaela Hrabalíková, Miloslav Janeček

Soil & Water Res. (accepted manuscript, under revision)

Abstract: Geographic information System (GIS) combined with soil loss models can enhance the evaluation of soil erosion estimation. SAGA and ARC/INFO geographic information system were used to estimate topographic (*LS*) factor of the Universal soil loss equation (USLE) soil erosion on a long-term experimental plots near Prague in the Czech Republic. Digital elevation model with high accuracy (1x1 m) and measured soil loss under simulated rainfall provided input for five alternate GIS based procedures in computing the combined slope length and steepness factor in (R)USLE for determining the influence of chosen algorithm in soil erosion estimates. Results of GIS based (R)USLE erosion estimates from the five procedures are compared with measured soil loss from experimental plot of given length 11 m from 38 rainfall simulations which were performed during 15 years. Results indicate GIS based (R)USLE predicted soil erosion estimates are in most variant lower than the observed measured average annual soil loss, only two methods over-predicted measured soil loss. One of them is the original manual method of the USLE which, however, predicted average soil of the lowest difference with measured average annual soil loss. The results from this study show the need for further work in using GIS and USLE for soil erosion estimation.

Key words soil loss; topographic factor; universal soil loss equation; geographic information system

INTRODUCTION

Recently, more than 80 soil erosion models are available to evaluate potential soil loss for different spatial or temporal scale (Karydas et al., 2014). However, one of the most used model is still the Universal Soil Loss Equation (USLE) which has been widely used all over the world either in the same (Wischmeier and Smith, 1978) or modified forms (Renard, 1997). When using the USLE or RUSLE, the components factors relating to rainfall erosivity (*R*), slope length and steepness factor (*LS*), which reflects the influence of terrain on soil erosion, soil erodibility (*K*), groundcover (*C*) and soil conservation practices (*P*) are multiplied to calculate the average annual soil loss per unit area. Wischmeier and Smith (1978) defined the slope length (*L*) as the distance from the point of origin of the surface flow to the point where each

slope gradient (*S*) decreases enough for the beginning of deposition or when the flow comes to concentrate in a defined channel.

According to literature (Liu et al., 2015, Kinnell, 2008, Desmet and Govers, 1996, Moore and Burch, 1986, Moore et al., 1991, Moore and Wilson, 1992, Zhang et al., 2013, Mitasova et al., 1996, Wilson et al., 2000), the extraction of the *LS* factor is a key issue in the applications of (R)USLE models (Oliveira et al., 2013). It is because, the *LS* factor is the most sensitive parameter of (R)USLE in the soil loss predictions (Truman et al., 2001, Tetzlaff and Wendland, 2012), moreover, the estimate of the topographic variables, although benefitted by automatic generation and spatial distribution (Desmet and Govers, 1996, Moore and Wilson, 1992, Mitasova et al., 1996) by the Geographical Information Systems (GIS's), is the target of controversy related to the formulation of applied algorithms (Oliveira et al., 2013, Desmet and Govers, 1997, Mitasova et al., 1997).

The procedure obtain the slope length and slope steepness factors was originally manual in these models (Wischmeier and Smith, 1965, Wischmeier and Smith, 1978, Renard, 1997, Moore and Wilson, 1992). Many methods have been developed seeking to include complex slopes to overcome restrictions given by equations for factor L developed by Wischmeier and Smith (1978), common in a context of hydrographic basins. The history of equations development of *LS* factors is described in the work of Garcia Rodriguez and Gimenez Suarez (2010).

To overcome limitations given by 1-D modelling, in the conceptual models the slope-length factor is substituted by the specific catchment area (Mitasova et al., 1996, Desmet and Govers, 1996, Moore and Burch, 1986, Moore et al., 1991) which allows to determine the drainage network considering the direction of the surface runoff and the accumulated flow from the digital elevation model (DEM). Incorporating this concept, Desmet and Govers (1996) modified the equations of Foster and Wischmeier (1974) for irregular slope. They compute the *LS*-factor in the form of finite difference in a grid of cells representing a segment of the hillside and compare GIS-based results with methods of Griffin (1988) and manual methods of Foster and Wischmeier (1974). Fu et al. (2006) adopted this same contributing area approach to *LS*-factor calculation in their application of the RUSLE and a sediment delivery model to evaluate the impacts of no-till practices on erosion and sediment yield. Another a GIS-based simplified equation for calculating the combined *LS*-factor over two-dimensional terrain (Moore and Wilson, 1992), based on unit stream theory, was shown to be equivalent to the RUSLE equations for the *LS*-factor (McCool et al., 1989). Other methods have sought to address the potential shortcomings of the aforementioned approaches, such as accounting for areas of deposition on the landscape that impact slope length (Hickey, 2000, Van Remortel et al., 2004, Van Remortel et al., 2001).

The work of Moore and Wilson (1992), Mitasova et al. (1996), Desmet and Govers (1996), Fu et al. (2006), Van Remortel et al. (2004), Liu et al. (1994, 2000, 2015) or Nearing (1997) include some comparison of the computed values for *LS* with values obtained using mostly manual methods of Wishmeier and Smith (1978) and/or McCool (1989). Yitayew et al. (1999) performed a study where they compared several different GIS-based approaches to *LS* calculation. However, they did not explicitly compare any of the GIS-based *LS* estimates with "ground-truth" values of LS, instead of it, they compare the GIS-based erosion predictions using RUSLE with observed sediment yield in the watershed.

Thus, it can be questioned to which degree available algorithms or equations for deriving the *LS* factor can influence the model results. The purpose of this study is to evaluate the effects of alternative algorithms on the erosion model results. Modelling of the *LS* factor was performed and comparisons of soil loss was made based on five different algorithms and/or equations at a fixed hill length of 11 m where soil loss was measured under simulated rainfall.

MATERIALS AND METHODOLOGY

The principle of comparison of different algorithms and/or equations for calculating *LS* factor is based on the calculation of the loss by the (R)USLE model. The methodology involved the use of the topographical factor in a GIS environment based on digital terrain model (DTM). Other factors of the (R)USLE was estimated from 38 rainfall simulations (factor *R, C*, and *P*) and soil surveys (factor *K*) during years 1994-2011. The influence of DTM resolution (Desmet and Govers, 1996, Moore et al., 1991), different flow (Freeman, 1991, Tarboton, 1997), and slope (Florinsky, 1998) algorithms on the (R)USLE results are neglected in this paper. Most of available *LS* algorithms are already implemented within GIS softwares such as IDRISI, SAGA GIS, GRASS, ArcGIS etc. SAGA GIS and raster calculator in ArcGIS ESRI were only two GIS softwares used for this study.

Experimental plots and field measurements

The long-term experimental site of the Research Institute for Soil and Water Conservation (RISWC) is situated close to the village Třebsín (49°51'15''N, 14°27'49''E) about 40 km in south-east direction from Prague. The experimental area consists of 9 experimental plots 35 - 38 m in length and 7 m in width, and 4 plots 2 m in width and 24 – 26 m in length maintained as a permanent fallow land (see Figure 1a) with north exposition and average slope of the plots vary between 7-8°. The soil is classified as silt, with quite low soil organic matter content, was identified as Haplic Cambisol (WRB, 2006) and no good moisture regime. The soil

structure of topsoil corresponds mainly to crumb structure (Kadlec et al., 2012, Kovář et al., 2012). The specific site-properties of experimental plots are described in more detail by Kadlec et al. (2012) and Kovář et al. (2012).

A rainfall simulator, construed by RISWC Prague, was used for experimental testing between years 1994-2011. The pipes, 3.0 m in height, are connected with tubes ended with a wide-angle spraying system created by four nozzles (fulljet type) where each nozzle is covering an area of angle 104° at a pressure of 34.5 kPa. The size of water drips is close to the size of natural rain drops (Kovář et al., 2012). The spraying intensity can vary from 0.5 to 2.0 mm·min^{-1}. The scheme of the portable rainfall simulator is shown in Figure 1b.

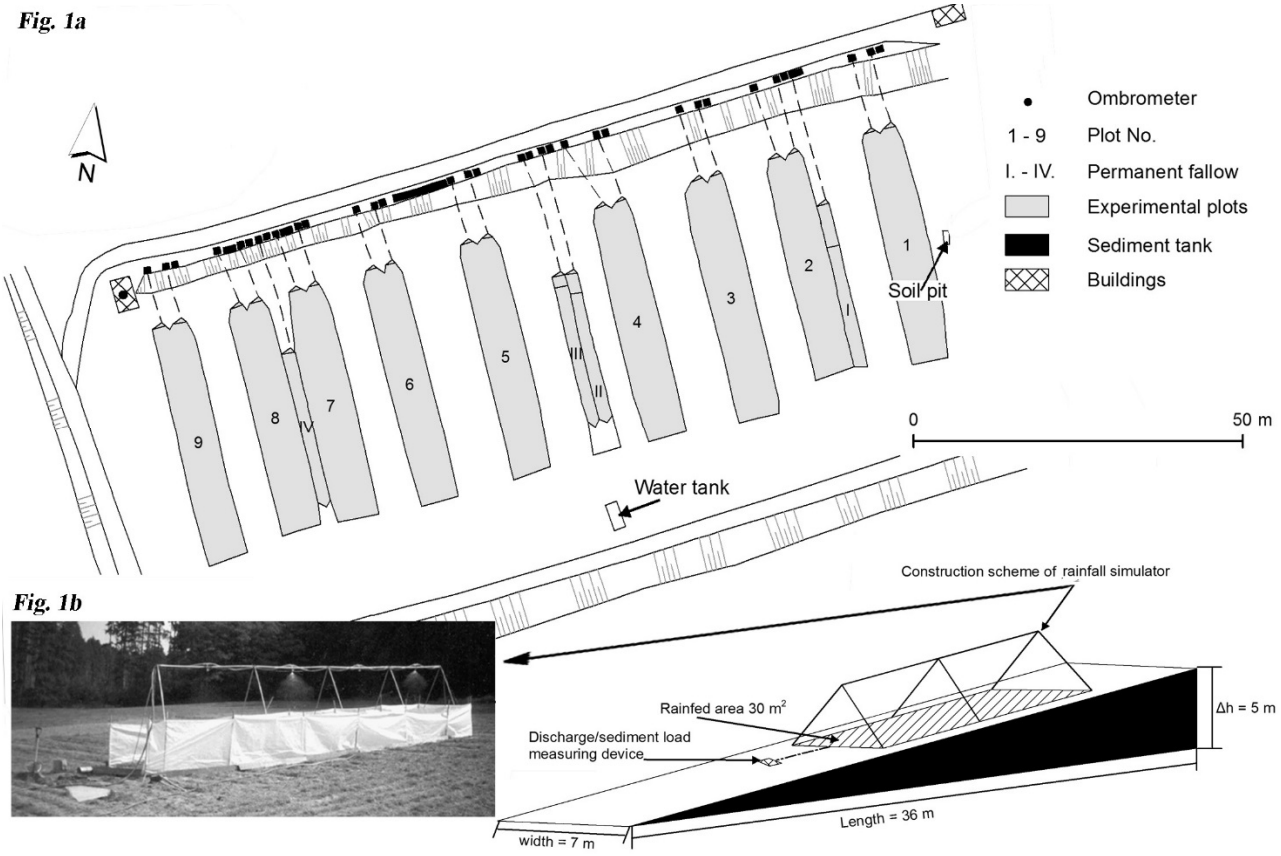

Figure 1a: Experimental runoff plots in Třebsín; Figure 1b: Scheme of portable rainfall simulator on the plot No. 4.

Rainfall simulations were used on the reduced size of the parcel area A = 30 m^2 (2.7 x 11 m). The simulator was always set over the middle part of the experimental plot and simulated rainfall experiments lasted until a constant runoff rate was reached (15–60 min). During each rainfall event with particular intensity: the beginning and amount of surface runoff, a rate of water infiltration into soil was recorded, and samples were collected at 3 min intervals which were afterward oven-dried at 105°C for 24 h to obtain soil loss.

For the purpose of this study, simulator measurement at the **experimental plot No. 4** were processed. Parcel No. 4 was selected on the basis of the most comprehensive available data set which contains 38 record of rainfall simulation, soil loss, and description of ground cover, soil management and soil moisture. The scheme of plot No. 4 is depicted in Figure 1. Slope of the plot No. 4 is 8° with slightly concave profile and plan curvature. The summary of soil loss measurements under simulated rainfall is available in the Table 1.

Input data, the USLE/RUSLE parameters

The conservation practices (*P*) factor values were chosen based on soil management practices at the plot No. 4 during years 1994-2011 (see notes below the Table 1). *P* factor for simulations has the value 1 with the exception of simulation in years 1996 and 1997, when corn was planted according to contours, and thus *P* factor is chosen as the value 0.7 according to table in Wischmeier and Smith (1978). **The soil erodibility (*K*) factor** was determined based on research published by Kadlec et al. (2012), where they estimated average *K* factor as the value of 0.046 ($t \cdot ha \cdot h \cdot ha^{-1} \cdot MJ^{-1} \cdot mm^{-1}$).

Rainfall erosivity index was calculated for each simulation from records taken during simulation tests (see eq. 1). The *R* factor based on 38 rainfall simulations was calculated as all the erosion indexes per year in which the simulation was done was summed up and the total sum was divided by the total number of years when the simulation was performed, i.e. 15 (see eq. 2). The *R* factor was determined by following relationship according to Foster et al. (1981) in Renard et al. (1997) which is the corresponding version for SI-units of equation developed by Wischmeier et al. (1978) in the USLE guide book:

$$E_m = 0.119 + 0.0873\ log_{10}(i_m) \tag{1}$$

$$R = \frac{\sum_{i=1}^{j}(EI_{30})_i}{N} \tag{2}$$

Where E_m is kinetic energy in $MJha^{-1}mm^{-1}$; and i_m is intensity in mm per hour ($mm \cdot h^{-1}$); I_{30} is the maximal 30-minute intensity which is in the case of rainfall simulator equal to intensity i_m; EI_{30} for simulated storm *i*, and *j* is the number of (simulated) storms in an *N*-year period.

The crop and management (*C*) factor were estimated according to the height of the crop (see Tab. 1), the test date and other records related to the cover of soil surface. Factor C for each simulation was determined according to handbook Wischmeier and Smith (1978). Given values of C factor have to be corrected according to partition coefficient rainfall within the year (Wischmeier and Smith, 1978). Since for soil loss evaluation the simulated rainfall was used, thus, it was assumed that the distribution of precipitation will be uniform for a whole

growing season. Therefore, the value of C factor was corrected by the partition coefficient for simulated precipitation, i.e. 0.14. Summary C factor of all 38 measurements was calculated as a sum up of average C factor of each year of simulation.

In order to utilize GIS-based approaches of ***LS*** factor calculations, the Digital Terrain Model of the Czech Republic of the 5th generation (DTM 5G) was used as a regular grid (1x1 m). The DTM 5G model is provided by the State Administration of Land Surveying and Cadastre of the Czech Republic in digital form with X, Y, H coordinates, where H means the altitude in the Baltic Vertical Datum with the total standard error of 0.18 m of height in the bare terrain. The model is based on the data acquired by altimetry airborne laser scanning of the Czech Republic territory between years 2009 and 2013. When calculating LS factor from DTM, following input parameters and algorithms were used: (i) Flow direction algorithm: a multiple flow direction (MFD) algorithm (Quinn et al., 1995); (ii) Slope algorithm: second order, central finite-difference scheme (Zevenbergen and Thorne, 1987); (iii) Specific Catchment Area (Upslope Area): contour length depend on aspect (Desmet and Govers, 1996).

The *LS* factor itself, was calculated by 5 different approaches, where λ is slope length in m, β is slope angle in radians, As is specific catchment area:

1) Manual method according to equations of Wischmeier and Smith (1978):

$$LS = (\lambda/22.13)^m \times (65.4sin^2\beta + 4.56sin\beta + 0.0654) \quad (3)$$

Where*:*

m = 0.5 if *β > 0.05*; *m = 0.4* if *0.03 < β > 0.05*; *m = 0.3* if *0.01 < β > 0.03*; *m = 0.2* if *β < 0.01.*

As variant 1b for GIS were slope length λ parameter replaced by specific catchment area *As*.

2) Manual method according to McCool et al. (1989):

$$LS = (\lambda/22.13)^m \times \begin{cases} (10.8sin\beta + 0.03) & if\ \beta < 0.09 \\ (16.8sin\beta - 0.5) & if\ \beta \geq 0.09 \\ (3sin^{0.8}\beta + 0.56) & if\ \lambda < 4.5\ m \end{cases} \quad (4)$$

$m = F/(1+F)$ where

$F = \frac{sin\beta/0.0896}{sin^{0.8}\beta+0.56}$ or *F=0* when there is deposition when *λ≤4.5* m (5)

As variant 2b for GIS were slope length λ parameter replaced by specific catchment area *As*.

3) L factor according to Desmet, Govers (1996), and S factor according to Nearing (1997):

$$L_{(i,j)} = \frac{\left(A_{(i,j),in}+D^2\right)^{(m+1)} - A_{(i,j),in}^{(m+1)}}{x_{(i,j)}^m \cdot D^{(m+2)} \cdot 22.13^m} \text{ and } S = -1.5 + \frac{17}{\left(1+e^{(2.3-6.1sin\beta)}\right)} \quad (6, 7)$$

Where *D* is the grid cell size (meters), $x_{i,j} = sin\ a_{i,j} + cos\ a_{i,j}$, *the* $a_{i,j}$ is the aspect direction of the grid cell (*i,j*) and *m* is related to the ratio *F* of the rill to interill erosion (McCool et al., 1989).

4) According to Moore and Burch (1986), and Moore and Wilson (1992):

$$LS = (A_s/22.13)^m \times (sin\beta/0.0896)^n \quad (8)$$

Where *m*=0.4 (the value range 0.4 to 0.6); *n*=1.3 (the value range 1.2 to 1.3)

5) The point method of Griffin et al. (1988) for L factor, and Moore and Wilson for (1992) S factor:

$$L = (m+1) \times (A_s/22.13)^m \text{ and } S = (sin\beta/0.0896)^n \quad (9)$$

Where *m*= 0.4 (the value range 0.2-0.6); *n*= 1.3 (the value range 1.0-1.3) (Mitasova et al., 1996)

Table 1: Soil loss measuring by rainfall simulator at the plot No. 4 between years 1994 – 2011.

No.	Year	Crop	Soil moisture	Crop height (cm)	Duration of rainfall (min)	Total rainfall (mm)	Intensity (mm/min)	Start of surface runoff (s)	Surface runoff (mm)	Infiltration (mm)	Soil loss (t/ha)
1	1994	Maize	Dry	NA	62.35	41.56	0.67	750	3.32	38.36	**0.054**
2	1995	Barley	Dry	NA	31.07	12.94	0.42	249	2.87	10.20	**0.447**
3	1995	Barley	Dry	NA	54.60	23.65	0.43	699	2.62	21.11	**0.278**
4	1996	Maize[1]	NA	NA	45.61	37.67	0.83	1780	1.35	36.45	**0.078**
5	1997	Maize[1]	NA	15	29.97	24.79	0.83	420	3.20	21.76	**0.307**
6	1998	Maize[2]	Dry	NA	20.12	18.2	0.90	220	7.37	11.17	**3.070**
7	1999	Maize	Dry	NA	29.88	23.64	0.79	48	10.58	13.47	**2.110**
8	1999	Maize	Dry	NA	30.05	24.43	0.81	120	8.93	16.90	**1.227**
9	2000	Fallow	Dry	NA	29.97	24.2	0.81	443	7.83	16.60	**6.566**
10	2001	Fallow	Dry	NA	45.00	38.97	0.87	1240	3.17	36.07	**0.443**
11	2001	Fallow	Dry	NA	44.92	37.34	0.83	1490	1.97	35.48	**0.166**
12	2002	Maize[3]	Dry	NA	30.17	25.85	0.86	120	7.4	18.75	**0.262**
13	2002	Maize[3]	Dry	NA	30.00	25.7	0.86	83	12.83	13.70	**3.556**
14	2004	Sunflower	Dry	NA	30.00	27.79	0.93	140	5.8	21.99	**0.603**
15	2004	Sunflower	Dry	NA	22.00	18.98	0.86	135	4.1	14.88	**0.260**
16	2007	Sunflower[4]	Dry	70	15.75	15.22	0.97	165	2.23	13.05	**0.113**
17	2007	Sunflower[4]	Wet	70	15.67	14.52	0.93	100	4.67	10.12	**0.096**
18	2007	Sunflower[4]	Dry	75	14.53	13.92	0.96	152	3.63	10.75	**0.155**
19	2007	Sunflower[4]	Wet	75	15.13	14.15	0.94	68	5.90	8.68	**0.137**
20	2008	Maize[4]	Dry	52	15.00	17.36	1.16	90	4.53	13.09	**1.472**
21	2008	Maize[4]	Wet	52	15.00	16.39	1.09	35	7.27	9.45	**2.151**
22	2008	Maize[4]	Dry	155	15.13	16.28	1.08	128	4.67	11.85	**1.475**
23	2008	Maize[4]	Wet	155	15.00	20.72	1.38	39	6.17	14.89	**1.792**
24	2008	Maize[4]	Dry	170	15.00	16.41	1.09	60	7.07	11.31	**1.654**

No.	Year	Crop	Soil moisture	Crop height (cm)	Duration of rainfall (min)	Total rainfall (mm)	Intensity (mm/min)	Start of surface runoff (s)	Surface runoff (mm)	Infiltration (mm)	Soil loss (t/ha)
25	2008	Maize[4]	Wet	170	15.00	13.94	0.93	20	9.4	5.14	**2.801**
26	2009	Maize[4]	Dry	90	15.00	12.47	0.83	95	5.77	8.2	**0.971**
27	2009	Maize[4]	Wet	90	15.00	12.87	0.86	43	7.43	6	**1.534**
28	2009	Maize[4]	Dry	140	15.00	11.67	0.78	140	10.8	2.13	**2.178**
29	2009	Maize[4]	Wet	140	15.00	11.47	0.76	130	7.83	4.3	**1.346**
30	2009	Maize[4]	Dry	205	15.00	8.13	0.54	68	4.13	4.13	**1.202**
31	2009	Maize[4]	Wet	205	15.00	9.33	0.62	26	6.17	3.4	**2.596**
32	2010	Maize[4]	Dry	53	15.00	14.7	0.98	100	3.6	11.43	**3.666**
33	2010	Maize[4]	Wet	53	15.00	14.8	0.99	43	5.83	9.37	**3.938**
34	2010	Maize[4]	Wet	135	14.92	13.9	0.93	55	5.47	8.9	**0.673**
35	2011	Maize[4]	Dry	160	15.00	13.47	0.89	50	7.33	6.6	**4.510**
36	2011	Maize[4]	Wet	160	15.00	13.80	0.92	36	8.73	5.93	**2.820**
37	2011	Maize[4]	Dry	200	15.00	13.66	0.91	40	9.37	5.02	**1.344**
38	2011	Maize[4]	Wet	200	15.00	13.57	0.90	25	10.30	3.83	**1.214**

1 - Contour tillage, 2 - Shallow aeration (3 cm) in each row 70 cm in the distance, 3 - without manuring, 4 - green manuring with white mustard (*Sinapsis alba*) as a winter cover.

RESULTS AND DISCUSSION

The basic parameters characterizing the erosion processes were calculated from simulated rainfall events with a particular intensity applied to a different vegetation cover over 15 years. A summary of the three USLE factor calculations (*R*, *C*, *P*) and measured soil loss from experimental plot No 4 summed up for particular year of measuring are given in Table 2. The Table 2 presents as well the average annual values of these factors as well measured average annual soil loss which are used for final evaluation of the influence of different LS-factor calculations on the USLE model results.

Table 2: The USLE factors (R, C, and P) calculated based on recorded data from simulations and measured soil loss summed up for particular years when simulations was performed

Year	No of measurements	R factor (MJ mm ha^{-1} h^{-1})	C factor (-)	P factor (-)	Measured ($t \cdot ha^{-1}$)
1994	1	430.15	0.036	1	0.054
1995	2	226.96	0.036	1	0.725
1996	1	498.35	0.105	0.7	0.078
1997	1	328.62	0.105	0.7	0.307
1998	1	267.13	0.105	1	3.070
1999	2	615.21	0.105	1	3.337
2000	1	312.02	0.14	1	6.566
2001	2	1041.91	0.14	1	0.609
2002	2	711.15	0.105	1	3.818
2004	2	683.02	0.105	1	0.863
2007	4	893.75	0.105	1	0.501
2008	6	1928.72	0.105	1	11.344
2009	6	782.81	0.105	1	9.827
2010	3	687.19	0.105	1	8.277
2011	4	803.79	0.105	1	9.888
Year average	**-**	**680.72**	**0.100**	**0.95**	**3.95**
Total	**38**	**-**	**-**	**-**	**59.26**

Topographic factor (*LS*) was calculated separately. The results of applying different algorithms of S-factor calculation are shown in the Table 3. The values of S-factors have similar range and there is no significant difference. Although the algorithm for L-factor looks same for method, expect method 5, it differ in exponent *m*. Influence of this exponent on the results can be clearly seen in the Table 4, where for method 1 was used *m*=0.5, for method 2a *m*=0.69, for method 2b and 3 the mean value was *m*=0.72 and for method 4 *m*=0.4. Liu et al. (2000) stated that the m=0.5 exponent is better adapted for very accentuate slopes. When the slope increases from 9% to 60%, the *m* exponent increases from 0.5 to 0.71. Therefore, in the equation 5 (McCool et al., 1989), the exponent *m* continues to increase with slope inclination, thus, the slope length effect is a function of the erosion ratio of rill to interrill.

Table 3: Values of L-factor based on different approaches (min, max, mean, range, and standard deviation)

Method	References	MIN	MAX	MEAN	STD	RANGE
1 (manual)	Wischmeier and Smith (1978)	-	-	1.97	-	-
1b (GIS)	Wischmeier and Smith (1978)	1.72	2.61	2.12	0.29	0.89
2 (manual)	McCool et al. (1989)	-	-	1.84	-	-
2b (GIS)	McCool et al. (1989)	1.65	2.28	1.94	0.20	0.63
3 (GIS)	Nering (1997)	1.56	2.17	1.83	0.20	0.61
4, 5 (GIS)	Moore and Wilson (1992)	1.60	2.23	1.88	0.21	0.64

Table 4: Values of L-factor based on different approaches (min, max, mean, range, and standard deviation)

Method	References	MIN	MAX	MEAN	STD	RANGE
1a (manual)	Wischmeier and Smith (1978)	-	-	0.71	-	-
1b (GIS)	Wischmeier and Smith (1978)	0.33	0.77	0.58	0.12	0.44
2a (manual)	McCool et al. (1989)	-	-	0.62	-	-
2b (GIS)	McCool et al. (1989)	0.21	0.72	0.48	0.14	0.50
3 (GIS)	Desmet and Govers (1996)	0.41	0.65	0.56	0.07	0.24
4 (GIS)	Moore and Wilson (1992)	0.41	0.82	0.64	0.11	0.40
5 (GIS)	Griffin (1988)	0.58	1.14	0.90	0.15	0.56

The mean *LS*-factor is given in the Table 5. Desmet and Govers (1996) determined that the GIS method generally predicted *LS* values 10% to 50% greater than the manual approach, which is in opposite of results given in the Table 5. GIS methods in this study generally generate *LS* values 10% to 30% lower than manual method of Wischmeier and Smith (1978), except Griffin's point methods which are giving higher *LS* values (22%). However, if we compare GIS method with manual method of McCool et al. (1989), the difference between is more or less for all methods (except Griffin's point method) ±10%.

Although the USLE and the RUSLE were not designed to predict soil loss from individual event (Wischmeier, 1976; Renard et al., 1997), they have been applied to predict soil loss from individual simulated event ($t \cdot ha^{-1}$) to highlight the difference in soil loss predicted by applying different approaches of LS-factor (see Figure 2). Such analysis showed, that the USLE over-predicted low soil losses and under-predicted high soil losses when it was applied at the event time-scale. These findings are in the agreement with Yitayew et al. (1999), their findings also showed that mean annual erosion was mostly under-predicted by the GIS methods. The Figure 2 shows the three algorithms, i.e. Moore's, McCool's and Desmet's, are able to estimated erosion similarly, but the Desmet's algorithm is consistently lower than the Moore algorithm. This stems from the procedure used for calculating slope steepness, and the

different algorithm used by each for determining the slope-length (i.e. *m* exponent). As it can be observed from Figure 2 and Table 5, the spatial variations in length-slope factors by the different procedures have significant effects on the total erosion calculation. All methods, except Wischmeier's (1a) and Griffin's (5) method, results in lower average annual soil loss than was measured. Best results are given by Wischmeier's method where slope-length was replaced by specific catchment area, and Moore's method. These two methods have almost same *LS*-factor, *LS*=1.23 for method 1b and *LS*=1.21 for method 4.

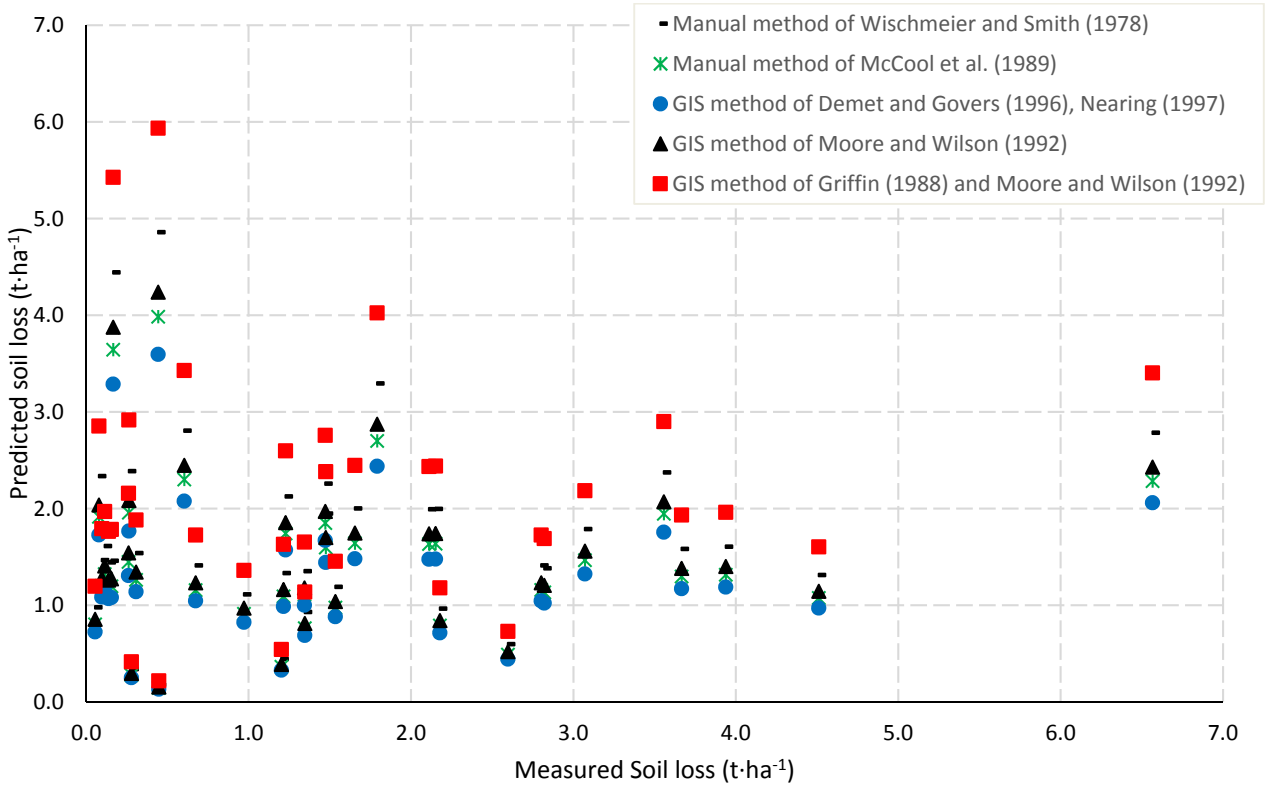

Figure 2: Comparison of predicted soil based on different LS-factor calculations with measured soil loss for all 38 simulations

Table 5: The calculated LS-factors, predicted average annual soil loss and its difference against measured average annual soil loss from plot 4

Methods	Calculated average soil loss (t/ha/y)	Difference from measured average (t/ha/y)	Difference in percentage	LS-factor
1a (manual)	4.17	0.22	5.48	1.39
1b (GIS)	3.69	-0.26	-6.66	1.23
2a (manual)	3.42	-0.53	-13.50	1.14
2b (GIS)	2.81	-1.14	-28.79	0.94
3 (GIS)	3.08	-0.87	-21.98	1.03
4 (GIS)	3.63	-0.32	-8.00	1.21
5 (GIS)	5.09	1.14	28.80	1.69

CONCLUSION

The analysis and obtaining of the topographic factors conducted in the digital environment have become a fundamental piece in erosion model progress, because they address the systematic analyses from specific GIS's tools, as well as allow the empirical processing of the data through adaptations of analogical techniques, thus maintaining researcher interpretation. In this study various methods of LS-factor calculation are presented. Various uncertainties are related to the results which may be e.g. DEM resolution, methods of flow estimation or computation of specific catchment area. The study evinces that there are approaches for GIS-based LS-factor calculation on hillslope scale giving acceptable agreement with measured data. Especially Moore's method or Wishmeier and Smith's method where the slope-length λ was replaced by specific catchment area *As* could be used as an alternative of manual methods. However, the comparison of the above-mentioned methods on a higher number of hillslopes of different shape and length seems to be appropriate.

Acknowledge: The study was supported by Ministry of Agriculture of the Czech Republic, Project No. QJ1520028 - Assessing and modelling of tillage and gully erosion under the framework of total soil loss evaluation on intensively farmed land.

References

DESMET, P. J. J. & GOVERS, G. 1996. A GIS procedure for automatically calculating the USLE LS factor on topographically complex landscape units. *Journal of Soil and Water Conservation,* 51**,** 427-433.

DESMET, P. J. J. & GOVERS, G. 1997. Modelling topographic potential for erosion and deposition using GIS - Comment. *International Journal of Geographical Information Science,* 11**,** 603-610.

FLORINSKY, I. V. 1998. Accuracy of local topographic variables derived from digital elevation models. *International Journal of Geographical Information Science,* 12**,** 47-61.

FOSTER, G. R. & WISCHMEI.WH 1974. EVALUATING IRREGULAR SLOPES FOR SOIL LOSS PREDICTION. *Transactions of the Asae,* 17**,** 305-309.

FREEMAN, T. G. 1991. Calculating catchment area with divergent flow based on a regular grid. *Computers & Geosciences,* 17**,** 413-422.

FU, G. B., CHEN, S. L. & MCCOOL, D. K. 2006. Modeling the impacts of no-till practice on soil erosion and sediment yield with RUSLE, SEDD, and ArcView GIS. *Soil & Tillage Research,* 85**,** 38-49.

GARCIA RODRIGUEZ, J. L. & GIMENEZ SUAREZ, M. C. 2010. Historical review of topographical factor, LS, of water erosion models. *Aqua-LAC,* 2**,** 55-61.

GRIFFIN, M. L., BEASLEY, D. B., FLETCHER, J. J. & FOSTER, G. R. 1988. Estimating soil loss on topographically non-uniform field and farm units. *Journal of Soil and Water Conservation,* 43**,** 326-331.

HICKEY, R. 2000. Slope Angle and Slope Length Solutions for GIS. *Cartography,* 29**,** 1-8.

KADLEC, V., HOLUBÍK, O., PROCHÁZKOVÁ, E., URBANOVÁ, J. & TIPPL, M. 2012. Soil organic carbon dynamics and its influence on the soil erodibility factor. *Soil and Water Research,* 7**,** 97-108.

KARYDAS, C. G., PANAGOS, P. & GITAS, I. Z. 2014. A classification of water erosion models according to their geospatial characteristics. *International Journal of Digital Earth,* 7**,** 229-250.

KINNELL, P. I. A. 2008. Sediment delivery from hillslopes and the Universal Soil Loss Equation: some perceptions and misconceptions. *Hydrological Processes,* 22**,** 3168-3175.

KOVÁŘ, P., VAŠŠOVÁ, D. & JANEČEK, M. 2012. Surface Runoff Simulation to Mitigate the Impact of Soil Erosion, Case Study of Trebsin (Czech Republic). *Soil and Water Research,* 7**,** 85-96.

LIU, B. Y., NEARING, M. A. & RISSE, L. M. 1994. SLOPE GRADIENT EFFECTS ON SOIL LOSS FOR STEEP SLOPES. *Transactions of the Asae,* 37**,** 1835-1840.

LIU, B. Y., NEARING, M. A., SHI, P. J. & JIA, Z. W. 2000. Slope length effects on soil loss for steep slopes. *Soil Science Society of America Journal,* 64**,** 1759-1763.

LIU, K., TANG, G., JIANG, L., ZHU, A. X., YANG, J. & SONG, X. 2015. Regional-scale calculation of the LS factor using parallel processing. *Computers & Geosciences,* 78**,** 110-122.

MCCOOL, D. K., FOSTER, G. R., MUTCHLER, C. K. & MEYER, L. D. 1989. REVISED SLOPE LENGTH FACTOR FOR THE UNIVERSAL SOIL LOSS EQUATION. *Transactions of the Asae,* 32**,** 1571-1576.

MITASOVA, H., HOFIERKA, J., ZLOCHA, M. & IVERSON, L. 1997. Modelling topographic potential for erosion and deposition using GIS - Reply. *International Journal of Geographical Information Science,* 11**,** 611-618.

MITASOVA, H., HOFIERKA, J., ZLOCHA, M. & IVERSON, L. R. 1996. Modelling topographic potential for erosion and deposition using GIS. *International Journal of Geographical Information Systems,* 10**,** 629-641.

MOORE, I. D. & BURCH, G. J. 1986. Physical Basis of the Length-Slope Factor in the Universal Soil Loss Equation. *Soil Science Society of America Journal,* 50**,** 1294-1298.

MOORE, I. D., GRAYSON, R. B. & LADSON, A. R. 1991. Digital terrain modelling: A review of hydrological, geomorphological, and biological applications. *Hydrological Processes,* 5**,** 3-30.

MOORE, I. D. & WILSON, J. P. 1992. Length-slope factors for the Revised Universal Soil Loss Equation: Simplified method of estimation. *Journal of Soil and Water Conservation,* 47**,** 423-428.

NEARING, M. A. 1997. A Single, Continuous Function for Slope Steepness Influence on Soil Loss. *Soil Science Society of America Journal,* 61**,** 917-919.

OLIVEIRA, A. H., SILVA, M. A. D., SILVA, M. L. N., CURI, N., NETO, G. K. & FREITAS, D. A. F. D. 2013. *Development of Topographic Factor Modeling for Application in Soil Erosion Models*.

QUINN, P. F., BEVEN, K. J. & LAMB, R. 1995. THE LN(A/TAN-BETA) INDEX - HOW TO CALCULATE IT AND HOW TO USE IT WITHIN THE TOPMODEL FRAMEWORK. *Hydrological Processes,* 9**,** 161-182.

RENARD, K. G. 1997. Predicting soil erosion by water : a guide to conservation planning with the revised universal soil loss equation (RUSLE). *Agriculture handbook no 703.* Washington, D.C.: USDA, Agricultural Research Service,.

TARBOTON, D. G. 1997. A new method for the determination of flow directions and upslope areas in grid digital elevation models. *Water Resources Research,* 33**,** 309-319.

TETZLAFF, B. & WENDLAND, F. 2012. Modelling Sediment Input to Surface Waters for German States with MEPhos: Methodology, Sensitivity and Uncertainty. *Water Resources Management,* 26**,** 165-184.

TRUMAN, C. C., WAUCHOPE, R. D., SUMNER, H. R., DAVIS, J. G., GASCHO, G. J., HOOK, J. E., CHANDLER, L. D. & JOHNSON, A. W. 2001. Slope length effects on runoff and sediment delivery. *Journal of Soil and Water Conservation,* 56**,** 249-256.

VAN REMORTEL, R. D., HAMILTON, M. E. & HICKEY, R. J. 2001. Estimating the LS Factor for RUSLE through Iterative Slope Length Processing of Digital Elevation Data within Arclnfo Grid. *Cartography,* 30**,** 27-35.

VAN REMORTEL, R. D., MAICHLE, R. W. & HICKEY, R. J. 2004. Computing the LS factor for the Revised Universal Soil Loss Equation through array-based slope processing of digital elevation data using a C++ executable. *Computers & Geosciences,* 30**,** 1043-1053.

WILSON, J. P., MITASOVA, H. & WRIGHT, D. J. 2000. Water resources applications of Geographic Information Systems. *Urisa Journal*.

WISCHMEIER, W. H. & SMITH, D. D. 1965. *Predicting rainfall-erosion losses from cropland east of the Rocky Mountains : guide for selection of practices for soil and water conservation,* Washington, D.C., Agricultural Research Service, U. S. Dept of Agriculture in cooperation with Purdue Agricultural Experiment Station.

WISCHMEIER, W. H. & SMITH, D. D. 1978. *Predicting rainfall erosion losses : a guide to conservation planning,* Washington, Purdue University. Agricultural Experiment Station, Science and Education Administration.

WRB, I. W. G. 2006. *World Reference Base for Soil Resources 2006: a Framework for International Classification, Correlation and Communication*, FAO, Rome.

YITAYEW, M., POKRZYWKA, S. J. & RENARD, K. G. 1999. Using GIS for facilitating erosion estimation. *Applied Engineering in Agriculture,* 15**,** 295-301.

ZEVENBERGEN, L. W. & THORNE, C. R. 1987. - Quantitative analysis of land surface topography. - 12**,** - 56.

ZHANG, H., YANG, Q., LI, R., LIU, Q., MOORE, D., HE, P., RITSEMA, C. J. & GEISSEN, V. 2013. Extension of a GIS procedure for calculating the RUSLE equation LS factor. *Computers & Geosciences,* 52**,** 177-188.

5 Celkové shrnutí a doporučení pro další výzkum

Využívání geoinformačních systémů v prostorově distribuovaném modelování a v oblasti tzv. „up-scalling“ modelů je díky překotnému vývoji v oblasti dálkového průzkumu země (např. projekty Copernicus, Corine nebo LUCAS, nebo přímo data ze satelitů jako jsou např. Sentinel, Landsat atd.) v centru vědeckého zájmu. Nespornou výhodou prostředí GIS je přímé propojení databázového systému obsahující půdní záznamy (např. digitalizace starých záznamů KPP, SOTER), obsahující informace o srážkách (databáze REDES) nebo i informace o využití půdy (např. propojení s LPIS) s digitálním modelem reliéfu (DMR) v různém rozlišení (např. ČÚZK poskytuje DMR ve vysokém rozlišení z LIDAR mapování).

Obecně dlouhodobým hlavním omezením, se kterým se v současnosti erozní modelování potýká, je nedostatek dlouhodobých dat a tudíž kvalitní kalibrace a validace modelů pro specifické podmínky. Podle Nearinga a Hairsine (2010) má tento trend z velké části na svědomí nastavení financování výzkumu, kdy se udělují granty v horizontu dvou až pěti let a tudíž vznikají různá úskalí z hlediska sběru dlouhodobých dat, která jsou přitom pro práci s modely nezbytnými.

Pokračování sběru dat a vytváření databázových systémů pro účely nejen erozního modelování bude mít i v budoucnu zásadní význam, protože nedostatek dat znamená omezení vývoje „spolehlivých“ modelů (Walling, 2005). Z praktického hlediska je do budoucna vyžadován takový model, který bude splňovat následující kritéria:

- Dostupná a spolehlivá vstupní data,
- Jednoduché uživatelské prostředí,
- Schopnost modelovat srážko-odtokové poměry,
- Schopnost určit trend ve vývoji degradace půdy erozí jakožto funkci protierozních opatření a měnícího se klimatu.

I přes velké množství podrobných dat, která jsou v současné době k dispozici, je empirické modelování stále jedním z nejvyužívanějších konceptů v erozním modelování v praxi. Svědčí o tom vznik RUSLE (Renard et al., 1997) a dalších modelů, které se řadí do tzv. „USLE family“, tj. základní koncept modelu je založen na USLE (např. SWAT). Velká výhoda této skupiny modelů spočívá v jejich jednoduchosti na pochopení pro uživatele, ale velmi často se již do úvahy neberou omezení a limity těchto modelů (Bagarello et al., 2015, Foster, 1982).

Nicméně v této oblasti je stále ještě třeba vyřešit mnoho problémů spojených s nejistotami spojenými se vstupními daty (např. DMR), ale i přímo nejistotami spojenými přímo

s modelem. Nejistoty budou podle Bevena a Alcocka (2012) hrát významnou roli v modelování i v budoucnu a možná povedou i k novým způsobům v myšlení a v modelování eroze (Wainwright et al., 2010). Přičemž ale propojení modelů s geoprostorovými informacemi bude i nadále hrát velmi významnou roli ve vývoji nových modelů (Wainwright et al., 2010, Hengl and Reuter, 2008).

Do budoucna je velmi důležité, aby se vzájemně porovnaly nejen samotné modely (ať už empirické, koncepční nebo fyzikálně založené), ale především algoritmy a další koncepty spojené s analýzou DMR a z nich odvozených atributů. Je třeba stanovit u jednotlivých algoritmů míru nejistoty, vstupní data (prostorové rozlišení) a pro uživatele jasně definovat jejich limity v použití, tak aby se zamezilo mis-aplikacím či mis-intepretaci výsledků modelu.

6 Použitá literatura

AMORE, E., MODICA, C., NEARING, M. A. & SANTORO, V. C. 2004. Scale effect in USLE and WEPP application for soil erosion computation from three Sicilian basins. *Journal of Hydrology,* 293**,** 100-114.

BAGARELLO, V., FERRO, V., GIORDANO, G., MANNOCCHI, F., PAMPALONE, V. & TODISCO, F. 2015. A modified applicative criterion of the physical model concept for evaluating plot soil erosion predictions. *Catena,* 126**,** 53-58.

BEASLEY, D. B., HUGGINS, L. F. & MONKE, E. J. 1980. ANSWERS - A MODEL FOR WATERSHED PLANNING. *Transactions of the Asae,* 23**,** 938-944.

BEVEN, K. J. 2011. *Rainfall-Runoff Modelling : The Primer (2nd Edition),* Hoboken, NJ, USA, John Wiley & Sons.

BEVEN, K. J. & ALCOCK, R. E. 2012. Modelling everything everywhere: a new approach to decision-making for water management under uncertainty. *Freshwater Biology,* 57**,** 124-132.

BOARDMAN, J. 2006. Soil erosion science: Reflections on the limitations of current approaches. *Catena,* 68**,** 73-86.

BOUGHTON, W. 1989. A review of the USDA SCS curve number method. *Soil Research,* 27**,** 511-523.

BRAZIER, R. 2004. Quantifying soil erosion by water in the UK: a review of monitoring and modelling approaches. *Progress in Physical Geography,* 28**,** 340-365.

BÖHNER, J. & SELIGE, T. 2006. Spatial prediction of soil attributes using terrain analysis and climate regionalisation. *Gottinger Geographische Abhandlungen,* 115**,** 13-28.

DE ROO, A. P. J. & JETTEN, V. G. 1999. Modelling soil erosion by water at the catchment scale. *Catena,* 37**,** 275-276.

DE VENTE, J., POESEN, J., GOVERS, G. & BOIX-FAYOS, C. 2009. The implications of data selection for regional erosion and sediment yield modelling. *Earth Surface Processes and Landforms,* 34**,** 1994-2007.

DE VENTE, J., POESEN, J., VERSTRAETEN, G., GOVERS, G., VANMAERCKE, M., VAN ROMPAEY, A., ARABKHEDRI, M. & BOIX-FAYOS, C. 2014. Predicting soil erosion and sediment yield at regional scales: Where do we stand? (vol 127, pg 16, 2013). *Earth-Science Reviews,* 133**,** 94-94.

DESMET, P. J. J. & GOVERS, G. 1996. A GIS procedure for automatically calculating the USLE LS factor on topographically complex landscape units. *Journal of Soil and Water Conservation,* 51**,** 427-433.

DUNN, M. & HICKEY, R. 1998. The effect of slope algorithms on slope estimates within a GIS. *Cartography,* 27**,** 9-15.

ELLISON, W. D. 1947. Soil erosion studies - Part I: Agric. Eng. 28:145-146.

FAIRFIELD J., LEYMARIE P. (1991) Drainage network from grid digital elevation models. Water Resources Research 27(5): 709-717.

FIENER, P., AUERSWALD, K., 2009. Spatial variability of rainfall on a sub-kilometre scale. Earth Surf. Process. Landf. 34, 848–859.

FLORINSKY, I. V. 1998. Accuracy of local topographic variables derived from digital elevation models. *International Journal of Geographical Information Science,* 12**,** 47-61.

FOSTER, G. R. 1982. RELATION OF USLE FACTORS TO EROSION ON RANGELAND. *Science and Education Administration Publications,* ARM**,** 17-35.

FOSTER, G. R., MEYER, L. D. & ONSTAD, C. A. 1977. EROSION EQUATION DERIVED FROM BASIC EROSION PRINCIPLES. *Transactions of the Asae,* 20**,** 678-682.

FOSTER, G. R. & WISCHMEI.WH 1974. EVALUATING IRREGULAR SLOPES FOR SOIL LOSS PREDICTION. *Transactions of the Asae,* 17**,** 305-309.

FOSTER, G.R., YODER, D.C., WEESIES, G.A., MCCOOL, D.K., MCGREGOR, K.C., BINGNER, R.L., 2003. Draft User's Guide, Revised Universal Soil Loss Equation Version 2 (RUSLE-2). USDA-Agricultural Research Service, Washington, DC.

FREEMAN, T. G. 1991. Calculating catchment area with divergent flow based on a regular grid. *Computers & Geosciences,* 17**,** 413-422.

GAREN, D., WOODWARD, D. & GETER, F. 1999. A user agency's view of hydrologic, soil erosion and water quality modelling. *Catena,* 37**,** 277-289.

GOVERS, G. 1991. Rill erosion on arable land in Central Belgium: Rates, controls and predictability. *CATENA,* 18**,** 133-155.

GOVERS, G. 2010. Misapplications and Misconceptions of Erosion Models. *Handbook of Erosion Modelling.* John Wiley & Sons, Ltd.

GRAYSON, R. B., MOORE, I. D. & MCMAHON, T. A. 1992. PHYSICALLY BASED HYDROLOGIC MODELING .1. A TERRAIN-BASED MODEL FOR INVESTIGATIVE PURPOSES. *Water Resources Research,* 28**,** 2639-2658.

GRIFFIN, M. L., BEASLEY, D. B., FLETCHER, J. J. & FOSTER, G. R. 1988. Estimating soil loss on topographically non-uniform field and farm units. *Journal of Soil and Water Conservation,* 43**,** 326-331.

HENGL, T. & REUTER, H. I. 2008. *Geomorphometry: Concepts, Software, Applications,* Amsterdam, Elsevier.

HOLMGREN P. (1994) Multiple flow direction algorithms for runoff modelling in grid based elevation models: an empirical evaluation. Hydrological Processes 8(4): 327-334.

KARYDAS, C. G., PANAGOS, P. & GITAS, I. Z. 2014. A classification of water erosion models according to their geospatial characteristics. *International Journal of Digital Earth,* 7**,** 229-250.

KAVKA, P. & ZAJICEK, J. Soil erosion model smoderp - 1D and 2D modelling. 13th International Multidisciplinary Scientific Geoconference and EXPO, SGEM 2013, 2013 Albena. International Multidisciplinary Scientific Geoconference, 895-902.

KOVÁŘ, P. & VAŠŠOVÁ, D. 2010. Impact of arable land to grassland conversion on the vegetation-period water balance of a small agricultural catchment (němčický stream). *Soil and Water Research,* 5**,** 128-138.

KOVÁŘ, P., VAŠŠOVÁ, D. & JANEČEK, M. 2012. Surface Runoff Simulation to Mitigate the Impact of Soil Erosion, Case Study of Trebsin (Czech Republic). *Soil and Water Research,* 7**,** 85-96.

LIU, B. Y., NEARING, M. A. & RISSE, L. M. 1994. SLOPE GRADIENT EFFECTS ON SOIL LOSS FOR STEEP SLOPES. *Transactions of the Asae,* 37**,** 1835-1840.

MCCOOL, D. K., BROWN, L. C., FOSTER, G. R., MUTCHLER, C. K. & MEYER, L. D. 1987. REVISED SLOPE STEEPNESS FACTOR FOR THE UNIVERSAL SOIL LOSS EQUATION. *Transactions of the American Society of Agricultural Engineers,* 30**,** 1387-1396.

MCCOOL, D. K., GEORGE, G. O., FRECKLETON, M., DOUGLAS, C. L. & PAPENDICK, R. I. 1993. TOPOGRAPHIC EFFECT ON EROSION FROM CROPLAND IN THE NORTHWESTERN WHEAT REGION. *Transactions of the Asae,* 36**,** 1067-1071.

MEYER, L. D. & WISCHMEIER, W. H. 1969. MATHEMATICAL SIMULATION OF THE PROCESS OF SOIL EROSION BY WATER. *Am Soc Agric Engrs-Trans,* 12**,** 754-758, 762.

MITASOVA, H., HOFIERKA, J., ZLOCHA, M. & IVERSON, L. R. 1996. Modelling topographic potential for erosion and deposition using GIS. *International Journal of Geographical Information Systems,* 10**,** 629-641.

MOORE, I. D. & BURCH, G. J. 1986. Physical Basis of the Length-Slope Factor in the Universal Soil Loss Equation. *Soil Science Society of America Journal,* 50**,** 1294-1298.

MOORE, I. D., GRAYSON, R. B. & LADSON, A. R. 1991. Digital terrain modelling: A review of hydrological, geomorphological, and biological applications. *Hydrological Processes,* 5**,** 3-30.

MORGAN, R. 2005. *Soil erosion and conservation*, Blackwell.

MORGAN, R. P. C. 2010. Model Development: A User's Perspective. *Handbook of Erosion Modelling.* John Wiley & Sons, Ltd.

MORGAN, R. P. C. & NEARING, M. A. 2011. *Handbook of erosion modelling,* Chichester, West Sussex, UK ; Hoboken, NJ, Wiley-Blackwell.

MOUSSA, R. 2003. On morphometric properties of basins, scale effects and hydrological response. *Hydrological Processes,* 17**,** 33-58.

NEARING, M. A. 1997. A Single, Continuous Function for Slope Steepness Influence on Soil Loss. *Soil Science Society of America Journal,* 61**,** 917-919.

NEARING, M. A. & HAIRSINE, P. B. 2010. The Future of Soil Erosion Modelling. *Handbook of Erosion Modelling.* John Wiley & Sons, Ltd.

NEARING, M. A. & NICKS, A. D. 1998. Evaluation of the water erosion prediction project (WEPP) model for hillslopes. *In:* BOARDMAN, J. & FAVISMORTLOCK, D. (eds.) *Modelling Soil Erosion by Water.* Berlin: Springer-Verlag Berlin.

O'CALLAGHAN J.F., MARK D.M., (1984) The extraction of drainage networks from digital elevation data. Computer Vision, Graphics, and Image Processing 28(3): 323-344.

OLIVEIRA, A. H., SILVA, M. A. D., SILVA, M. L. N., CURI, N., NETO, G. K. & FREITAS, D. A. F. D. 2013. *Development of Topographic Factor Modeling for Application in Soil Erosion Models*.

QUINN, P., BEVEN, K., CHEVALLIER, P. & PLANCHON, O. 1991. THE PREDICTION OF HILLSLOPE FLOW PATHS FOR DISTRIBUTED HYDROLOGICAL MODELING USING DIGITAL TERRAIN MODELS. *Hydrological Processes,* 5**,** 59-79.

QUINN, P. F., BEVEN, K. J. & LAMB, R. 1995. THE LN(A/TAN-BETA) INDEX - HOW TO CALCULATE IT AND HOW TO USE IT WITHIN THE TOPMODEL FRAMEWORK. *Hydrological Processes,* 9**,** 161-182.

RENARD, K. G. 1997. Predicting soil erosion by water : a guide to conservation planning with the revised universal soil loss equation (RUSLE). *Agriculture handbook no 703.* Washington, D.C.: USDA, Agricultural Research Service,.

ROSE, C. W., WILLIAMS, J. R., SANDER, G. C. & BARRY, D. A. 1983a. A MATHEMATICAL-MODEL OF SOIL-EROSION AND DEPOSITION PROCESSES .1. THEORY FOR A PLANE LAND ELEMENT. *Soil Science Society of America Journal,* 47**,** 991-995.

ROSE, C. W., WILLIAMS, J. R., SANDER, G. C. & BARRY, D. A. 1983b. A MATHEMATICAL-MODEL OF SOIL-EROSION AND DEPOSITION PROCESSES .2. APPLICATION TO

DATA FROM AN ARID-ZONE CATCHMENT. *Soil Science Society of America Journal,* 47**,** 996-1000.

SPEIGHT, J. G. 1974. A parametric approach to landform regions. *Progress in Geomorphology, Special Publication No.7.* Oxford: Institute of British Geographers, Alden & Mowbray Ltd at the Alden Press.

TARBOTON, D. G. 1997. A new method for the determination of flow directions and upslope areas in grid digital elevation models. *Water Resources Research,* 33**,** 309-319.

TETZLAFF, B., FRIEDRICH, K., VORDERBRUEGGE, T., VEREECKEN, H. & WENDLAND, F. 2013. Distributed modelling of mean annual soil erosion and sediment delivery rates to surface waters. *Catena,* 102**,** 13-20.

THALACKER, R. J. 2014. *Mapping techniques for soil erosion: Modeling stream power index in eastern North Dakota.* 1560010, The University of North Dakota.

TIWARI, A. K., RISSE, L. M. & NEARING, M. A. 2000. Evaluation of WEPP and its comparison with USLE and RUSLE. *Transactions of the Asae,* 43**,** 1129-1135.

VERSTRAETEN, G., POESEN, J., DEMARÉE, G., SALLES, C., 2006. Long-term (105 years) variability in rain erosivity as derived from 10-min rainfall depth data for Ukkel (Brussels, Belgium), implications for assessing soil erosion rates. J. Geophys. Res. 111, D22109 (11 pp.).

VRIELING, A. 2006. Satellite remote sensing for water erosion assessment: A review. *Catena,* 65**,** 2-18.

WAINWRIGHT, J., PARSONS, A. J., MULLER, E. N., BRAZIER, R. E. & POWELL, D. M. 2010. Standing proud: a response to 'Soil-erosion models: where do we really stand?' by Smith et al. *Earth Surface Processes and Landforms,* 35**,** 1349-1356.

WALLING, D. E. 2005. Tracing suspended sediment sources in catchments and river systems. *Science of The Total Environment,* 344**,** 159-184.

WILSON, J. P. & GALLANT, J. C. 2000. *Terrain analysis : principles and applications,* New York, Wiley.

WISCHMEIER, W. H. & SMITH, D. D. 1965. *Predicting rainfall-erosion losses from cropland east of the Rocky Mountains : guide for selection of practices for soil and water conservation,* Washington, D.C., Agricultural Research Service, U. S. Dept of Agriculture in cooperation with Purdue Agricultural Experiment Station.

WISCHMEIER, W. H. & SMITH, D. D. 1978. *Predicting rainfall erosion losses : a guide to conservation planning,* Washington, Purdue University. Agricultural Experiment Station, Science and Education Administration.

YOUNG, R. A. & ONSTAD, C. A. 1990. *AGNPS - A TOOL FOR WATERSHED PLANNING,* New York, Amer Soc Civil Engineers.

YOUNG, R. A., ONSTAD, C. A., BOSCH, D. D. & ANDERSON, W. P. 1989. AGNPS - A NONPOINT-SOURCE POLLUTION MODEL FOR EVALUATING AGRICULTURAL WATERSHEDS. *Journal of Soil and Water Conservation,* 44**,** 168-173.

YU, B. & ROSE, C. W. 1999. Application of a physically based soil erosion model, GUEST, in the absence of data on runoff rates I. Theory and methodology. *Soil Research,* 37**,** 1-12.

ZHANG, H., YANG, Q., LI, R., LIU, Q., MOORE, D., HE, P., RITSEMA, C. J. & GEISSEN, V. 2013. Extension of a GIS procedure for calculating the RUSLE equation LS factor. *Computers & Geosciences,* 52**,** 177-188.

ZHANG, L., ONEILL, A. L. & LACEY, S. 1996. Modelling approaches to the prediction of soil erosion in catchments. *Environmental Software,* 11**,** 123-133.

Seznam erozních modelů

Zkratka	Název modelu
ACTMO	Agricultural Chemical Transfer MOdel
ACRU	Agricultural Catchments Research Unit
AGNPS	Agricultural Non-Point Source pollution
AnnAGNPS	Annualized AGNPS
ANSWERS	Areal Nonpoint Source Watershed Environmental Response Simulation
ARM	Agricultural Runoff Management
BTOPMC	Block-wise use of TOPMODEL with Muskingum-Cunge flow routing method
CASC2D-SED	CASCade 2-Dimensional SEDimentation
CORINE	COoRdinate INformation on the Environment
CREAMS	Chemicals, Runoff and Erosion from Agricultural Management Systems
CSEP	Climatic index for Soil Erosion Potential
CSSM	Coleman and Scatena Scoring Model (named partially after the authors Coleman and Scatena)
DWSM	Dynamic Watershed Simulation Model
EGEM	Ephemeral Gully Erosion Model
EHU	Erosion Hazard Units
EPIC	Erosion Productivity Index Calculator (original name) or Environmental Policy Integrated Climate (current name)
EPM	Erosion Potential Method (identical to Gavrilovic model)
EROSION 2D/3D	EROSION 2-Dimensional/3-Dimensional
EUROSEM	EUROpean Soil Erosion Model
EUROWISE	EUROpe WIthin Storm Erosion (named partially after the project 'Modelling Within Storm Erosion Dynamics')
FKSM	Fleming and Kadhimi Scoring Model (named partially after the authors Fleming and Kadhimi)
FSM	Factorial Scoring Model

G2	Geoland2 (named after the project ‘geoland2’)
Gavrilovic/EPM	(named after the main author)/Erosion Potential Model
GAMES	Guelph model for evaluating the effects of Agricultural Management systems on Erosion and Sedimentation
GLEAMS	Groundwater Loading Effects of Agricultural Management Systems
GUEST	Griffith University Erosion System Template (named partially after the university-developer)
HSPF	Hydrologic Simulation Program - FORTRAN
IHACRES-WQ	Identification of unit Hydrographs And Components flows from Rainfall, Evaporation and Streamflow data – Water Quality
IQQM	Integrated Quantity and Quality Model
KINEROS	KINematic EROsion Simulation
LASCAM	LArge Scale CAtchment Model
LEAP	Land Erosion Analysis Programs
LISEM	LImburg Soil Erosion Model (named partially after the university-developer)
MEDALUS	MEditerranean Desertification And Land USe impacts
MEDRUSH	MEdalus Desertification Response Unit SHe
MEFIDIS	Modelo de Erosao FIsico e DIStribuido (Portuguese acronym for ‘Physically Based Distributed Erosion Model’)
MESALES	Modèle d'Evaluation Spatiale de l'ALéa Erosion des Sols (French acronym for Spatial Model Evaluation of Soil Erosion Hazard) (identical to PESERA model)
MIKE/SHE	MIKE (named partially after the author Michael (Mike) Abbott) – SHE (see below)
MMF	Morgan-Morgan-Finney (named after the initials of the authors Morgan, Morgan, and Finney)
MULTSED	MULTiple-watershed SEDiment-routing
MUSLE	Modified USLE
OPUS	(not an acronym)
PALMS	Precision Agricultural-Landscape Modeling System

PEPP	Process-orientated Erosion Prediction Program
PESERA	Pan European Soil Erosion Risk Assessment
PRMS	Precipitation-Runoff Modeling System
PSIAC	Pacific Southwest Inter-Agency Committee
RDI	Regional Degradation Index
RHEM	Rangeland Hydrology and Erosion Model
RillGrow	(not an acronym)
RillGrow2	(not an acronym)
Rose	(named after the main author)
RUNOFF	(not an acronym)
RUSLE	Revised USLE
SCALES	Spatialisation d'éChelle fi ne de l'ALéa Erosion des Sols (French acronym for 'large-scale assessment and mapping model of soil erosion hazard)
SEDD	SEdiment Delivery Distributed
SEDEM	SEdiment DElivery Model (identical to WATEM)
SedNet	SEDiment River NETwork
SEM	Soil Erosion Model
SEMMED	Soil Erosion Model for MEDiterranean areas
SHE	Système Hydrologique Européen (French acronym for 'European Hydrologic System')
SHE-SED	SHE – SEDimentation
SHETRAN	SEDiment TRANsport modelling system
SIMWE	SIMulation of Water Erosion
SLEMSA	Soil Loss Estimation Model for Southern Africa
SMODERP	Simulation Model of OverlanD flow and ERosion Processes
STREAM	Sealing, Transfer, Runoff, Erosion, Agricultural Modification
SWAT	Soil and Water Assessment Tool
SWIM	Soil and Water Integrated Model

SWRRB	Simulator for Water Resources in Rural Basins
TOPMODEL	TOPographic MODEL
TOPOG	TOPOGraphy
TREX	Two-dimensional Runoff, Erosion, and eXport
USLE	Universal Soil Loss Equation
USLE-M	USLE - Modification
USPED	Unit Stream Power based Erosion Deposition
VSD	Vegetation Surface material Drainage density
WATEM	Water and Tillage Erosion Model
WEHY	Watershed Environmental HYdrologic
WEPP	Water Erosion Prediction Process
WESP	Watershed Erosion Simulation Program
WSM	Wallingford Scoring Model (named partially after the company-developer)

Část seznamu převzata z: Christos G. Karydas, Panos Panagos & Ioannis Z. Gitas (2014): A classification of water erosion models according to their geospatial characteristics, International Journal of Digital Earth, 7(3): 229-250 (DOI:10.1080/17538947.2012.671380)